Preliminary Research Findings on the Effect of Coarse Aggregate on the Performance of Portland Cement Concrete Paving

B. F. McCullough, Dan Zollinger, and
Brent T. Allison

RESEARCH REPORT 1244-5

PROJECT 0-1244

CENTER FOR TRANSPORTATION RESEARCH
BUREAU OF ENGINEERING RESEARCH
THE UNIVERSITY OF TEXAS AT AUSTIN

OCTOBER 1993

1. Report No.	2. Government Accession No.	3.
FHWA/TX-94+1244-5		

4. Title and Subtitle	5. Report Date
PRELIMINARY RESEARCH FINDINGS ON THE EFFECT OF COARSE AGGREGATE ON THE PERFORMANCE OF PORTLAND CEMENT CONCRETE PAVING	October 1993
	6. Performing Organization Code
7. Author(s)	8. Performing Organization Report No.
B. F. McCullough, Dan Zollinger, and Brent T. Allison	Research Report 1244-5
9. Performing Organization Name and Address	10. Work Unit No. (TRAIS)
Center for Transportation Research The University of Texas at Austin 3208 Red River, Suite 200 Austin, Texas 78705-2650	11. Contract or Grant No. Research Study 0-1244
	13. Type of Report and Period Covered
12. Sponsoring Agency Name and Address	Interim
Texas Department of Transportation Research and Technology Transfer Office P. O. Box 5051 Austin, Texas 78763-5051	14. Sponsoring Agency Code

15. Supplementary Notes

Study conducted in cooperation with the U.S. Department of Transportation, Federal Highway Administration. Research study title: "Evaluation of the Performance of Texas Pavements Made with Different Coarse Aggregates"

16. Abstract

This report focuses on aggregates used in the construction of continuously reinforced concrete pavements (CRCP). Specific chapters address (1) past research regarding aggregates used in asphalt concrete paving, (2) field and laboratory investigations of asphalt concrete pavements, and (3) CRCP behavior and distress. Also addressed are research activities related to aggregates used in asphalt cement concrete pavements. The report reviews such topics as spalling and punchout distresses in continuously reinforced and jointed pavements, aggregate shape characterization using fractals, and the determination of sawcut depth using fractal analysis. Some of these activities relate directly to improving pavement performance, regardless of aggregate type used for construction. Early recommendations based on the project's significant findings have already been presented to the Texas Department of Transportation.

17. Key Words	18. Distribution Statement
Aggregates, portland cement concrete pavements, chemical modeling, aggregate properties, CRCP, fractal analysis, steel design, sawcutting, curing methods, tie bar modifications	No restrictions. This document is available to the public through the National Technical Information Service, Springfield, Virginia 22161.

19. Security Classif. (of this report)	20. Security Classif. (of this page)	21. No. of Pages	22. Price
Unclassified	Unclassified	112	

PRELIMINARY RESEARCH FINDINGS ON THE EFFECT OF COARSE AGGREGATE ON THE PERFORMANCE OF PORTLAND CEMENT CONCRETE PAVING

by
B. F. McCullough
Dan Zollinger
and
Brent T. Allison

Research Report 1244-5

Research Project 0-1244
Evaluation of the Performance of Texas Pavements Made with Different Coarse Aggregates

conducted for the

Texas Department of Transportation

in cooperation with the

U.S. Department of Transportation
Federal Highway Administration

by the

CENTER FOR TRANSPORTATION RESEARCH
Bureau of Engineering Research
THE UNIVERSITY OF TEXAS AT AUSTIN

October 1993

IMPLEMENTATION STATEMENT

The recommendations presented in this report can lead to improved coarse aggregate selection and, thus, improved pavement performance. The field and lab data collected and evaluated as part of this study can also serve as the basis for improving existing design equations. Finally, improvement in material selection for pavement construction can translate into a direct cost benefit to the Texas Department of Transportation (TxDOT). The following are specific practices that TxDOT may implement immediately:

1. Concrete placement should not be permitted between the hours of 10:00 a.m. and 3:00 p.m., when the ambient temperature is expected to rise above 92° F (33.3° C).
2. The steel design should be adapted to the specific site conditions and to the materials proposed for use by the contractor. A bidding scheme should be established in the specification that permits TxDOT to adjust pavements based on the various blendings, and to eliminate aggregate types based on critical conditions.
3. The use of early-age saw cutting has tremendous promise for crack control and for use with longitudinal joints. The early-age sawing is considerably less expensive and should eliminate the problem of longitudinal cracks forming outside the joint area.
4. Aggregate blends should be used to maximize performance and to minimize cost.
5. TxDOT should consider modifying the current specifications regarding curing (especially under hot-weather conditions).

Prepared in cooperation with the Texas Department of Transportation and the U.S. Department of Transportation, Federal Highway Administration.

ACKNOWLEDGMENTS

The authors wish to thank Dr. Tang, Mr. Terry Dossey, and Mr. Eric D. Moody for their assistance in the preparation of this research report.

DISCLAIMERS

The contents of this report reflect the views of the authors, who are responsible for the facts and the accuracy of the data presented herein. The contents do not necessarily reflect the official views or policies of the Federal Highway Administration or the Texas Department of Transportation. This report does not constitute a standard, specification, or regulation.

NOT INTENDED FOR CONSTRUCTION, BIDDING, OR PERMIT PURPOSES

B. F. McCullough, P.E. (Texas No. 19914)
Research Supervisor

TABLE OF CONTENTS

SUMMARY

This report focuses on aggregates used in the construction of continually reinforced concrete pavements. Specific chapters address (1) past research regarding aggregates used in continually reinforced concrete paving, (2) field and laboratory investigations of continually reinforced concrete pavements, and (3) continually reinforced concrete pavement behavior and distress. Also addressed are research activities related to aggregates used in asphalt concrete pavements. The report reviews such topics as spalling and punchout distresses in continuously reinforced and jointed pavements, aggregate shape characterization using fractals, and the determination of saw-cut depth using fractal analysis. Some of these activities relate directly to improving pavement performance, regardless of aggregate type used for construction. Early recommendations based on the project's significant findings have already been presented to the Texas Department of Transportation.

CHAPTER 1. INTRODUCTION

Included in Texas' 73,000 center-line miles (117,482 km) of highway are both rigid pavements (portland cement concrete, or PCC) and flexible pavements (asphalt concrete). Most of these pavements were constructed using crushed limestone (LS) and/or siliceous river gravel (SRG) as coarse aggregates. It is commonly known that the type of coarse aggregate used in construction significantly affects the performance of pavement structures (since 60 to 80 percent of the pavement volume is some type of coarse aggregate). Thus, it is necessary in the evaluation of the performance of rigid and flexible pavements that the coarse aggregate type be included as a variable. In determining the different physical and chemical characteristics of these aggregates—in addition to determining the characteristics that will affect pavement performance—one can make different design adjustments for pavement construction.

1.1 BACKGROUND

In the past, the design and construction of both asphalt concrete (AC) and portland cement concrete (PCC) pavement in Texas did not take into account the variation in coarse aggregate material properties. Generally, during the bidding process, a contractor selects the aggregate type based on competitive prices received from the various aggregate suppliers. The contractor will then construct the pavement required by the project with the coarse aggregate of his own choosing, even though field tests have indicated that pavement performance will vary significantly, depending on the physical properties of the aggregate.

For portland cement concrete pavements, the design process is based on the premise that concrete volume affects the random occurrence of transverse cracks/joints that are allowed to develop along continuously reinforced concrete pavements (CRCPs) and that are formed or sawed at prescribed spacings for jointed concrete pavements (JCPs). The spacing and width of cracks in CRCP are controlled by the longitudinal steel placed in the concrete slab. Thus, the crack pattern of CRCP is one of the most important physical performance characteristics of the pavement.

Although not reflected in current concrete specifications, the physical properties of the coarse aggregate have a significant effect on the crack pattern developed in CRCP. The chemical properties serve as indicators as to how the physical properties will perform. In the past, this has not been fully recognized in the design/construction process, the result being numerous problems with CRCPs. The principal physical properties of concrete that vary with coarse aggregate type include modulus of elasticity (E), the coefficient of contraction and expansion (α), strength, and shrinkage. All of these have a direct effect on crack spacing, crack width, and corresponding pavement performance.

During the late 1970s and early 1980s, the Center for Transportation Research (CTR) conducted a project entitled "Evaluation of the Performance of Texas Pavements Made with Different Coarse Aggregates" for the State Department of Highways and Public Transportation (presently the Texas Department of Transportation). One phase of the study dealt with condition surveys for the Department that were used to establish criteria for selecting projects for

rehabilitation. In addition, the condition survey data were used to develop numerous improvements in construction procedures and in the design process. One of the major observations that came out of the study was that, generally, CRCPs placed with limestone coarse aggregates had longer service lives than CRCPs placed with siliceous river gravel coarse aggregates (Ref 1). As a result of these studies, several districts have utilized a plan note requiring crushed limestone as the coarse aggregate. This note was accepted without much question during Texas' economic boom of the 1980s. At that time the suppliers were marketing aggregates as rapidly as they could produce them, especially in the building construction industry.

A second major contribution of the study was the development of a CRCP-1 computer program that provided the designer with an analysis method for utilizing the concrete properties, climatic conditions, and friction conditions of the subbase to predict crack spacing, steel stress, and crack width as a function of time. This program permitted the user to analyze the performance, over time, of any given design.

As the building frenzy subsided in Texas, especially in the Houston area, there was considerable concern regarding the use of the plan note. Consequently, the Department requested that CTR utilize the CRCP program to develop a design that would incorporate siliceous river gravel. This information was developed and, subsequently, a proposed standard design—CRCP (B-89B)—was executed by the Highway Design Division.

The purpose of the analysis was to provide a design whereby the crack spacings would be very similar for both aggregate types. Unfortunately, because SRG produces numerous cracks relative to limestone (a result of SRG's higher thermal coefficients and modulus of elasticity), the design standard required more steel for limestone than for SRG. Of course, this presented a problem to aggregate producers, since those who chose to use the limestone aggregate that was providing a better performance (from the standpoint of cracking) were in effect being penalized by the requirement that they use more steel.

Thus, the Department initiated Project 1244, "Evaluation of the Performance of Texas Pavements Made with Different Coarse Aggregates," as a CTR and Texas Transportation Institute (TTI) joint study. Over the past few years, numerous observations, findings, and conclusions relative to this study have been presented by the two institutions. This report was developed to provide a summary of the progress made thus far.

1.2 SUMMARY OF RESEARCH REPORTS TO DATE

To date, four research reports have been published under Project 422/1244. The following provides a brief summary of each.

1.2.1 Report 1244-1: Field Evaluation of Coarse Aggregate Types: Criteria for Test Sections

This report develops design and layout plans for pavement test sections constructed at four state locations (Ref 1). After construction, the sections were subjected to both short-term (from construction to 1 month after construction) and long-term monitoring. Two relatively short

lengths of CRCP were placed, so that one length used a crushed limestone coarse aggregate and the other used a siliceous river gravel coarse aggregate. Each pavement would be subdivided into four 200-foot (61 m) test sections (with a small transition length between sections). In addition to the different aggregates, slab thicknesses of 10 (25.4 cm), 11 (27.94 cm), and 15 (38.1 cm) inches were used, and steel reinforcement varied between 0.1 percent lower than optimal to 0.1 percent higher than optimal (using No. 5 bars). Also, the effect of bonding was tested by using larger steel reinforcing bars, while maintaining the same optimal steel percentage (No. 6 bars).

The purpose of the outlined experiment was to test the effectiveness of the proposed CRCP design standards using various aggregates and aggregate blends from across the state. One proposed standard, CRCP (B) - 89 B, specifies steel percentage based on aggregate type, whereas a later standard, CRCP (B) - 89 C, calls for percent reinforcement based on a compromise of what is needed for each aggregate type. Neither standard has been adequately tested, since existing CRCPs in the state had very little variation in steel quantity or in pavement thickness. The experiment developed in this report will provide the field data necessary for evaluating the proposed design standards and for selecting the best approach.

1.2.2. Report 1244-2: Characterization of Concrete Properties with Age

This report describes the technique and results of the Phase II laboratory testing (Ref 2). Eight coarse aggregates commonly used in Texas pavements were tested for their effect on portland cement concrete material properties. Concrete compressive strength, tensile strength, modulus of elasticity, and drying shrinkage were monitored over a period of 28 to 256 days while the specimens were cured at a constant temperature and humidity (75°F [23.8°C] at 40 percent R.H.). Statistical tests performed on the data revealed significant differences in performance between the aggregates (Table 1.1).

As shown in the table, coarse aggregate type had a significant effect on all four of the concrete properties tested. Further statistical tests were used to determine which aggregates were significantly different given the four concrete properties tested, as shown in Tables 1.2 through 1.5. These tables indicate that researchers may classify the aggregates by using two to four groups, depending on the property considered. Thus, in formulating a design standard or specification, generally two groupings would suffice (with a maximum of four groupings). This is significant in that a standard will not be required for each aggregate type in the state.

Simple log models were calculated to describe the relationship of the four concrete properties to curing set time, for each aggregate. These models are shown in Figures 1.1 through 1.4. The curves were developed from the equations for each aggregate type using the significant variables shown in Table 1.1. Since the curve fits were excellent, these curves are very representative of the actual data.

Using the chemical composition of each aggregate (determined by oxides remaining after fusion), researchers developed additional models that could predict, approximately, concrete properties for specimens that have not undergone comprehensive laboratory testing. A computer program, CHEM1, was written to implement this procedure. The significance of these results is

that, with the computer program and a simple chemical test, any new source may be characterized (obviating a detailed laboratory testing program).

Table 1.1. ANOVA results for tested aggregates (Ref 2)

Concrete Property	Coefficient of Determination	Number of Observations	Predictor Variables	Significance
f_c	0.96	95	Time Aggregate Time * Agg	Yes
f_t	0.94	95	Time Aggregate Time * Agg	Yes
E	0.86	96	Time Aggregate Time * Agg	Yes
Z	0.99	64	Time Aggregate Time * Agg	Yes

f_c = compressive strength E = modulus of elasticity
f_t = tensile strength Z = drying shrinkage

Table 1.2. Comparison of means for 28-day compressive strength (Ref 2)

Grouping*	Mean (psi**)	N	Aggregate
A	4,999	3	LS
A	4,967	3	GR
A	4,870	3	SRG
B A	4,465	3	DL
B	4,139	3	WT
B	4,093	3	BTT
B	4,008	2	VG
B	3,989	3	FR

*Means with the same letter are not significantly different. Least significant difference = 634.98 for a = 0.05.
**1 psi=6894.757 Pa

Table 1.3. Comparison of means for 28-day tensile strength (Ref 2)

Grouping*	Mean (psi**)	N	Aggregate
A	529	3	GR
B A	494	3	DL
B A	476	3	FR
B	455	3	SRG
B	441	3	VG
B	441	3	BTT
B	432	3	LS
B	432	3	WT

*Means with the same letter are not significantly different. Least significant difference = 65.6 for a = 0.05.
**1 psi=6894.757 Pa

Table 1.4. Comparison of means for 28-day elastic modulus (Ref 2)

Grouping*	Mean (psi, millions**)	N	Aggregate
A	4.86	3	DL
B	4.23	3	SRG
B	4.11	3	FR
C B	4.09	3	BTT
C B D	3.88	3	VG
C E D	3.63	3	WT
E D	3.47	3	GR
E	3.37	3	LS

*Means with the same letter are not significantly different. Least significant difference = 0.488 for a = 0.05.
**1 psi=6894.757 Pa

Table 1.5. Comparison of means for 28-day drying shrinkage (Ref 2)

Grouping*	Mean (in.**/in. 10^{-3})	N	Aggregate
A	330	2	GR
A	317	2	FR
B	227	2	VG
B	217	2	WT
C B	206	2	LS
C B D	187	2	SRG
C D	170	2	BTT
D	157	2	DL

*Means with the same letter are not significantly different. Least significant difference = 43.0 for a = 0.05.
**1 inch=2.54 cm

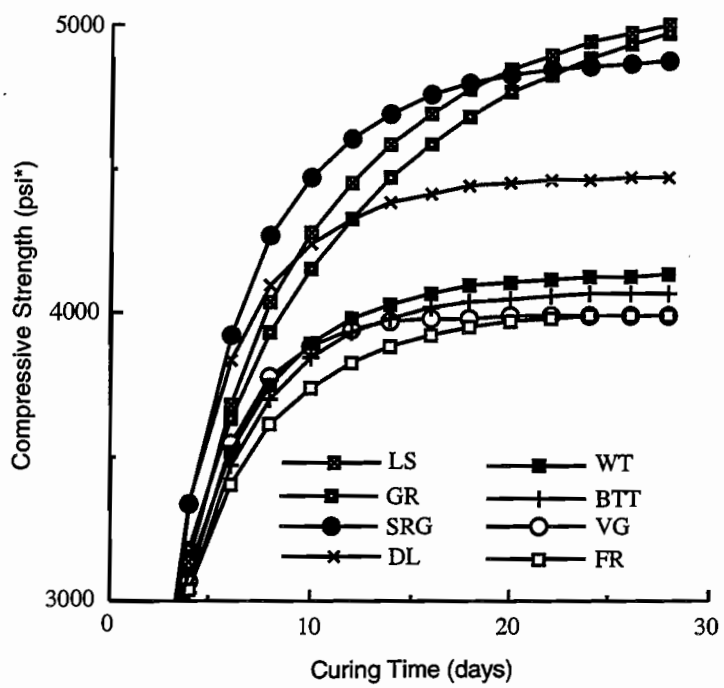

1 psi=6894.757 Pa

Figure 1.1. Curing set curves for compressive strength (Ref 2)

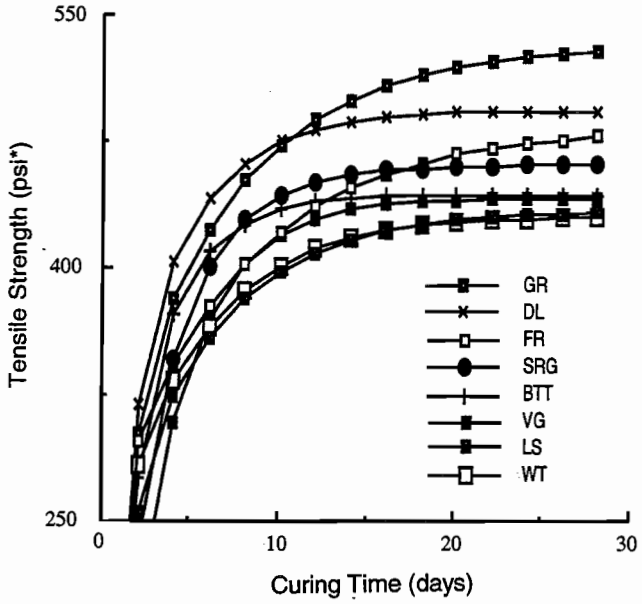

1 psi=6894.757 Pa

Figure 1.2. Curing set curves for tensile strength (Ref 2)

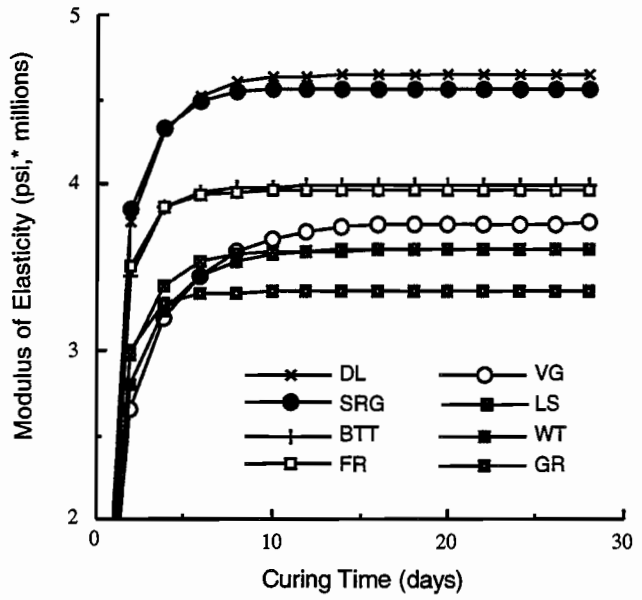

1 psi=6894.757 Pa

Figure 1.3. Curing set curves for elastic modulus (Ref 2)

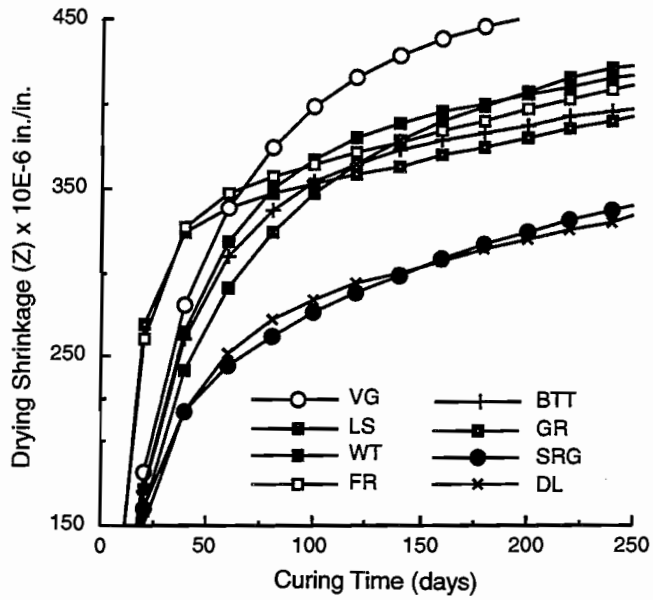

1 inch=2.54 cm

Figure 1.4. Curing set curves for drying shrinkage (Ref 2)

1.2.3 Report 1244-3: Early Age Behavior of Continuously Reinforced Concrete Pavement and Calibration of the Failure Prediction Model in the CRCP-7 Program

This report (Ref 3) documents the short-term performance of the test pavements, described in Report 1244-1, for continuously reinforced concrete. This report is focused on (1) the importance of the heat of hydration in connection with early-age behavior of CRCP; (2) the effect on early-age cracking of the construction season and the time of placement during the day; (3) the detrimental characteristics of the early-age cracks in terms of their shapes and widths; (4) the effect of coarse aggregate type on cracking; (5) the factors affecting crack width; (6) the determination of setting temperature, which is used as a reference temperature in the calculation of temperature-induced stresses; and (7) the correlation between the shrinkage of concrete pavement in the field and that of lab-cured cylinders. Based on these observations and findings, the study recommends how the early-age observations may be simulated in the CRCP program. Recommendations for future design and construction are also presented.

Long-term distress curves having various reliabilities (the probability of achieving the stated performance level) were developed for CRCP; the curves were based on the number of failures per mile derived from the Rigid Pavement Database available at the Center for Transportation Research. Figure 1.5 shows how the rate of failure is affected by aggregate, soil types, and ESALs.

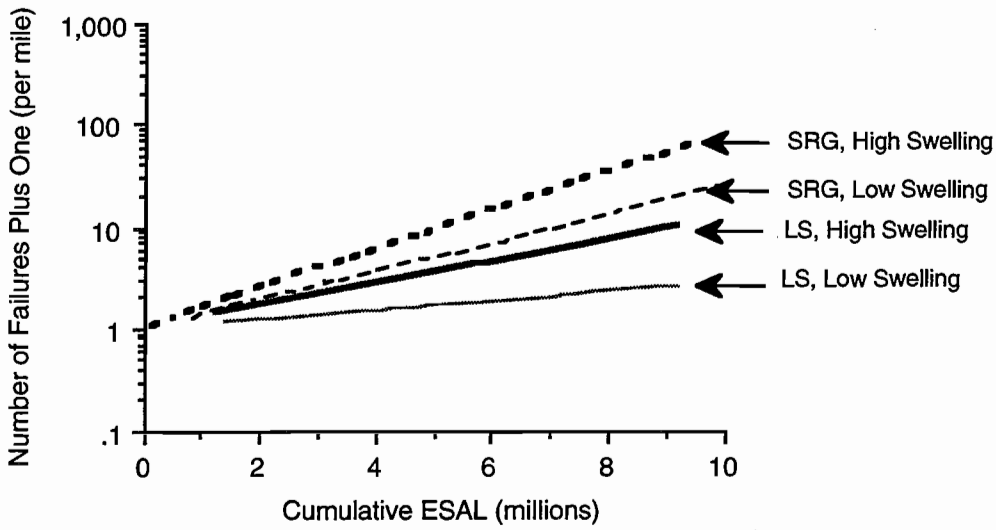

1 mile=1.61 km

Figure 1.5. Mean failure curves for different coarse aggregate types and subbase swelling conditions

Failure curves with various reliabilities were also developed. Figure 1.6 shows an example for limestone aggregate and swelling subgrade.

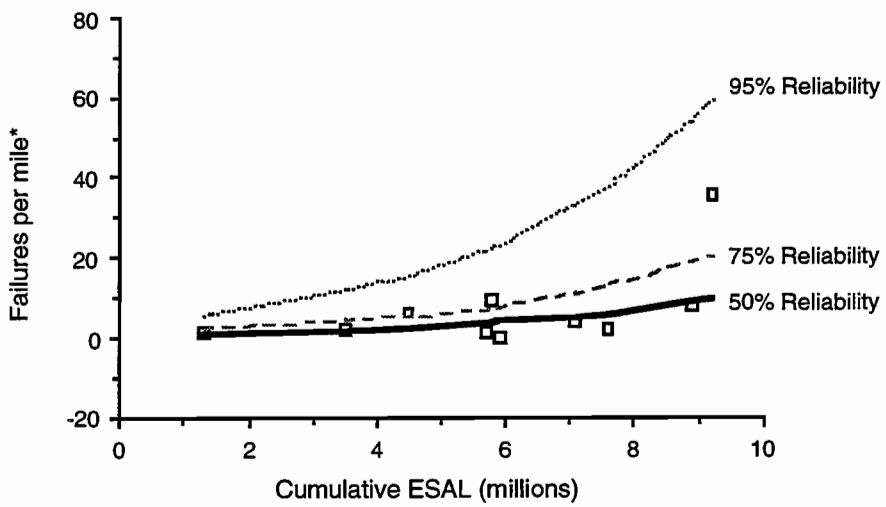

1 mile=1.61 km

Figure 1.6. Failure curves with various reliabilities (LS, high swelling) (Ref 3)

Using these distress curves, researchers calibrated the failure prediction model in the CRCP-7 computer program. The report offers the following conclusions and recommendations, drawn from the short-term monitoring:

(1) For all the paired test sections, there were significant differences in both crack spacing and crack width between the Siliceous River Gravel (SRG) sections and the Limestone (LS) sections. The LS sections, without exception, experienced fewer cracks and larger crack spacings than the SRG sections. The LS sections also experienced smaller crack widths than the SRG sections, even though the crack spacings were larger.

(2) Generally, with the winter projects, crack spacing and crack width decreased as the percent steel increased. At the age of 1 month, a change in bond area, achieved by the use of different bar sizes (No. 6 and No. 7 bars), had not shown a significant difference in cracking.

(3) The location of the new crack between the two adjacent old cracks in CRCP seemed to depend on the distance between the two old cracks (longitudinal length of the slab segment). There was a relatively consistent trend in the location of the new crack in a slab segment when the slab segment was less than about 8 feet long. When the slab segment was about 3 feet long, the new crack within the slab segment occurred, almost without exception, near the middle of the slab segment. Longer slab segments showed greater scattering of the new cracks near the middle of the slab segment. When the slab segments were longer than about 8 feet, the locations of the new cracks were randomly distributed. This supports the assumptions made in CRCP-5 or CRCP-7, that the variability of crack spacing is primarily caused by tensile strength variation and the application of a normal distribution of strength.

(4) Factors that significantly affect crack width were construction season, coarse aggregate type, amount of steel, and time of crack occurrence. Hot-weather placement showed much wider cracks at a given slab surface temperature condition than cool-weather placement. The use of SRG aggregates resulted in wider cracks than the use of LS aggregates, and the difference was larger at lower temperatures. The greater the amount of longitudinal steel, the narrower the crack width. Cracks occurring during the first three days of construction were significantly wider than those that occurred later.

(5) Shrinkage of a concrete cylinder cured in the laboratory at 75°F and 40 percent relative humidity, without removing the cylinder mold, sufficiently represented the field shrinkage of the concrete slab.

Observations and findings from the short-term monitoring that require further research or modification of the CRCP program are outlined below.

(1) The heat caused by the hydration of the cement significantly affects the pattern of the concrete temperature in the pavement slab during the first 24 hours after construction, and consideration should be given to controlling the temperature especially in summer placements. Fresh concrete temperature, ambient temperature conditions, and solar radiation influence the pattern of concrete temperature during hydration. Since the reaction of the hydration is chemically controlled, the rate of hydration is very sensitive

to the ambient temperature conditions. A higher ambient temperature condition results in a higher rate of hydration. The higher the rate of hydration, the higher and the earlier the maximum peak of the concrete temperature will be.

(2) There were significant differences in the crack patterns between summer construction and winter construction. For the summer construction, numerous early-age cracks and several longitudinal cracks were observed, whereas a much smaller number of early-age cracks and no longitudinal cracking were observed in the winter construction. This may be related to the higher temperature change associated with summer construction (a result of the higher rate of hydration).

(3) Early-age cracks observed within the first several days after construction in the summer project tended to be wide and to meander badly. This tendency will increase the future probability of Y-cracking, punchouts, spalling, and steel rupture.

(4) The frequency of early-age cracking in the summer project varied even with the time of placement during a day. The frequency of cracking was always greater in the area placed earlier in the morning than in the areas placed later during the day. For winter construction, however, the effect of placement time was negligible.

(5) For the summer construction, the transverse cracks that occurred during the first several days did not differ significantly with the amount or size of the reinforcing steel. This may be because placement time and temperature are more important than reinforcing steel.

(6) The Randomness Index (RI), which is a mathematical model for objectively quantifying the randomness of cracks by their shapes, has been developed. The RI can be used in identifying the factors affecting the randomness of cracks and in quantifying the effects resulting from the factors. The reliability of concrete pavements can be increased by controlling the randomness.

(7) The results of a statistical analysis conducted on the randomness indices of the cracks in the test sections showed that the construction season, coarse aggregate type, and time of crack occurrence were significant factors influencing the randomness of cracks. Cracks that occurred with summer placement, in the concrete containing SRG aggregate, in the initial day, showed much more random shapes than those that occurred with winter placement, in the concrete containing Limestone aggregate and, at later periods, respectively.

(8) Contrary to the general belief that the greater the crack spacing the wider the cracks, no significant correlation was observed between crack spacing and crack width during the short-term monitoring. It is recommended that the correlation be checked again during long-term monitoring of the test sections.

(9) A method for determining the curing set temperature used in calculating the temperature-induced stress in concrete pavements has been developed by monitoring the concrete temperature and the movement of concrete within a modified cylinder mold.

Recommendations for future testing are provided below.

(1) This study has documented problems associated with early-age cracks in summer construction. To avoid these unwanted early-age cracks, it is better to place concrete in cool weather, since early-age cracks are a product of hot-weather concreting. Because the bond between steel and concrete is not fully developed during the first several days after construction, it may be difficult to control early-age cracks by controlling the amount of longitudinal steel.

(2) If it is necessary to place concrete during hot weather, it is recommended (for reducing early-age cracks) that placement begin in the afternoon rather than in the morning, since afternoon construction produces less temperature rise. Night construction should also be considered.

(3) Since problems occur owing to the temperature rise by hydration during the construction day and subsequent cooling during the night, a reduction of the temperature rise during construction by certain techniques would also decrease the tendency toward unwanted early-age cracks. These techniques could include pre-cooling, the use of pozzolanic material, and the use of retarder. A much lower variation in concrete temperature could be expected if the concrete temperature could be controlled by these techniques so that the main heat generation period of hydration occurred during the night when the ambient temperature was lower. Reducing the temperature rise by these methods would delay the time of crack occurrence; moreover, a substantial amount of the tensile stresses induced by the drying shrinkage and temperature drop could be relieved by creep. The pavement benefits most from the creep effect when the time of cracking is delayed as long as possible. The curing set temperature (setting temperature) of the concrete could also be lowered by reducing the temperature rise, resulting in a lower concrete tensile stress and smaller crack width.

(4) Because of the high temperature variations, the use of aggregate with a low thermal coefficient, such as Limestone, is recommended for hot-weather placement. The use of aggregates having a high thermal coefficient, such as Siliceous River Gravel, in hot-weather construction should be minimized (unless measures for lowering the peak temperature are implemented).

(5) It should be noted that longitudinal cracks began to occur during the first night after the construction day. To avoid unwanted longitudinal cracks, it is recommended that the longitudinal joint of the concrete pavement placed in hot weather be sawed during the evening of the day of construction as soon as the concrete gains enough strength for the sawing operation. A proposed sawing schedule is given in the report.

(6) Many of the transverse cracks occurred over the transverse steel bars, a phenomenon that was more significant in the sections with double-layered steel. Cracking over the steel bars increases the possibility of water reaching the steel, resulting in a much higher possibility of steel corrosion. A staggered steel layout is recommended to reduce this problem.

(7) All the manhole areas showed two to five meandering cracks around the manhole. Within one year after construction, these areas showed punchouts or severe spalling along the cracks. Relocation of the manholes is recommended at the design stage,

based on a long-term cost-benefit analysis; the design of the area surrounding the manhole could also be improved.

1.2.4 Report 1244-4: Monitoring of Siliceous River Gravel and Limestone Continuously Reinforced Concrete Pavement Test Sections in Houston Two Years After Placement, and Development of a Crack Width Model for the CRCP-7 Program

This is the second report concerning the performance of the continuously reinforced concrete pavement (CRCP) test sections (described in Report 1244-1); that is, the report evaluates the test sections' performance up to 2 years after construction (Ref 4). This report examines how CRCP performance is affected by (1) coarse aggregate type, (2) quantity of reinforcing steel, (3) amount of steel bond area, and (4) pavement thickness. Toward this end, test section monitoring included measurements of crack spacing, crack width, and concrete slab temperatures—all collected during the early age of the test sections (i.e., before construction and up to 1 month after construction) and for 2 consecutive years following construction. The construction itself was scheduled so that the seasonal effects on CRCP performance could also be studied.

Using the data collected over the 2 years, along with the data previously collected in the early-age monitoring (Ref 3), the study team developed a model to predict crack width based on the day of crack occurrence. This model is designed to be used with the CRCP-7 computer program, a software program devised several years ago to predict CRCP performance from an empirical/theoretical standpoint. While early versions of the program predicted average transverse crack spacing and crack width (in addition to predicting the steel stress in the reinforcement), later improved versions included a model to estimate the crack spacing distribution. Using field measurements of crack width dimensions, the project team developed a new prediction model to replace the existing model (Eq 1).

$$CW = 0.028 + 740*Z_3 - 260.4e^{-11}*E_i + 29*a*DT - 203e^{-4}*(\%)*(\emptyset) \qquad \text{(Eq 1.1)}$$

where:

- CW = crack width, in.,
- Z_3 = residual shrinkage, as previously defined, in./in.,
- E_i = elastic modulus on the day the crack occurred, psi,
- a = thermal coefficient of the concrete, in./in./°F,
- DT = temperature differential as previously defined, °F,
- $\%$ = reinforcing steel percentage (0.00), and
- $\emptyset$ = reinforcing bar diameter, in.

Figure 1.7 shows the improvement over the existing model through a comparison of results computed with Equation 1.1. The data indicate that the new model gives a much better representation of the field measurements.

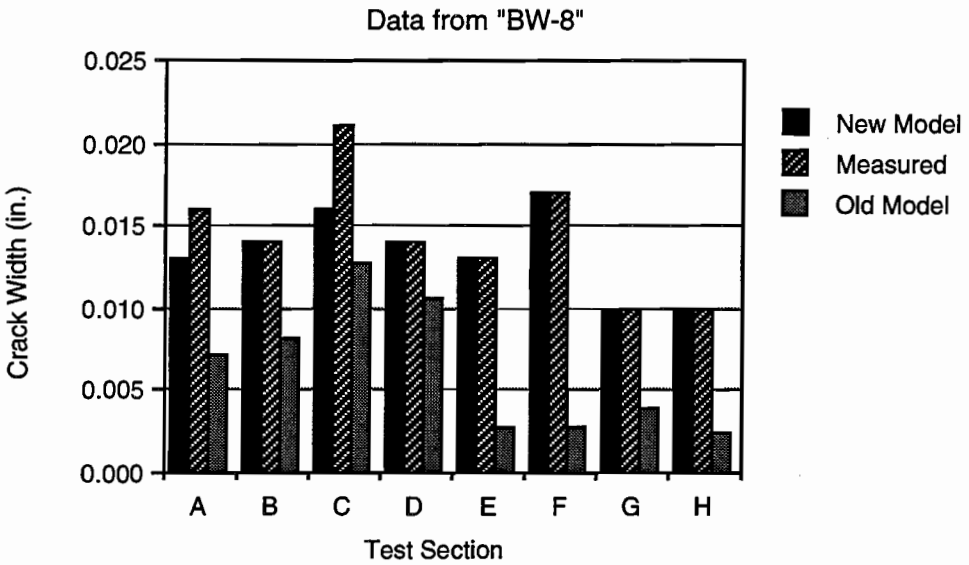

Figure 1.7. Crack width comparison between new model, measured data, and old model (Beltway 8 in Houston) (Ref 4)

The primary objectives of this study were (1) to document the field performance of continuously reinforced concrete pavements constructed with different coarse aggregates (siliceous river gravel and limestone) in the early life of the pavement (1 and 2 years after construction), (2) to evaluate (for crack spacings and crack widths) the recently developed CRCP (B)-89 B design detail for calculating the reinforcing steel for continuously reinforced concrete pavements, and (3) to compare the measured crack spacing and crack width parameters with the values predicted by the CRCP-7 program. In addition, two models were developed: (1) a model to calculate concrete pavement temperatures based on air temperatures reported by the U.S. Weather Bureau, and (2) a model to predict crack widths for CRCP based on concrete properties and climate data. The analysis documented in the report supports the following conclusions and recommendations:

1.3 CONCLUSIONS

(1) The CRCP test sections constructed in Houston were monitored for 2 consecutive years after construction. In general, crack spacing and crack width performance of the winter-constructed test sections was satisfactory. The test sections constructed in the summer had (poor) crack spacing consisting of a high percentage of meandering cracks and a high concentration of crack spacings below the 3.5-ft (1.06 m) AASHTO limit.

This is due to the typically high temperatures that occur during the summer months. Significant differences were found between the paired (equivalent) limestone and SRG sections, with the limestone sections experiencing both larger crack spacings and smaller crack widths. The SRG test sections are already experiencing minor punchouts. The crack widths measured in the test sections constructed in the summer, though wider than those measured in the equivalent winter test sections, are still well below the AASHTO limits.

(2) The CRCP-89(B) design detail performance was satisfactory, despite some significant differences found in the performance of the test sections. The differences of SRG and LS coarse aggregates are much smaller than those found in pavements built with the previous design details, which did not take into account the coarse aggregate type.

(3) The CRCP-7 computer program's ability to predict average crack spacing, crack spacing distribution, and crack width was evaluated. In general, the computer program gives a very good prediction of average crack spacing (given the different variables considered) and an acceptable prediction for the crack spacing distribution. Because the predicted crack width values are dependent on the crack spacing, a new model is proposed that accounts for the age at which a crack occurs.

1.4 RECOMMENDATIONS

(1) Long-term monitoring of the test sections should be continued to evaluate their performance.

(2) The proposed method for calculating set temperature should be studied in more detail. Several tables should be developed to calculate temperature increase using placement temperature for each different coarse aggregate type.

(3) Installation of manholes on CRCP should be avoided; if necessary, these manholes should be located on the shoulder or median (to avoid the pavement distress associated with them).

(4) Future research should investigate the effect of subbase friction on crack widths, so that different subbase materials may be included in the mix design.

(5) A weak plane in the concrete created by multiple stacking of transverse steel should be avoided. When more than one layer of steel is needed, it should be placed in an alternating pattern. A diagonal placement should also be considered.

(6) The use of low thermal coefficient coarse aggregates is recommended. If one with a high thermal coefficient is used, or when hot weather construction is proposed, provisions should be made to minimize the concrete set temperature to maintain the lowest possible thermally induced stresses.

1.5 SUMMARY

The findings from these reports documented the evolution and calibration of the CRCP-7 computer program, which may be used to analyze an existing CRCP or to predict pavement

performance over time relevant to crack spacing, crack width, steel stress, and the punchouts expected with 18-kip ESAL applications. The field measurements and the computer program verify for CRCP what has long been known but not quantified for PCC pavements in general. Specifically, crack width, crack spacing, and punchout prediction models have been improved and calibrated. In addition, a computer program has been developed that uses results from simple and economical chemical tests to predict and to characterize a the physical properties of a specific coarse aggregate without an expensive matrix of laboratory tests. Hence, the feasibility is established of a specification and design standard that has various classifications of coarse aggregates.

The results also show that the performance of a CRCP is dependent on the coarse aggregate type; consequently, designs should be based on the materials delivered in order to extend the service life of the pavement. The field studies also revealed that pavement performance and service life can be affected significantly by the climatic condition during and shortly after placement. The effects of large pavement temperature changes, time of placement, and cure set, among other things, establish a "fingerprint" for future performance. Hence, the specifications and construction guidelines should reflect this information.

1.6 OBJECTIVES

Given the numerous activities being conducted at both CTR and TTI in connection with the study, this report has the following objectives:

1. Provide an overview of work that has not been published to date, one that gives information to the designers, construction personnel, contractors, and research staff.
2. Provide guidelines for trial implementation of the preliminary results.
3. Provide for the Department insight into the work activities currently being conducted by the research staff at CTR and TTI.

1.7 REPORT ORGANIZATION

Chapters 2 through 5 present results of current activities in the area of full-scale studies, the chemical model of the aggregate properties, and the analysis of intricate components of a CRCP pavement. Chapter 6 provides trial implementation and guidelines for preliminary application by the Department. Chapter 7, the report's final chapter, provides insight into the project's future direction. Conclusions and recommendations are provided throughout the report.

CHAPTER 2. FULL-SCALE FIELD STUDIES

This chapter presents the experiment design, construction, instrumentation, data collection, and testing for the various test sections located in Houston, Texas (Figure 2.1).

2.1 BELTWAY 8, STATE HIGHWAY 6, AND INTERSTATE 45

The experiment included CRCP test sections placed at four locations in Houston. At each location, 1,840 feet (560.8 m) of CRCP were placed, with one-half of the length (920 feet [280.4 m]) constructed with SRG and the other half constructed with LS. Each of these lengths was then subdivided into four test sections. One of the four test sections for each coarse aggregate type used the same quantity of longitudinal steel as proposed in the new design standard (hereafter termed "medium" steel).

Two other test sections used an amount of longitudinal steel about 0.1 percent higher (hereafter termed "high" steel) and 0.1 percent lower (hereafter termed "low" steel), respectively, than the medium steel; these three test sections also used a 3/4-inch-diameter (19 mm-diameter) bar size (No. 6 bar). The fourth test section used medium steel with a larger-sized bar (7/8-inch diameter [22 mm-diameter], or No. 7 bar), an arrangement permitting an investigation of the interactive effect of bond area and concrete volume ratio.

The thickness of the concrete slab varied with the project, with the vertical location of the steel (a single layer of steel) in the slab most often at mid-depth; in the case of IH-45 winter, double layers of steel were used. The following describes each project in detail.

2.1.1 SH 6 and Huffmiester—Summer

These sections, located on the two outside northbound lanes of SH 6 approximately one-half mile (.8 km) south of US 290 in Houston, Texas, were the first to be constructed. The layout of the test sections is shown in Figure 2.2. The concrete slab, 11 inches (27.9 cm) thick, used a single layer of steel. The SRG sections were placed on June 16, 1989. The LS sections were placed on June 19, 1989, with the construction of the sections in the sequencing of increasing letter designations as shown.

2.1.2 Beltway 8 and Antonie—Winter

The second set of test sections was placed on Beltway 8 (North) on the eastbound frontage road on the inside two of the three lanes. Section A begins 315 feet (96.0 m) east of the centerline of Antoine Road, with the sections continuing east.

The location and layout of the test sections are shown in Figure 2.3. The concrete slab, 10 inches (25.4 cm) thick, used a single layer of steel. The SRG sections were placed on November 24, 1989, while the LS sections were placed on November 25, 1989. It should be noted that, because of a breakdown at the mixing plant, fly ash was not included in the construction of section H, and only partly included in the construction of section G.

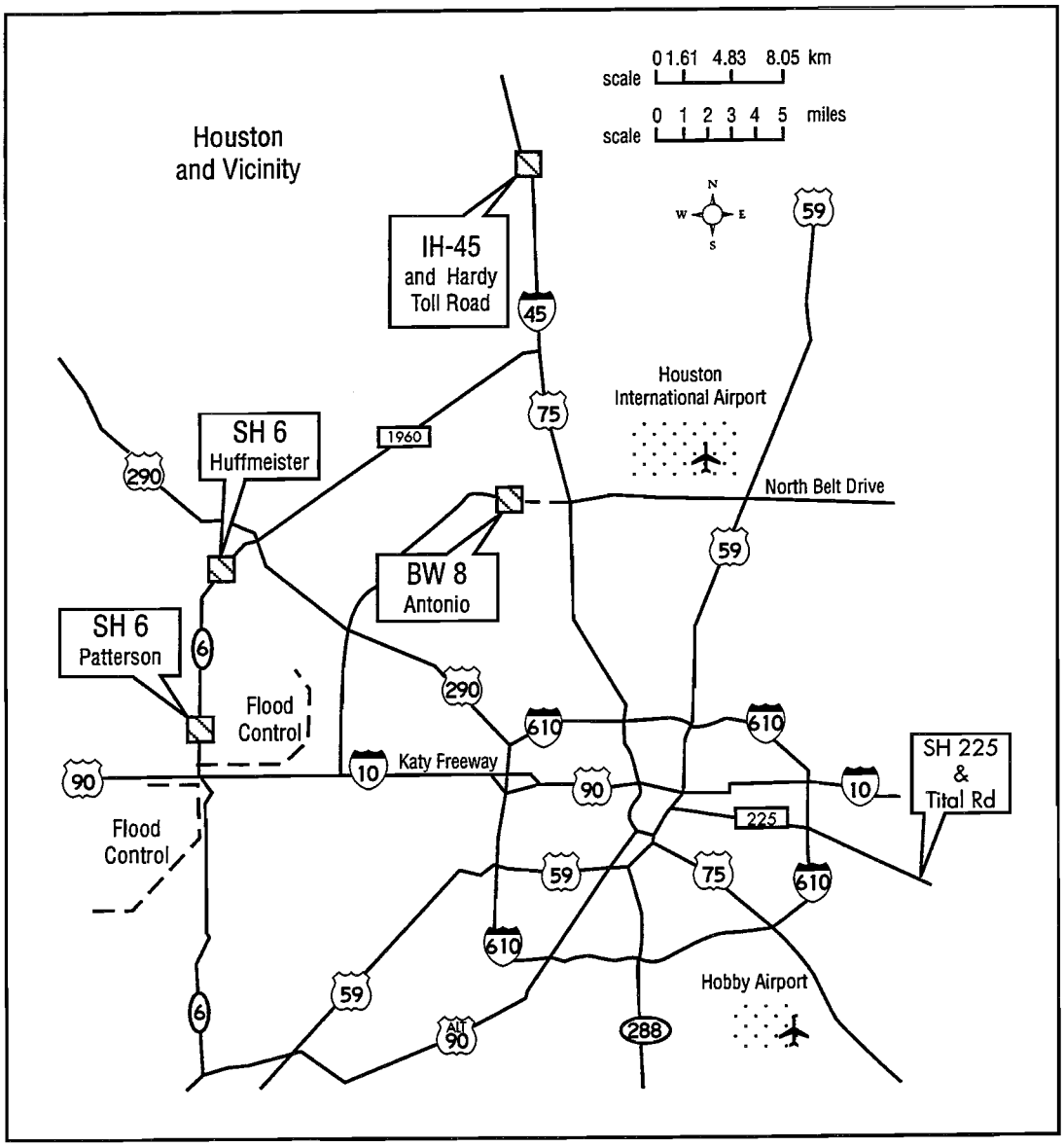

Figure 2.1. Location of the various Houston test sections

2.1.3 SH 6 and Patterson—Winter

The third set of test sections was placed on State Highway 6 just south of Patterson Road, which is about 2 to 3 miles (3.2 to 4.8 km) north of Interstate Highway 10. Test sections are on the two outside southbound lanes in a fill area marked by reinforced earth retaining walls. A concrete shoulder lies between the sections and the retaining wall. The layout of the test sections is shown in Figure 2.4.

The concrete slab was 11 inches (27.9 cm) thick and used a single layer of steel. The construction of the test sections began on January 10, 1990. Sections A and B were placed on

January 10; sections C, D, and E were placed on January 11; sections F, G, and H were placed on January 12. The shoulder was placed a few days after the test sections. Because the contractor did not have a sufficient supply of crushed limestone, SRG aggregates were used in the last 50 feet (15.24 m) of section H (the last section).

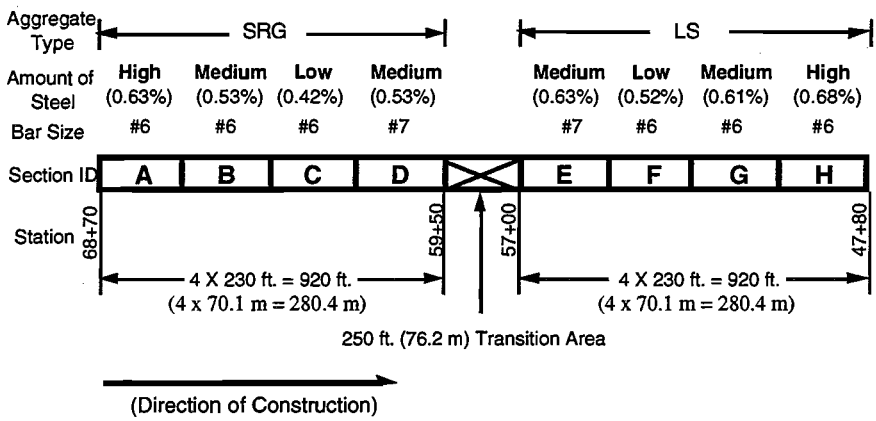

Figure 2.2. Location and layout of the first set of test sections

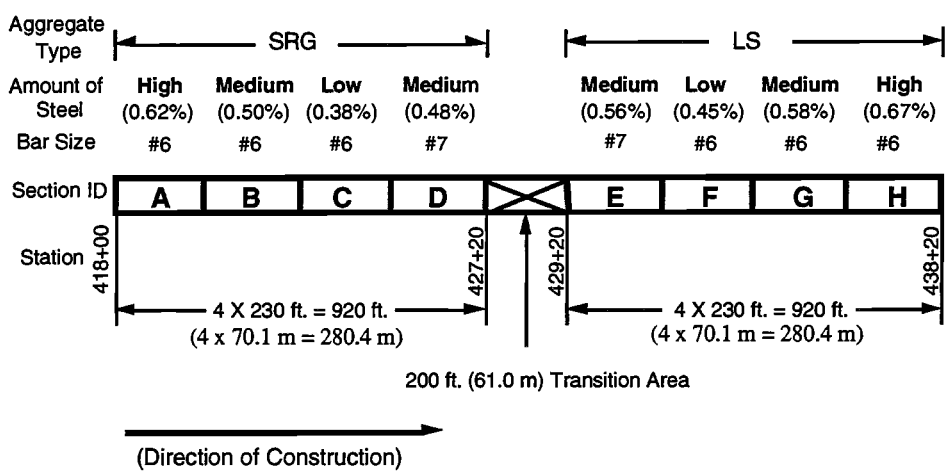

Figure 2.3. Location and layout of the second set of test sections

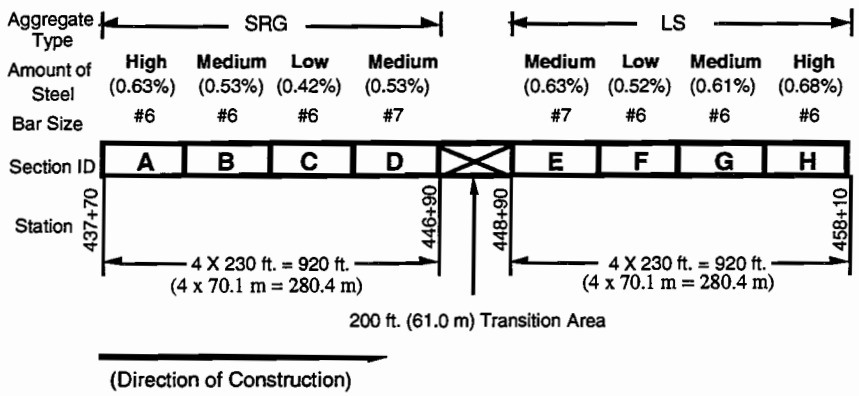

Figure 2.4. Location and layout of the third set of test sections

2.1.4 IH-45 and Hardy Toll Road—Winter

The last set of test sections was placed on Interstate Highway 45 on the north side of Houston at the Hardy Toll Road Interchange near Spring Creek. The cross section includes four lanes with a full-depth CRCP shoulder and an inside median. The test sections are on the two inside northbound lanes, with the median located next to the inside lane. (This location was chosen because it would allow for future observations using the inside median without having to control traffic). The layout of the test sections is shown in Figure 2.5, where it may be noted that the order of placement of the test sections was opposite that of other projects; that is, section D was placed first in SRG sections, and section H was placed first in LS sections.

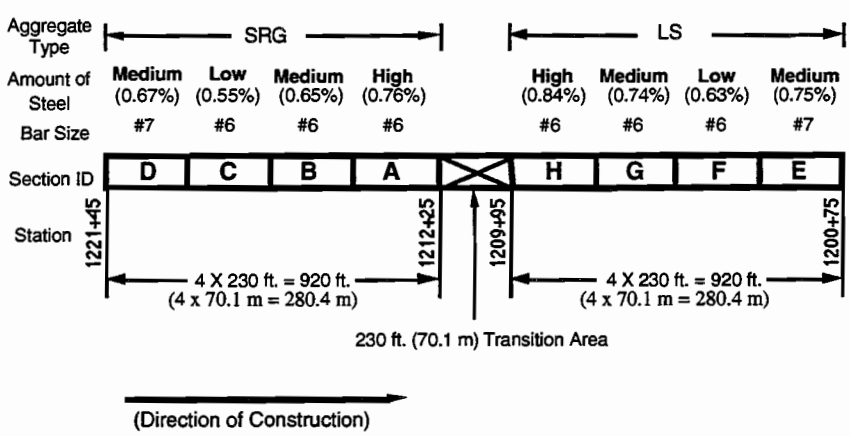

Figure 2.5. Location and layout of the fourth set of test sections

The concrete slab for these sections was 15 inches (38.1 cm) thick and used double layers of steel. While the SRG sections were placed on January 14, 1990, the placement of the LS sections was delayed (because of bad weather) until January 21, 1990. The overall placement of the test sections was performed in good order, with no unusual construction problems occurring.

2.1.5 Instrumentation, Data Collection, and Testing

The primary instrumentation installed in the test sections included thermocouples and D-mac points for monitoring the concrete temperature and slab movement. Layout of the D-mac points was designed to measure the slab movement longitudinally along a pavement from crack to crack. All instrumentation was placed about 3 feet (.9144 m) from the pavement edge for ease of measuring.

To provide a vertical temperature distribution throughout the slab, thermocouples were positioned 1 inch (2.54 cm) from the surface, at mid-depth, and 1 inch (2.54 cm) from the bottom of the slab. Four to seven sets of thermocouples were imbedded at various locations in each project.

To measure slab movement, 20 to 30 D-mac points were placed at 10-inch (25.4-cm) intervals (SH 6 summer used 8-inch [20.32-cm] intervals) on the surface of the concrete. For each project, two sets of brass D-mac points (one for SRG sections and the other for LS sections), covering a length of about 15 to 20 feet (4.57 to 6.10 m), were installed in sections with medium steel (sections B and G).

Data collected during the short-term monitoring (about 1 month after construction) included (1) air and concrete temperature, (2) atmospheric conditions, (3) slab movement, and (4) transverse and longitudinal crack locations. Data were collected periodically over 24 hours for several days after construction. Although new cracks were monitored at various times throughout the day, most often they were surveyed in the morning, when the concrete temperature was low and when crack visibility was enhanced by the wider crack width associated with morning. Instruments were used for measuring temperature, solar radiation, and slab movement. In addition, crack width and concrete movement of experimental slabs were measured.

To determine the concrete properties of the test sections, about 74 to 94 cylinders from each project were cast at the job sites using the same concrete used in the test sections. The material was obtained from four different trucks for each project: two from the SRG sections and two from the LS sections.

On the day following casting, about one-half of the cylinders in each project were transported to the lab at the Center for Transportation Research in Austin for storage (until they could be tested in a chamber having a temperature of 75° F [23.89° C] and a relative humidity of 45 percent). The remaining cylinders were cured in the field in the same manner as the pavement and transported to the lab 1 day before testing. The results of these tests were then used to compare the properties of the concretes cured under the two different conditions.

The lab-cured cylinders were tested at 3, 7, and 28 days, while the field-cured cylinders were tested at 7 and 28 days. Properties tested included splitting tensile strength, compressive modulus of elasticity, compressive strength, drying shrinkage, and thermal coefficient.

2.1.6 Summary of Four Test Sections

The performance of CRCP constructed with siliceous river gravel (SRG) coarse aggregate differs significantly from that of CRCP constructed with limestone (LS) coarse aggregate. Specifically, for the same steel design, pavements containing siliceous river gravel experience substantially more distress (e.g., cracks, spalling, and punchouts) than those containing limestone. Because a large percentage of a pavement's concrete volume consists of coarse aggregates, researchers have tended to conclude that the various coarse aggregates affect differently the overall properties—and, hence, performance—of concrete. In Texas, such observations led to the development of the new CRCP design standard, CRCP (B) - 89 B.

In creating this new design standard, researchers at the Center for Transportation Research at The University of Texas at Austin first analyzed the properties of concrete samples constructed with both SRG and LS coarse aggregates and then entered the results in the CRCP-4 computer program as input values to predict the performance of pavements containing these materials. For various slab thicknesses and steel designs, the program predicted the performance of each pavement in terms of crack spacing, crack width, and steel stress. Using the CRCP design criteria, an optimum longitudinal steel design could be selected for each combination of slab thickness and coarse aggregate type.

Based on the results of this early analysis, the Texas State Department of Highways and Public Transportation (SDHPT, now the Texas Department of Transportation, or TxDOT) developed new design standards for both SRG and LS aggregates. These standards include different coarse aggregate types; for a given slab thickness, different bar spacings were used with same-sized bars. The major feature of the new design standard was the use of different amounts of longitudinal steel for different coarse aggregate types in a manner such that similar crack spacings for the two aggregate types would be expected within the limiting design criteria. Since the major distresses of CRCP (i.e., punchouts and spalling) have a strong correlation with crack spacing, the new design standard sought to minimize the distress by controlling the crack spacing. And because SRG-constructed pavements showed narrower crack spacing than LS-constructed pavements, the new design for SRG concrete specified less longitudinal steel than specified for LS concrete.

2.2 STATE HIGHWAY 225, LAPORTE, TEXAS

Concrete placement on SH 225 in Houston began on November 11, 1992. The monitoring and testing of the test sections were joint efforts of the Center for Transportation Research (The University of Texas at Austin) and the Texas Transportation Institute (Texas A&M University). This section discusses (1) the purpose of the LaPorte test sections, (2) placement activities, (3) testing and past monitoring, and (4) future monitoring of the test sections.

2.2.1 Research Purposes

The primary purpose of the LaPorte test sections is to determine the effect of varying curing technique, saw cut technique, and placement of skewed transverse steel on the performance of CRCP. The primary parameters that have been measured to evaluate the affects of varying curing technique, saw cut technique, and placement of skewed transverse steel on CRCP include (1) crack width, (2) crack spacing, and (3) concrete strength.

2.2.2 Placement

The test sections are located on SH 225 a few miles east of Beltway 8 on the east side of Houston. The test sections were originally designed to be the "warm weather placement test sections" for this project. Because of the time of year placed, weather, and temperature, optimum conditions for warm weather placement were not present. The temperature at the beginning of the placement on November 11 was in the high 50s (mid teens C) and peaked at 69° F (20.56° C) before dropping back into the high 50s (mid teens C) during evening. The effect of the temperature allowed the newly placed concrete to solidify much slower than would have been expected during warm weather placement.

Nine consecutive test sections, each 250 feet (76.2 m) long, were placed in the eastbound lanes. A 150-foot (45.72-m) buffer zone was placed at each end of the test sections. Figure 2.6 shows the general layout of the test sections.

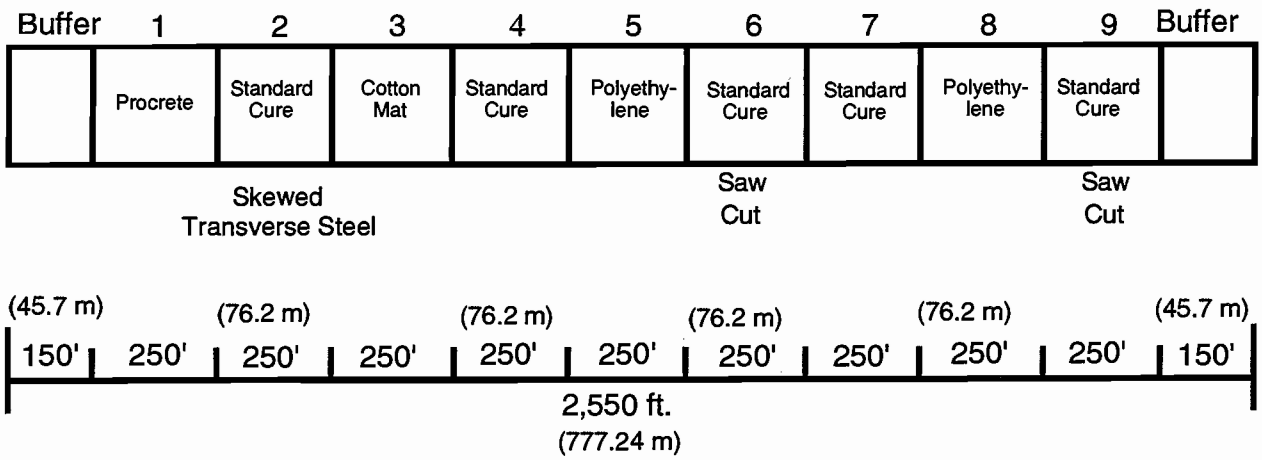

Figure 2.6. Layout of test sections by distance, cure type, and unique features

On November 26, the shoulder was paved along the outside lane of the test sections. In section 2, skewed transverse steel was placed at a 45-degree angle for the full 250 feet (76.2 m). Various methods of curing were done on each test section. Figure 2.6 summarizes the cure methods completed in each section.

2.2.3 Testing

Various types of testing have been employed to determine the crack width, crack spacing, and concrete strength. Each of these testing methods are listed below and will be discussed in this section.

1. D-mac strain gage measurements
2. Thermocouple concrete temperature measurements
3. Maturity meter
4. Condition surveys
5. Microscope crack width measurements
6. Saw methods
7. Coring
8. Crack spacing
9. Crack randomness
10. Cure methods

Table 2.1 offers a brief summary of the locations and types of tests conducted.

Table 2.1. Summary of testing locations and times

Section	D-mac	R-Humid	Strain Gage		Temperature	
			Conc.	Steel	Conc.	air
1	X	X			X	
2	X	X			X	
3	X	X			X	
4		X			X	
5	X	X			X	
6		X	X	X	X	X
7		X			X	
8		X			X	
9		X	X	X	X	X

Time in Hours/Days

a. Hours: 12, 18, 24.

b. Days: 3, 7.

2.2.4 D-mac Strain Gauge Measurements

Thirty D-mac points were placed in the concrete at the test sections. The D-mac bolts were placed in four locations along the test sections (sections 1, 2, 3, and 5). In sections 1-3, five bolts

were placed. In section 5, fifteen bolts were placed. The strain gauge measures are accurate to 0.001 of an inch (.0254 mm). The strain gauge measurements were used to measure the expansion and contraction of the pavement. The measurement is also extremely useful in obtaining accurate crack width data. Cracks appeared within the D-mac points located in section 2 and section 5. Data obtained from D-mac location 2 were plotted in Figure 2.7. While three of the lines in Figure 3 remain fairly straight, the fourth line identifies a crack in the pavement. This crack varies as much as 1/25 of an inch (1.016 mm), depending on the temperature of the concrete at the time of measurement.

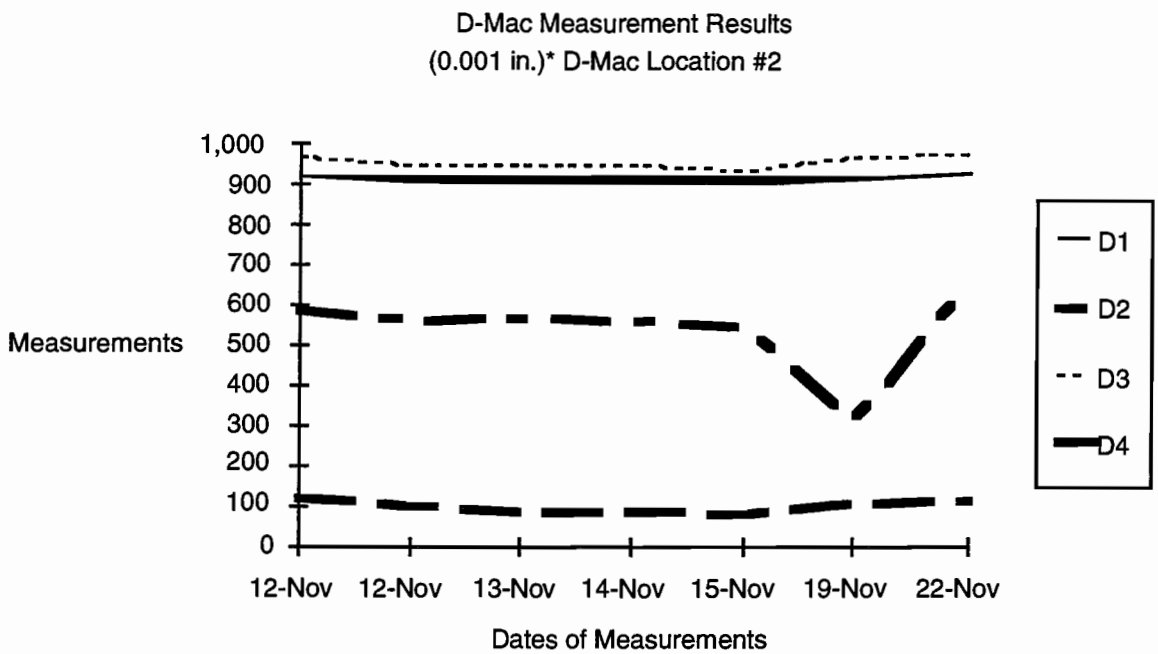

*.001 in. = .0254 mm

Figure 2.7. D-mac crack width measurement at location 2

2.2.5 Thermocouple Concrete Temperature Measurements

Two sets of thermocouples were placed in the concrete at the test sections (sections 2 and 5). The thermocouple wires are designed to measure the temperature at four different levels of the pavement. Four insulated copper wires were attached to a small wood dowel and placed in the concrete overlay just after the paving train had passed over and while the concrete was still plastic. Because of the overcast weather on the placement date and the dates immediately following, the pavement temperature never exceeded 95° F (35° C). This is a relatively very mild temperature, considering that the surface temperature may exceed 200° F (93.3° C) on a hot day.

2.2.6 Maturity Meter

A maturity meter was placed in section 5 alongside the D-mac location #4. The team was not able to obtain any data from the maturity meter left in the field because of a mechanical breakdown. The maturity meter had been tampered with and was not working on the return trip to Houston one week after placement of the overlay.

2.2.7 Condition Surveys

A detailed condition survey was taken a week after the pavement placement was placed. This survey marks out the sites of the various tests and accurately maps the cracks that have occurred in the pavement thus far. Much of the data collected in the condition surveys will prove useful for future reference. The following items were contained in the condition survey:

1. Crack spacing
2. Crack randomness
3. Testing sites
4. Cure types
5. Soft cut saw joints
6. Section location

2.2.8 Microscope Crack Width Data

Five cracks in each section were measured for crack width using the microscope. At each crack, there were three measurements taken (Figure 2.8), all within the outside lane. The first measurement was taken in the outside wheel path, the second in the center of the lane, and the third in the inside wheel path.

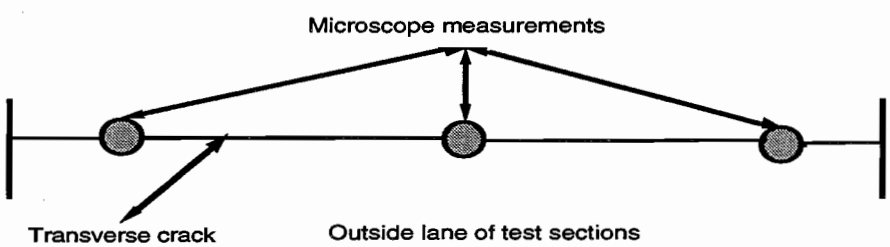

Figure 2.8. Diagram of microscope measurement technique

A mark was placed around the base of the microscope on the pavement at each location in order that future measurements could be taken. The microscope measures down to the nearest 1/1,000 of an inch (.0254 mm). The results of the measurements are given in 1/1,000 of an inch (.0254 mm). In graphing the results of the microscope measurements, it was found that the bar size, cure type, and other factors did not have near the influence on crack width that the time of

placement did. The sections placed at the start of the day have larger crack widths than those placed in the afternoon and evening. In Figure 2.9, which shows crack width average vs. section, one can see a general pattern of smaller crack widths in relation to the sections being placed progressively later in the day. These results may lead to the research examining the time of placement for controlling crack width and spacing.

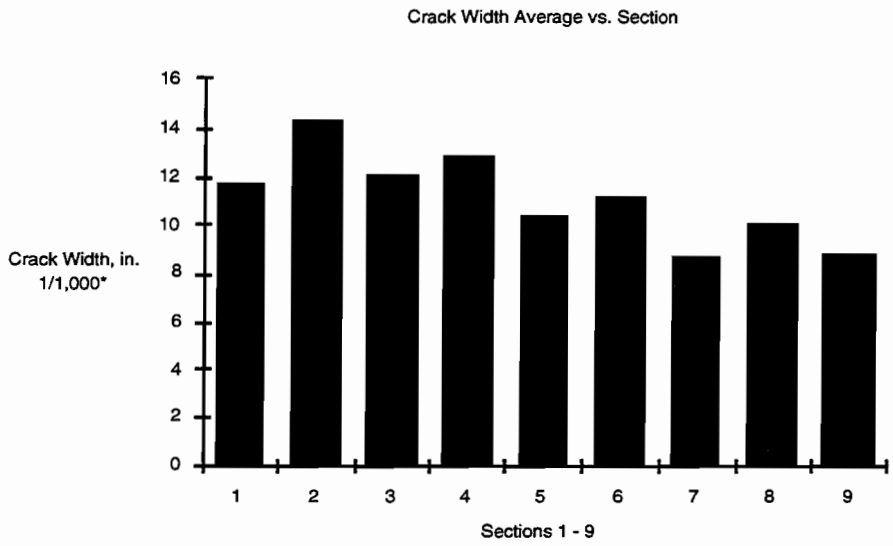

* 1/1000 in. = .0254 mm

Figure 2.9. Microscope crack width measurements by section/time

2.2.9 Saw Methods

A "dry sawing" technique was used on the test sections (i.e., water was not used). After the pavement was placed and after both the concrete and curing compound had solidified to a point where it could support the saw and operator, the dry cut sawing began. The saw used in the cutting was manufactured by Soft Cut. The saw produces a 1/8-inch-by-3/4-inch (.3175 cm by 1.905 cm) cut in a single pass. The longitudinal joint was sawed for the entire length of the sections. Transverse cracks were sawed every 3 feet (.9144 m) starting at the beginning of section #6 and running for 57 feet (17.37 m). In section 6 from 57 feet (17.37 m), where the 3-foot (.9144 m) spaced joints ended, to 127 feet (38.7 m), transverse joints were sawed every 5 feet (1.524 m). The major problem encountered with the dry sawing technique is the time required for the curing compound to dry sufficiently. The Procrete cure, which dries much faster than the standard curing compound, allows the sawing to take place earlier. With the standard curing compound, the cracks seem to begin before the sawing can be done. If the dry sawing is used with the right curing compound (e.g., Procrete), the cracking can be somewhat controlled. Other curing methods that worked well with the dry sawing at these test sections included the cotton mat

method and the polyethylene sheeting method. Both methods allow the sawing to be performed soon after placement of the pavement.

2.2.10 Coring

A total of two cores were taken from each of the test sections. These cores were tested for modulus of elasticity, coefficient of thermal expansion, permeability, and compression strength.

2.2.11 Crack Spacing

In Figure 2.10, which shows the number of cracks vs. section, there is seen a pattern of cracking related to the time of placement of the pavement—as was the case with the earlier test sections. Figure 2.11 illustrates that there is a considerable amount of variation in crack spacing in each section. This is shown by the fact that the standard deviation is high. There were several places within the test sections where clump cracking occurred. In clump cracking, there may be four or five cracks within a 10-foot (3.048 m) space, and perhaps not another crack for 20 or 30 feet (6.096 or 9.144 m).

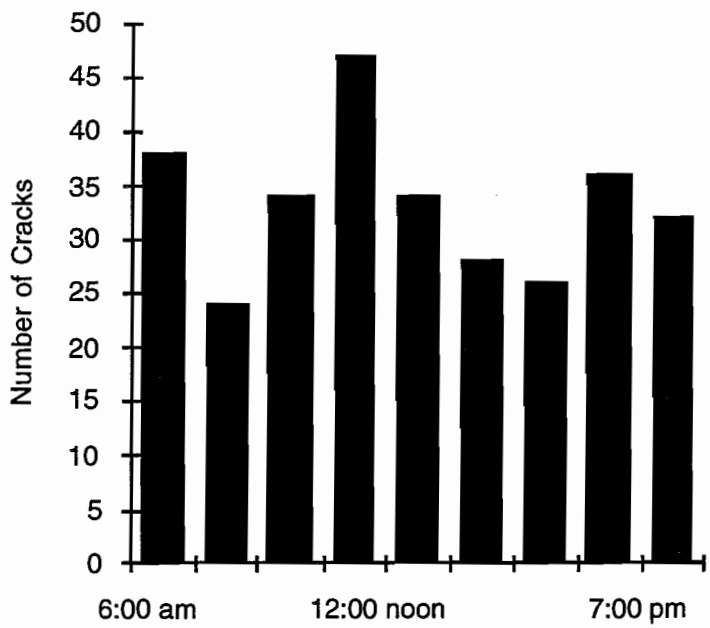

Figure 2.10. Number of cracks vs. section

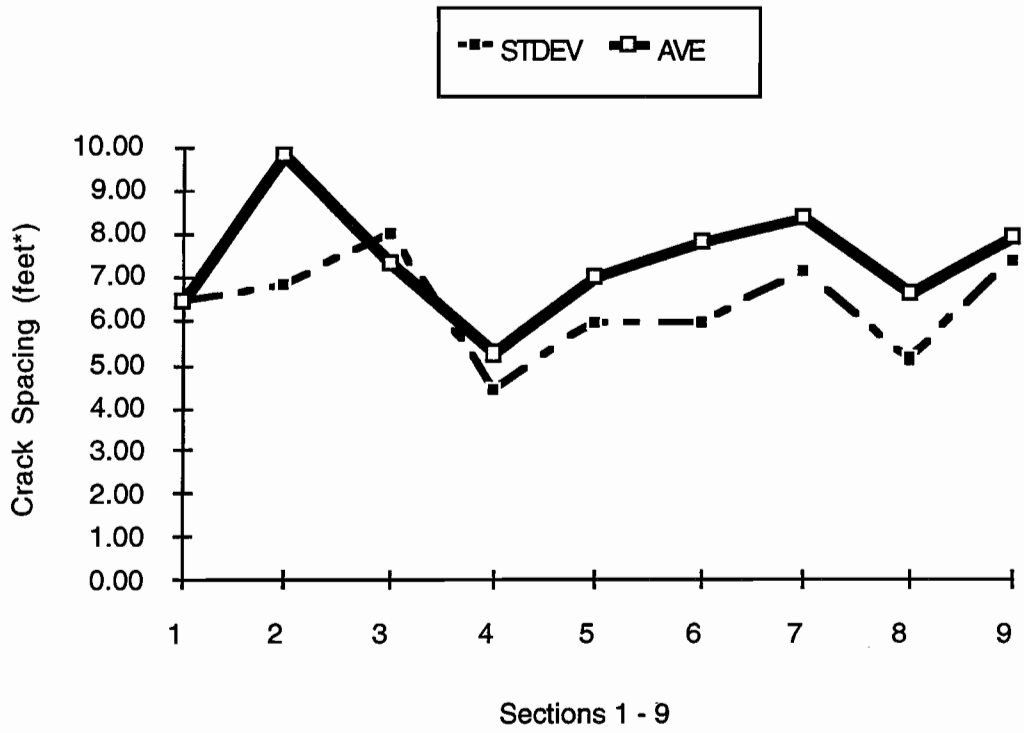

* 1 foot = .3048 m

Figure 2.11. Averages and standard deviation of crack spacing

2.2.12 Crack Randomness

The randomness index was performed on ten cracks in each of the nine sections. For the most part, the randomness of the cracks was very small. This means that the cracks that have occurred are almost completely transverse, even in the skewed steel section.

2.2.13 Cure Methods

As illustrated in Figure 2.6, four types of curing methods were used in the test sections, namely:

1. Cotton mat
2. Polyethylene sheeting
3. Standard curing compound
4. Procrete curing compound

The cotton mat curing method seems to do the job and has the advantage of being able to reuse the cotton mats indefinitely. The problem associated with the cotton mats is the weight. The mats absorb water, causing them to be very heavy and difficult to handle.

The polyethylene sheeting method solves the problem of having bulky weight material to handle. By providing a non-absorbent and lightweight cover for the concrete, the sheeting can be easily placed and removed.

The standard cure method consists of applying a membrane curing compound to the pavement soon after placement. The compound is thick and sticky and takes several hours to dry. The standard cure method does not work well with the dry sawing because the wet compound tends to bind up the saw. If allowed time to dry before the dry saw is used, the cracks have already begun to form, thus voiding the purpose of the sawing. While the standard cure method is widely used for the sawing operation, in this study it has not proven effective thus far.

Procrete curing compound seems to be the best alternative to use with the soft cut sawing. Procrete can be quickly applied to the surface soon after placement of the pavement. Because it is more of a water-based compound, Procrete is not sticky (even when wet). This means that dry sawing can take place within just a few hours of pavement placement (given average temperatures and weather conditions).

2.2.14 Other Testing

TTI conducted testing for concrete and steel strength using concrete and steel strain gauges. In addition to the strain gages, TTI conducted all testing of cylinders and beams made at the test sections.

2.2.15 Future Monitoring of the Test Sections

Crack spacing in the test sections will continue to be monitored semi-annually. New cracks will continue to be added to the database as they occur. Crack widths, spalling, and any other anomalies that occur in these test sections will also be noted.

2.3 F.M. 559 IN TEXARKANA TEST SECTIONS

This section summarizes the intermediate reports on the Texarkana test section under Project 1244. It is intended to report concisely what was found in the field investigation on concrete pavement performance.

2.3.1 Background

Two test sections, one on SH 225 in LaPorte for CRCP, and another on FM 559 in Texarkana for JPC pavement, were paved from October 14 to November 11, 1991. Each test section was subdivided into several sub-sections. Different orientations of the transverse steel reinforcing, different curing methods, different cracking control methods, different mix design with different type or amount of coarse aggregate were applied in the test sections. The purpose of the field investigation was not only to detect the factors that affect the cracking behavior of the CRCP, but also to improve the performance of concrete pavement by controlling construction procedure and using new techniques. Many physical parameters and responses characterizing concrete properties and performances were measured in the field for providing sufficient data to

verify and calibrate mechanistic-based algorithms to realistically model the performance of concrete pavement. Crack information, including number, spacing, shape, and width, was collected continuously. FWD testing was also conducted on different joint types and cracks to estimate the load transfer efficiency and the effective modulus. This study provides a preliminary summary of findings in the field investigation. The test will be continuously monitored throughout the duration of this research project.

2.3.2 Mix Designs Used in Field Test

To evaluate the performance of concrete pavement with different coarse aggregates, five mixes were carefully designed using different types and proportions of coarse aggregates in the Texarkana test section, as shown in Table 2.2.

Table 2.2. Aggregates used in different mix designs

Mix Design	Coarse Aggregate	Intermediate Aggregate	Fine Aggregate
1 Control Mix	1_" SRG (100%) Item 360.1 (3)	None	Little River Sand (100%) Item 360.1 (4)
2	1_" L.S. (50%) _" SRG (50%) Item 360.1 (3)	Buckshot	Little River Sand (35%) Crushed Sand (65%) Item 360.1 (4)
3	1_" SRG (100%) Item 360.1 (3)	Same as above	Same as above
4	_" SRG (100%) Item 421.2	Same as above	Same as above
5	1_" L.S. (100%) Item 360.1 (3)	Same as above	same as above

1"=2.54 cm

SRG=siliceous river gravel

LS=crushed limestone

Mix Design 1 is the control mix design for the experimental sections. In the other four mix designs, buckshot was added as an intermediate aggregate to improve gradation of aggregates. With no intermediate aggregate, "gaps" are formed between coarse aggregate grains. The volume of these gaps is so small that it cannot be occupied by the coarse aggregate and must, therefore, be provided by mortar. With intermediate aggregate, medium particles fill in these gaps and decrease the amount of mortar. As a result, the volume of voids in the concrete is decreased by adding intermediate aggregate. This effect of the intermediate aggregate will be shown by the cored specimens of this experimental pavements.

Mix Design 5 used crushed limestone as the coarse aggregate. Mix Design 2 used a blend of siliceous river gravel and crushed limestone as the coarse aggregate. Previous investigations have shown that pavement of river-gravel concrete tends to crack more in the early ages than crushed-limestone concrete. Mix Design 3 and Mix Design 5 were proposed to compare effects of river gravel and crushed limestone on joint formation. Mix Design 2 was proposed to observe how a hybrid of crushed limestone and river gravel changes concrete properties. One of the primary purposes was to prove that adding small coarse river gravel in the concrete, which is designed to use crushed limestone as the coarse aggregate, helps joint formation. The data indicate that this purpose has been achieved in this field experiment. Different from Mix Design 3, Mix Design 4 used smaller siliceous river gravel as the coarse aggregate. These two mix designs were designed to reveal size effects of coarse aggregates. Data presented later show smaller coarse aggregates caused the pavement to be more brittle at early ages. In all these mix designs, the design water/cement ratio was 0.39 and the design slump was 1.5 inches (3.81 cm). The proportioning, aggregate gradation, and other material characteristics of each mix design are provided in the detailed report.

2.3.3 Field Investigation of Concrete Performances and Properties

2.3.3.1 New Method for Field Measurement of Relative Humidity. Temperature and relative humidity are two important variables for concrete. Changes in either of these conditions can induce stresses in the pavement and can affect the rate of the strength gain of the concrete. The influence of the parameters is very apparent during the early ages of the concrete. Both temperature and relative humidity in the test sub-sections were measured with two different digital systems. One was manufactured by Vaisala, in which the sensor is a capacitor. It monitors the change in capacitance of a thin polymer film as it absorbs water vapor. The other, manufactured by General Eastern, measures the change in electric resistance of a bulk polymer sensor with the moisture the sensor absorbs.

To implement these instruments, a PVC tube was inserted in the pavement from the pavement top surface. The lateral wall of the tube was tightly fitted into the pavement concrete in which the concrete was exposed to the sensor though the opening end of the tube. When the temperature and relative humidity were measured, the probe of the measuring system was inserted in the PVC tube with a rubber seal fastened around it to make up a small closed space between the sensor unit and the concrete. After the measurement, the probe was removed and a PVC cap was placed on the top end of the tube to prevent air exchange between the space inside the tube and the atmosphere.

For each sub-section, holes one-and-half-inch (3.81 cm) deep were formed in the pavement surface in which the probe was inserted. Thus, the temperature and relative humidity measurements were made near the pavement top surface. Where these measurements were made automatically by a portable data recording system, the data were downloaded from the data logger system for analysis. In this way, continuous recording was possible. Three channels in the data logger (with one probe per channel) were used to record the temperature and relative humidity at

three different depths in the pavement—1 inch (2.54 cm), 2 inches (5.08 cm), and 4 inches (10.16 cm). For security, the logger system had to be dismantled during off-hours, during which time no data were recorded. The digital records and the graphs are included in the report on the LaPorte test section. As shown in the graphs, a period of time is necessary to achieve a stable record of the relative humidity. The readings over 100 percent were caused by the state of saturation of the sensor element and should be considered showing 100 percent relative humidity in the closed space. Two of the three channels had good calibration for temperature measurement; the other required calibration before the reading could be interpreted properly.

The curing method used in each of the sections is indicated in Figure 2.6. It is speculated that the cotton mat kept the pavement from the solar radiation and, as a result, the temperature in Sub-Section 3 was lower than in other sections. The polyethylene film covering the pavement (Sub-Section 5) caused a "greenhouse" effect, which made the temperature in Sub-Section 5 higher than that in sub-sections using other curing methods. However, change in temperature of pavement was caused by complicated environmental conditions as well as by properties of concrete mix. On the other hand, the relative humidity in Sub-Section 5 was the highest, since the polyethylene film isolated the pavement top surface from the atmosphere and kept the moisture in the pavement from evaporating. Between the two membrane curing methods, the standard method (Item 360) caused a lower temperature and higher relative humidity in the pavement than the proprietary product.

2.3.3.2 Field Determination of Concrete Properties. Cylindrical specimens and beam specimens were prepared and cured in the field while each mix design was placed. The cylindrical specimens were 6 inches (15.24 cm) in diameter and 12 inches (30.48 cm) tall. Data from the compression tests are shown in Table 2.3.

Note that data marked with '*' are the average of three tests performed by Southwestern Laboratory, Texarkana, Texas. Other data are the average of three tests performed at Texas Transportation Institute.

Table 2.3. Compressive strengths of concrete specimens prepared on-site

Mix Design	Specimen Preparation Date	Average Compressive Strength**	Age of Concrete Specimens
1	October 16, 1991	4,970 psi	56 days
3	October 14, 1991	5,480 psi	58 days
4	October 22, 1991	1,680 psi*	1 day
		2,620 psi	2 days
		5,600 psi	50 days
5	October 26, 1991	1,190 psi*	1 day
		5,780 psi	46 days

**1psi = 6894.757 Pa

Four beam specimens of different sizes were prepared in the field for each of Mix Designs 3, 4, and 5. The support span of the beam specimen was 2.5 times the depth of the specimen. The depth of the specimen was 4.5 inches (11.43 cm), 6 inches (15.24 cm), 9 inches (22.86 cm), and 12 inches (30.48 cm), respectively. A notch was cut before testing (the length of the notch was a quarter of the beam depth and the width of notch was about 1/8 inch [.3175 cm]). Three-point-bending flexure tests were performed on the specimens 24 hours after preparation of the specimens, as illustrated in Table 2.4. Two fracture parameters were calculated from the flexure test, using the peak loads of the four tests, based on the size effect law for a nonlinear fracture model for concrete. For the details of the test method, see the intermediate report on the Texarkana Test Section. Table 2.4 shows the two fracture parameters: K_{If} (the critical stress intensity factor for an infinite specimen) and c_f (the effective critical crack increase for an infinite specimen). They are both material parameters.

Table 2.4. Two fracture parameters at 1 day measured in the field

Mix Design	Concrete Age (day)	K_{1f} (psi$\sqrt{in}$)*	c_f (in)
3	1	717	1.98
4	1	687	0.56
5	1	827	1.31

* 1psi = 6894.757 Pa
1 inch = 2.54 cm

Mix Design 4, using smaller coarse aggregate than Mix Design 3, had Lower K_{If} and c_f value than Mix Design 3. Mix Design 5, which used crushed limestone as the coarse aggregate, had a higher K_{If} value, at 1 day, than the other two mix designs in Table 2.4, which both used siliceous river gravel as the coarse aggregate. Table 2.4 gives comparison of K_{If} values for the three mix designs.

The two fracture parameters are material parameters; that is, they are independent of specimen. Although the loading condition of the concrete pavement is more complicated than three-point bending, these two parameters obtained from bending beams also apply to the pavement. So long as stresses caused by temperature variation and concrete drying shrinkage were known in the pavement, another index "brittleness number" could be calculated. In the experimental section, pavements of different mix designs were of the same size and the same geometry. Provided it is assumed that the same thermal and shrinkage-caused stress distribution was caused in different pavements, the brittleness number of the pavement is inversely proportional to c_f. If the brittleness number of the pavement of Mix 5 is given $ß_5$ at the 1-day age, then $ß_3 = 0.66\ ß_5$ and $ß_4 = 2.33\ ß_5$, where $ß_3$ and $ß_4$ are the brittleness numbers of the pavement of, respectively, Mix 3 and Mix 5 at 1 day. The relative brittleness number in the figure is the ratio of the brittleness number of the specific pavement to the brittleness number of the pavement of

Mix 5. It will be seen later in this report that the larger the brittleness number at the 1-day age, the more saw cuts cracked at early ages.

In summary, the SRG mixes are more susceptible to fracture than a LS mix. Hence, for a similar set of conditions, the SRG has a higher probability of cracking than LS.

2.3.3.3 Early-Aged Saw Cutting to Control Cracking in Concrete Pavement. The longitudinal joint in the test sections was cut using early-aged saw cutting techniques in Texarkana. This technique is different from conventional saw cut methods that use external sources of water to cool the blade during cutting operations. This method does allow the concrete to be saw cut at an early age, with minimal or no raveling, which is typically much earlier than what is possible using conventional saw cut methods. The notch placed by the early-aged method was approximately 1 inch (2.54 cm) in depth.

The early-aged technique was used to place transverse saw cuts at specified intervals in Sub-Sections 6 and 9. A series of transverse saw cuts 175 feet (53.34 m) in length was placed in Sub-Section 6. Within the series, the spacing of the transverse saw cuts was 3 feet (.9144 m) for a length of 57 feet (17.37 m), and in the remaining portion, the spacing of the transverse saw cuts was 5 feet (1.524 m). The transverse saw cut operations started at 9:00 p.m. on November 11, or about 7 hours after placement of the concrete in Sub-Section 6. Four saw cut machines were used simultaneously in order to meet the pavement cutting schedule. Saw cutting operations Sub-Section 6 ended at 9:00 a.m., November 12. No raveling of the saw cut joints was evident. Twenty-five feet (7.62 m) of Sub-Section 9 were saw cut transversely.

As described previously, two saw cut techniques were used for longitudinal and transverse joints: conventional saw cutting and early-aged saw cutting. The early-aged saw cut technique uses a light and portable saw cut machine that allows the pavement to be cut earlier than does the conventional saw cut technique. The early-aged saw cut technique is different from the conventional saw cut method, which uses water to cool the blade during cutting operations.

The spacing of the transverse joints in this experimental pavement was 15 feet (4.572 m). The notch cut by the early-aged saw cut method was approximately 1 inch (2.54 cm) deep. The conventional method was used to cut the pavement D/4 which was approximately 3 inches (7.62 cm) deep. Two different types of diamond blades were used with the early-aged saw cutting method. One was T-shaped, the other was a straight blade.

Early-aged saw cut operations generally started 4.5 to 5.5 hours after placement of the concrete. When the weather was cold and humid, dry saw cutting was delayed until the pavement was solid enough to walk on. In some instances, this delay was extensive. For example, in the test section where Mix Design 3 was used, the paving started at 9:00 a.m. but was not saw cut until midnight. No apparent raveling occurred along the notches saw cut by the early-aged saw cut technique.

2.3.3.4 Effect of Different Curing Methods on Cracking in Concrete Pavement. Four different curing methods were employed. The curing method applied to each section is indicated in Figure 2.6. These curing methods included:

(1) membrane curing compound, Item 360.2 (13), is referred to as the standard curing method and noted as "Standard Cure;"

(2) membrane curing compound, Item 360.2 (13), using Procrete, a proprietary product, is noted as "Procrete;"

(3) cotton mat curing, Item 360.2 (15), plus membrane curing, Item 360.2 (13), noted as "Cotton Mat;" and

(4) polyethylene film curing, Item 360.2 (12), plus membrane curing, Item 360.2 (13), noted as "Polyethylene."

The buffer sections were cured using standard curing methods.

2.3.3.5 Effect of Different Coarse Aggregates. Comparing mix designs 1 and 3 would have the effect of an optimum gradation, with the buckshot aggregate (mix 3) indicating that, with the optimum gradation, a higher percentage of cracks at saw cuts is acquired. Similarly, comparing mix 2 (which has 50 percent river gravel and limestone) with mix 5 (which has 100 percent limestone), produces a higher percentage of cracks at saw cuts when the limestone quantity is reduced (or the river gravel content is increased). Similar observations can also be deduced from mixes 1 and 5 (for type of coarse aggregate) and also mixes 3 and 4 (for maximum size of coarse aggregate). Comparison of mixes 3 and 4 indicates that very little effect is introduced to the percent of saw cuts cracked by changing the maximum aggregate size. In general, it appears from the data in Table 2.6 that, for pavements using siliceous river gravel aggregate, saw cutting may have a positive effect in having the transverse cracks form at the same locations.

2.3.4. Monitoring Concrete Pavement Performance

2.3.4.1 Crack Survey—Observation of Formation of Joint and Crack. Crack surveys were conducted on all the test sections. Sub-Section 6, which was transversely saw cut after paving, was surveyed on November 14 (3 days after paving), November 15 (4 days after paving), November 19 (8 days after paving), November 22 (11 days after paving), and November 26 (15 days after paving) in 1991. It was surveyed again on March 16, 1992 (125 days after paving). Other sub-sections were surveyed 3, 15, and 125 days after paving. All the sections were opened to the traffic on December 12, 1992.

In Sub-Section 6, most cracks were initiated from the saw cuts; in other sections, many cracks were initiated from the steel rebars. Many of these cracks initiated from the steel rebars finally developed and moved completely through the pavement.

Among the four different curing methods, Cotton mat and Polyethylene reduced daily temperature variation in the pavement and slowed down the concrete drying process, which was seen in the section "Measurement of Pavement Temperature and Relative Humidity." As a result, an increase in the number of surface cracks in Sub-Sections 3, 5, and 8 was suppressed in the first 3 days, though more surface cracks were formed between the third and fifteenth day (Cotton Mat

and Polyethylene were removed 7 days after paving). It appears that the formation of these surface cracks was delayed by the effect of these two curing methods.

Data listed in Table 2.5 are the results of the survey conducted on the fifteenth day, which indicates that cracks were mostly initiated from the interfaces of the steel rebar and mortar or the saw cut tips, because of the stress concentration at these locations, where structure geometry, or/and material properties changed sharply. Besides surface cracks, or cracks that went through the top surface of the pavement, there were many cracks observable on the edge surface of the pavement (which would potentially develop to form new surface cracks). These cracks observed on the pavement edge but which did not extend to the pavement surface are called "edge cracks" for convenience. Except for Sub-Section 6 and Sub-Section 2, most of cracks, either surface cracks or edge cracks, were initiated from steel rebars.

Table 2.5. Crack survey result at day 15

Section Number	0	1	2	3	4	5
No. of surface cracks	11	21	24	24	26	26
No. of surface cracks initiated at steel	7	17	11	18	21	26
No. of edge cracks not developed into surface cracks	19	46	18	7	21	3
No. of edge cracks not developed into surface cracks, and initiated at steel	16	43	12	2	16	3
Total No. of surface & edge cracks	30	67	42	31	47	29
Percentage of cracks initiated at steel	77	90	55	65	79	100

Many more cracks were observed on the pavement edge than on the pavement top surfaces. All the surface cracks could be traced to cracks observable on the pavement edge, though many cracks, observed on the pavement edge (called edge cracks), did not reach the pavement top surface. It is speculated that cracks were mostly initiated from the pavement edge. Because the edge was exposed to the ambient conditions, the change of temperature and moisture condition possibly was more rapid there than on the pavement top surface. This two-dimensional effect deserves further consideration in further test pavements. Different curing methods have effects on the number of cracks initiated from the transverse steel rebars. Cotton mat (Section 3) and Polyethylene (Section 5) made less rebars initiate cracks than the two membrane curing methods—Procrete (Section 1) and the white pigments (Section 4).

It would be interesting to note the distribution of the number of surface cracks with respect to the location of the sub-section. The number of surface cracks either at the 15th day or at the 125th day has a shape of the half-sine function (which is not surprising). Formation of cracks results from interaction between stresses induced by temperature variation in the pavement and drying shrinkage and restraint of the pavement movement. In CRCP, the restraint is caused by the

pavement weight, rebar reinforcement, subgrade support forces, and friction. Apparently, greater restraint exists in the middle section of the pavement than at the ends of the pavement. Since Sections 0 and 10 are shorter than other sections, it is more reasonable to study the crack distribution in terms of number of surface cracks per unit length, which is called "crack density," instead of the number of total cracks for each section. A regression on the half-sine function based on the least square method is given in each of the figures.

Crack densities for Sub-Sections 6, 8, and 9 at the fifteenth day are far apart from the regression, which was calculated from the data for Sub-Sections 0, 1, 2, 4, 7, and 10. This may mean that saw cutting and polyethylene curing caused higher crack densities than the other crack control and curing methods. Sub-Section 3 was cured with cotton mat and had fewer cracks than the sub-sections cured by membrane methods at the third day, but its crack density at the fifteenth day had increased to where it was close to the regression curve. Sub-Section 5 was cured with polyethylene. Although it did not obtain an increase in the crack density as rapid as Sub-Section 8, it did obtain a higher crack density from the third day to the fifteenth day. However, at the 125th day, the crack densities for Sub-Sections 6, 5, and 8 were lower than the regression, which was calculated from the data for Sub-Sections 0, 1, 4, 7, 9, and 10. In other words, these preliminary results indicate that saw cutting developed cracking in early ages but reduced the crack density on a long-term basis. Besides Sub-Sections 5, 6, and 8, Sub-Section 2 had a low crack density at the 125th day, showing that skewed transverse rebars may cause reducing cracking. Sub-Section 3 (cotton mat cured) did not deviate from the regression curve in the crack density.

2.3.4.2 Load Transfer Efficiency and Effective Modulus. Falling weight deflectometer (FWD) testing was conducted on several saw cut joints, construction joints, and cracks on the morning of February 20, 1992. Locations of these joints and cracks are listed in the first column of Table 2.6. The testing equipment was a trailer-mounted FWD weighing approximately 1,500 pounds (680.39 kg). The impulse force is created by dropping masses. The load, measured by a transducer, is transmitted to the pavement through a load plate having a radius of 5.9055 inches (15 cm). Deflections are measured by using velocity transducers mounted on a bar that is lowered simultaneously with the load plate to the pavement surface. The loading plate and deflection sensors layout is on 12-inch (30.48 cm) centers. Eight sensors are mounted on the bar. One of the eight sensor measures the deflection at the load, noted as D_0. Six sensors are an one side of the load at 12 inches (30.48 cm), 24 inches (60.96 cm), 36 inches (91.44 cm), 48 inches (121.92 cm), 60 inches (152.4 cm), and 72 inches (182.88 cm) away from the load position. Deflection measured by these sensors are designated as D_1, D_2, D_3, D_4, D_5, and D_6, respectively. Another sensor is on the other side of the load, 12 inches (30.48 cm) away from the load position. It measures the deflection noted as D_{-1}.

The results of the FWD field measurements are described in terms of the load plate deflection (D_0), the load transfer efficiency (LTE), and the effective stiffness (E_c) at the joint. The LTE is equal to the change in deflection on the unloaded side of the joint divided by the change in deflection on the loaded side of the joint. The effective stiffness E_c is determined from the

Westergaard solution for slab-on-grade deflections at an interior load position. Simplified forms of the Westergaard solutions rearranged to solve for the modulus of subgrade reaction K.

2.3.5. Primary Conclusions and Further Research

2.3.5.1 Findings. It was found that much cracking occurs at early age on concrete pavement that uses river gravel as its coarse aggregate; by contrast, cracks occur gradually on limestone concrete pavement. Field measurements of concrete strength show that, at early age, limestone concrete is stronger than river gravel concrete. However, at 28 days river gravel concrete grows stronger than limestone concrete. Smaller-sized aggregates produce a more brittle concrete at early age.

In comparison with the membrane curing method (using white pigments or Procrete), cotton mat and polyethylene film reduced daily temperature variation and slowed down pavement concrete drying. Accordingly, the number of surface cracks (cracks that went transversely through the top surface of the pavement) in test sections cured with cotton mat or polyethylene film was lower than that found in test sections cured with membrane in the first 3 days after paving. After the mat or the film was removed, the number of surface cracks increased in the sections that were initially covered by the mat or film.

The crack density (number of surface cracks per unit length of pavement) was affected by the restraints inherent within by the pavement system (longitudinal steel rebars, subbase friction, etc.). Its distribution with respect to the distance from the pavement end (over a 1-day placement) may be expressed in terms of a half-sine function. Regression was made for the crack-density distribution on the 15th day and on the 125th day. On the 125th day, or 4 months after paving, crack density in sections cured by polyethylene film was lower than the regression curve (based on the data from membrane-cured sections), while crack density in the section cured by cotton mat was very close to the regression curve.

A 175-foot-long (53.34 m) test section cured by the standard membrane curing method was transversely cut with the early-aged saw cut technique at an interval of 3 feet (.9144 m) and 5 feet (1.524 m). In contrast to the conventional saw cut method, no water cooling was used and the depth of the cut was approximately 1 inch (2.54 cm) (i.e., a depth less than that specified in the D/4 or D/3 method used for conventional saw cutting of joints in jointed concrete pavement). In the saw cut section, the average crack spacing decreased more rapidly than any section that was not saw cut. The average crack spacing in the saw cut part was ultimately larger than that in the non-saw cut sections.

The saw cut not only reduced the number of cracks; it also controlled the location of the crack. In the saw cut portion, most cracks were initiated from the saw cut, while the rest of cracks were initiated from the transverse steel positions.

No significant raveling occurred, though the saw cutting operation started relatively early, which indicates an improved saw cut efficiency with this type of an approach. Data analysis, which shows that early-aged saw cutting can occur without raveling when the pulse velocity reaches 5,000 ft/sec (1524 m/sec), verifies the same conclusions drawn in the previous field tests performed on the Texarkana test sections.

Table 2.6. Results of FWD tests

Station	Mix Design #	Date of Paving	Type of Joint or Crack	Downstream LTE (%)	Upstream LTE (%)	Upstream Effective Stiffness (ksi)*
255+51.	3	10-14-91	early-aged saw cut	88.89	No data	No data
254+61	3-5		construction joint	82.06	81.28	1,154
254+41	1	10-16-91	early-aged saw cut	81.06	78.18	568
254+11	1	10-16-91	conventional saw cut	78.31	79.36	967
253+96	1	10-16-91	conventional saw cut	80.20	78.00	571
253+66	1	10-16-91	conventional saw cut	81.96	79.58	559
252+18	5	10-18-91	early-aged saw	87.80	79.62	504
251+73	5	10-18-91	early-aged saw cut	78.99	85.64	1,845
251+58	5	10-18-91	early-aged saw cut	84.16	80.34	776
250+91	5	10-18-91	crack	67.15	82.58	974
250+26	5		construction joint	81.05	79.64	770
249+24	5	10-26-91	crack	84.69	81.09	819
248+42	5		construction joint	79.39	82.91	1,151
247+41	5	11-6-91	early-aged saw cut	80.79	77.68	2,694
246+51	5-2		construction joint	87.11	78.14	998
245+83	2	11-8-91	early-aged saw cut	85.97	89.28	1,475
245+53	2	11-8-91	early-aged saw cut	85.86	88.08	1,788
244+33	2	11-8-91	conventional saw cut	89.74	85.56	1,433
243+88	2	11-8-91	conventional saw cut	87.65	85.55	1,252
243+91	2-4		construction joint	87.17	87.35	1,475
242+74	4	10-23-91	early-aged saw cut	99.73	86.52	1,384
242+40	4	10-23-91	early-aged saw cut	92.92	87.44	1,738
241+31	4	10-23-91	early-aged saw cut	88.10	94.67	4,208

* 1 ksi = 6894757 Pa

A large percentage of the transverse steel rebars initiated cracks, part of which developed as surface cracks. This means that these surface cracks are not random cracks, but actually were initiated from the rebars transverse positions. Designers may suggest that cracking at the rebar interface should be avoided to improve the utility of the reinforcement. It is apparent, however, that the transverse steel can be used to control cracking that occurs randomly between rebars.

Some cracks may have been initiated on the lateral edge surface of the pavement from the rebar interface, since temperature varies more widely and drying proceeds more rapidly on the edge than on any other pavement surface area. Even in the cotton mat and polyethylene film curing methods, the edge surface was not covered by the mat or film, but, rather, was left exposed

to the air. More moisture can evaporate from the surface so that, at the same depth, moisture content could be lower near the edge than at greater distances from the edge. Heat could dissipate faster from the edge surface as a result of the increased surface area. This two-dimensional effect needs to be investigated in future test sections.

The General Eastern digital system, used for temperature and relative humidity measurement in pavements, provided significant data to show different effects of different curing methods. This system may serve well for quality control purposes. To detect the two-dimensional effect described previously, distributions of temperature and relative humidity on the edge surface and in the depth from the edge surface should be considered in future tests.

Since skewed transverse steel rebars constituted weak bonding not perpendicular to the direction of the maximum tensile stress, the number of surface cracks in the skewed rebar reinforced pavement section was lower than the half-sine regression curve on the 125th day after paving. It may be appropriate to provide guidelines on the implementation of polyethylene film curing method, saw cutting crack-control method, and the arrangement of skewed rebars in the construction of concrete pavements.

In the first 1 or 2 days after placement of the concrete, an increase in the compressive strength of the concrete used to pave the test sections may be expressed in terms of a linear relation with the concrete age. Formulas to correlate the pulse velocity and fracture toughness with the compressive strength were constructed for the concrete used in the test sections. These formulas may be improved to better reflect the relationships among these parameters after more data are accumulated in further research.

2.3.5.2 Recent Research. Timing is important when using a saw cutting technique to control cracks. A criterion needs to be developed to inform contractors when to saw cut. In addition, optimum saw cut spacing needs to be determined based on experience, type of coarse aggregate, subbase material, weather conditions, and structural analyses of the concrete pavement system.

It is expected that cracking can be induced by an interior device, namely, a crack inducer or crack initiator. It was found that transverse rebars can act as crack formers, and a crack will almost certainly form along the line of a rebar. In some circumstances, the crack-forming influence can be so strong that the crack spacing and widths are entirely controlled by the spacing of the transverse rebars. The problem is that it is not clear under what circumstances this will happen, though it seems to be relatively unlikely in normal CRCP. Research needs to be conducted to improve the performance of concrete pavement by controlling the crack patterns (including the crack spacing, crack opening, and crack shape).

It is known that pavement cracking is a long-term process influenced mainly by the concrete shrinkage induced by moisture loss. Control of crack opening can be achieved not only by designing uniform predetermined saw cut spacing or transverse rebar spacing; it can also be achieved by carefully designing the size, location, and amount of reinforcing steel used in concrete pavement. Toward this end, laboratory tests and theoretical analyses need to be performed.

CHAPTER 3. CHEMICAL MODELING OF AGGREGATE PROPERTIES

3.1 BACKGROUND

Earlier in this project, concrete specimens were cast from eight coarse aggregate sources commonly used in Texas. The specimens were then tested for tensile strength (f_t), compressive strength (f_c), elastic modulus (E), drying shrinkage (Z), and thermal coefficient (a), after various lengths of curing. Subsequent analysis based on this testing developed descriptive models (based on aggregate type and on the length of time the specimen was allowed to cure) and predictive models (based on curing time and physical properties based on chemical composition) (Ref 5).

In order to easily apply the chemical models, a computer program, CHEM1, was developed for the IBM PC (Ref 5). This program requires as input the percentage by weight of certain oxide residues produced by standard fusion testing. It then outputs graphs predicting f_t, f_c, E, and Z for time allowed for curing, ranging from 1 to 28 (256 for Z) days. The object of the program was to give a rough prediction of material properties for concrete made with a new aggregate source prior to actual laboratory testing. However, the accuracy of the program was necessarily limited by the model inference space, which consisted of only eight aggregates.

The overall purpose of predicting concrete material properties for various aggregates is to determine design parameters (steel percent, bar size, etc.) needed to attain a desired level of performance. Using design tools such as the CRCP programs, these factors can be estimated. In this way, it is hoped that equal performance from very different aggregates can be obtained.

3.2 CHEM2 MODEL OBJECTIVES

Currently, Phase III testing is being performed. Data from this experiment should make it possible to produce an improved version of the program, which will be called CHEM2. The mix design for the Phase III testing will match the Phase II testing as closely as possible, so that data from Phase II and Phase III can be combined. This should greatly improve the accuracy and usefulness of the program.

3.2.1 Improved Models for Limestones and River Gravels

CHEM1 attempts to use one model to predict for all types of aggregates. Better results could be obtained if the program could first identify the type of aggregate and then predict using a model specifically developed for that aggregate class. This is especially important for aggregate types that produce similar oxide residues (e.g., SRG and granite, both high in SiO_2) but which differ in mineral composition and, consequently, exhibit characteristic differences when cast in concrete. The program could either identify the class of aggregate by direct user input, or determine it through a simple set of IF statements or probabilistically via a discriminant function. Once the class is determined, the original mineral content could be backcalculated from the oxide residue stochiometrically.

Since limestones and river gravels are the focus of the overall study, special attention will be given to these aggregates. By including two new limestones and two new river gravels in Phase III, sufficient additional data should be produced to make specific models possible. These models would estimate differences in strength, modulus, shrinkage, and expansion based on small differences in the characteristic minerals composing the aggregates, presumably calcium carbonate (Ca_2CO_3) and dolomite ($CaMgCO_3$) for limestone, and quartz (SiO_2) for river gravel.

CHEM2 predictions for aggregates other than limestone or river gravel would simply consist of identifying the aggregate (e.g., granite) and producing the absolute or normalized curing set curves determined in Phase II.

3.2.2 Prediction of Thermal Coefficient

CHEM1 does not predict thermal coefficient of expansion. This is a vitally important property, particularly for pavements placed in the summer season, when temperature extremes are high and when peak ambient temperature may coincide with peak heat of hydration (as in morning placements). Under such conditions, for a given steel design, a high thermal coefficient tends to produce more closely-spaced early-age cracking, compared with an aggregate having a lower coefficient.

Despite the desirability of such a model, inconsistencies in the Phase II data and field testing prevented the development of a definitive model. Although Phase I testing reported that thermal coefficient does not change with time allowed for curing (age), some doubt remains as to the validity of this conclusion. Phase III testing should settle the issue, providing at the same time additional data that can be used to develop a model predicting thermal coefficient from chemical composition. If at all possible, CHEM2 will predict thermal coefficient.

3.2.3 Predictions for Aggregate Blends

CHEM2 would also add a facility for predicting the performance of blended aggregates. The proposed Phase III testing also includes an experiment to determine the effect of blending limestone with river gravel at various proportions. This should reveal the shape of the "blending curves" (Figure 3.1), which could then be normalized for each material property and be used to predict the performance of blends. Currently, it is not known whether the properties of a blended aggregate are simply multiplied by the weighted average for the two aggregates (Figure 3.1, curve A, linear) or a non-linear combination (Figure 3.1, curves B & C).

3.3 PROPOSED PROGRAM FLOW

The proposed CHEM2 program would operate as follows: (1) User input of chemical composition data is obtained, (2) prediction models for the five material properties are produced, (3) potential problem areas are highlighted (e.g., excessively high thermal coefficient), (4) at the user's option, a parametric series of curves is produced predicting the performance of the original aggregate blended 75/25, 50/50, and 25/75 with a standard or user-input limestone (see Figure 3.2). These graphs (Figure 3.3) would have gridlines so that the user could screen-print them and

determine the approximate blending level needed to produce the materials properties that result in a desired level of performance.

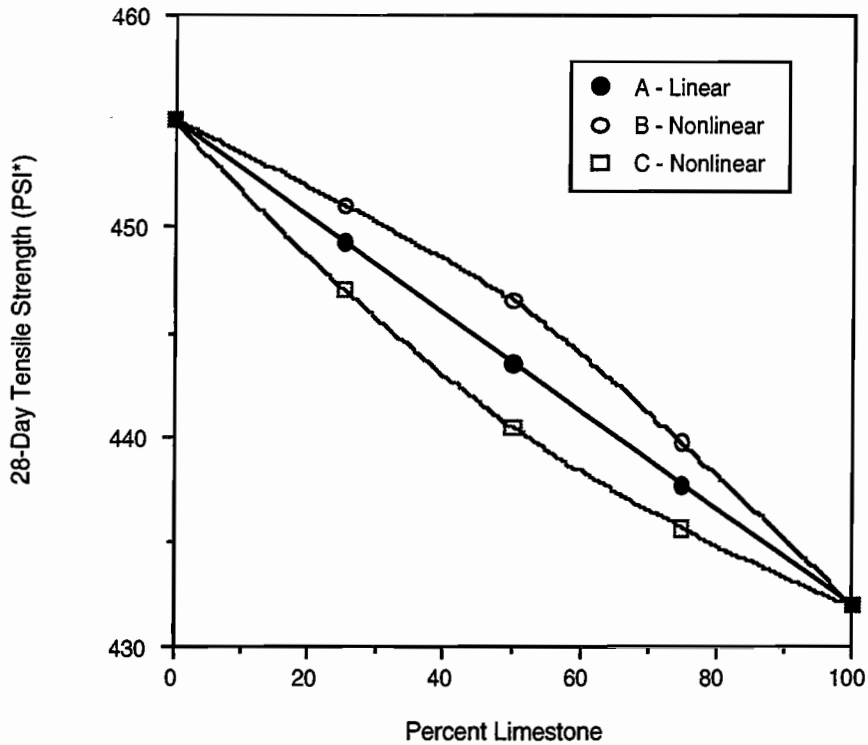

* 1 psi = 6894.757 Pa

Figure 3.1. Possible performance shapes for blended river gravel

3.4 STOICHIOMETRIC ANALYSIS

A problem encountered in developing the Phase II chemical models was that only the oxide residues were considered as predictors. Since different minerals may be oxidized to the same compound (e.g., dolomite and calcite both contribute to the calcium oxide residue), direct empirical modeling based on oxide residue is problematic. Therefore, a methodology is presented for backcalculating the percentage by weight of the various minerals that compose the aggregates used in the Phase II study. Mineral composition determined in this way can then be used to develop more robust predictive models for such aggregate-dependent concrete properties as tensile strength, compressive strength, elastic modulus, drying shrinkage, and thermal coefficient of expansion.

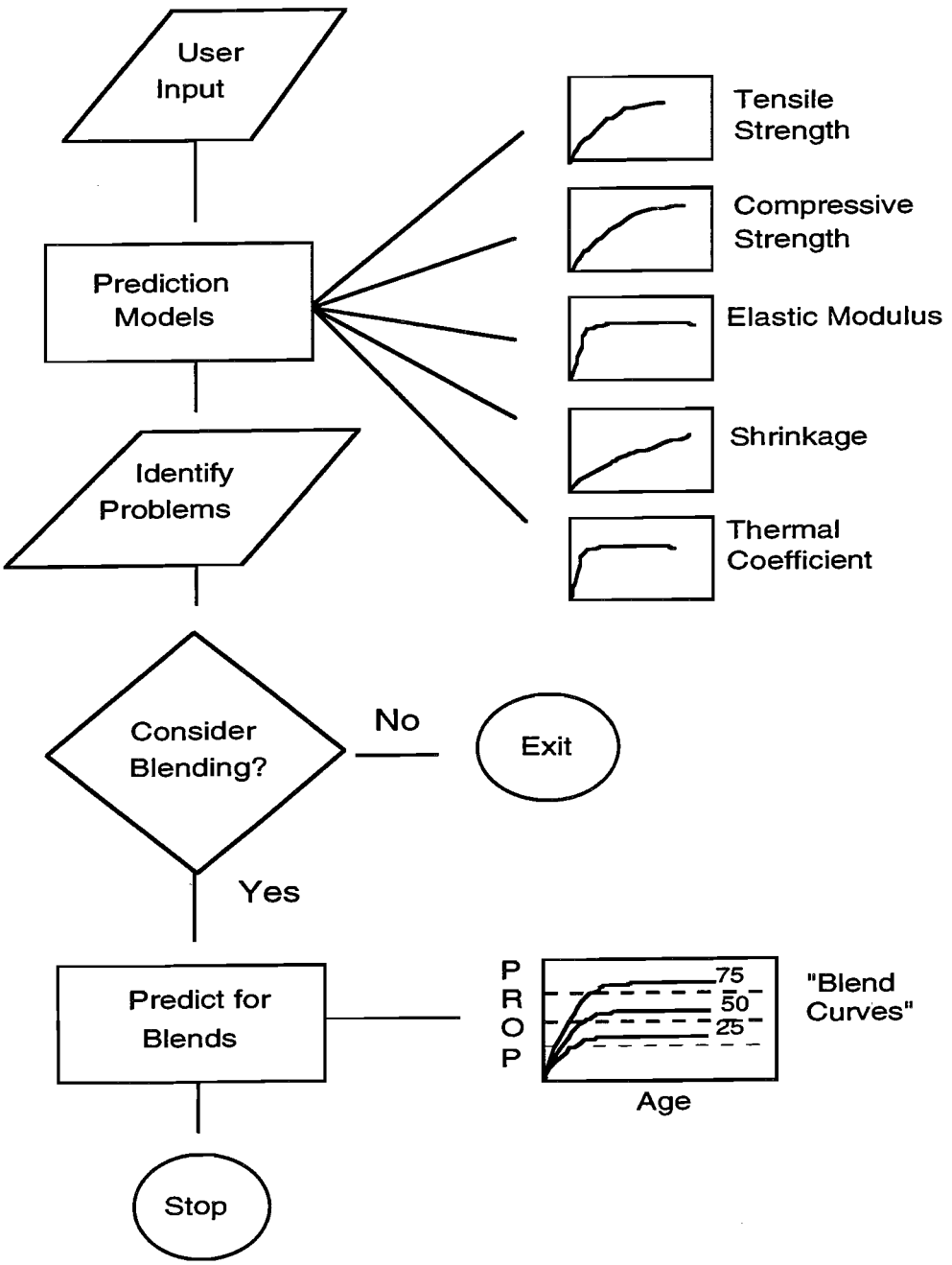

Figure 3.2. Proposed CHEM2 program flow

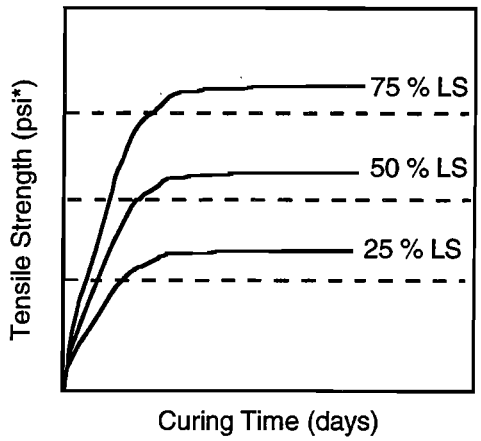

Figure 3.3. Parametric curves for blend design (example)

3.4.1 Problems with Existing Chemical Models

Phase II testing under this project collected aggregate chemical composition data for eight aggregates commonly used in Texas pavements, as well as for a number of additional aggregates (Ref 5). Three analytical procedures were performed, including determination of principal mineral composition by x-ray diffraction and oxide residue analysis after fusion.

An effort was made to predict aggregate performance based solely on oxide residues (Ref 5). Although some useful models were developed, some of the models were later determined to have weak predictive ability outside the inference space of the eight tested aggregates. The problem with oxide-based models is that few of the oxides measured actually existed in the aggregate prior to fusion; in fact, most of the oxides were formed by the burning of more complex minerals in the sample. For example, little if any calcium oxide (CaO) was present prior to fusion; some was produced by the oxidation of calcite ($CaCO_3$), while some came from dolomite ($CaMg(CO_3)_2$).

This situation gives rise to a fundamental problem: Since the amount of each oxide is proportional not to a single mineral but to several, no strong direct correlation is observed between oxide percentage and concrete material properties. The models developed attempt to compensate by considering interactions (Ref 5). These interactions serve as surrogate variables (or indirect indicators) for the original mineral content of the sample.

3.4.2 Methodology

A much better method would be to develop models based directly on the original mineral composition of the aggregates. Fortunately, stoichiometric analysis can be used to backcalculate these percentages.

Using the results from x-ray crystallography (Table 3.1) the principal minerals in each sample have been determined. Most are composed primarily of calcite ($CaCO_3$), quartz (SiO_2), and/or dolomite ($CaMgCO_3$). A notable exception is Scotland Granite, which contains a substantial amount of the sodium feldspar albite ($Na_2O{\bullet}Al_2O_3{\bullet}6SiO_2$). It is the albite (and other feldspars) in granite that cause it to be an outlying point in much of the previous analysis. For instance, the granite (GR) and Vega (VG) aggregates tested had thermal coefficients of 5.7 and 6.5 respectively; yet GR has an SiO_2 residue of 71.3 percent vs. 66.9 percent for VG. Since quartz is so thermally expansive, this is counter-intuitive. Because the oxidation of albite yields additional SiO_2, granite appears to have had the second highest mineral quartz content of the tested aggregates; however this is not the case. Much of the SiO_2 residue came from albite, not quartz. Albite and quartz have very different physical properties (such as thermal coefficient of expansion). The technique presented here will eliminate this type of problem.

3.4.3 Assumptions

Mined aggregate is a complex blend of many minerals; it would be impossible from the rudimentary information given in Table 3.1 to determine the exact mineral composition of the aggregates. Fortunately, a methodology to backcalculate the principal minerals should be all that is needed to develop more robust models. Accordingly, the following imprecise but essentially correct assumptions were made:

1. All SiO_2 residue in the sample came from quartz or feldspar (granite is composed of quartz and feldspar). Only the three most commonly occurring feldspars — albite, orthoclase, and microcline ($K_2O{\bullet}Al_2O_3{\bullet}6SiO_2$) — were considered in this analysis. (Orthoclase and microcline have the same chemical composition.)
2. All CaO residue in the sample came from calcite or dolomite.

These two assumptions imply the following decomposition reactions:

$CaCO_3 \rightarrow CaO + CO_2$	calcite decomposition	(Eq 3.1)
$CaMg(CO_3)_2 \rightarrow MgO + CaO + 2CO_2$	dolomite decomposition	(Eq 3.2)
$Na_2OAl_2O_3{\bullet}6SiO_2 \rightarrow 6SiO_2 + Al_2O_3 + Na_2O$	albite decomposition	(Eq 3.3)
$K_2OAl_2O_3{\bullet}6SiO_2 \rightarrow 6SiO_2 + Al_2O_3 + K_2O$	kalinite decomposition	(Eq 3.4)
$SiO_2 \rightarrow SiO_2$	quartz, no reaction	(Eq 3.5)

3.4.4 Computational Method—Carbonates

Using the molecular weights for the compounds (Table 3.2) and the balanced equations above, it is a simple matter to determine the weight ratios relating the oxides to the original mineral content. For instance, from Equation 3.2 it can be seen that dolomite oxidizes to MgO in a 1:1 ratio. Since the molecular weight of dolomite is 184.407 and the molecular weight of MgO

is 40.305, then 184.407/40.305 = 4.575 grams of dolomite must have existed for each gram of MgO in the fused sample. Therefore:

$$\% \text{ dolomite} = \% \text{ MgO} \bullet 4.5752 \qquad \text{(Eq 3.6)}$$

Table 3.1. Mineral composition of Phase II aggregates

		Minerals Found		
Source	Aggregate Code	Most Abundant	Second	Third
McCelligan # 1	DL	Dolomite	Calcite	Quartz
Western-Tascosa	WT	Quartz	Calcite	
Tin-Top # 1	BTT	Calcite	Quartz	
Bridgeport	BTT	Calcite	Dolomite	Quartz
Feld (TCS)	LS	Calcite	Dolomite	Quartz
Fordyce	SRG	Quartz	Calcite	
Vega	VG	Quartz	Calcite	
Ferris # 1	FR	Calcite	Quartz	
Scotland Granite	GR	Quartz	Albite	
TXI-Boonesville	BO	Calcite	Quartz	
McCelligan # 2	DL2	Dolomite	Calcite	Quartz
Ferris # 2	FR2	Calcite	Quartz	
TCP-Cleburne # 51	CL	Calcite	Quartz	
Ingram Whitehead	IW	Calcite	Quartz	
TXI-Tin Top # 2	TT2	Calcite	Quartz	
Pioneer-Landess Pit	PI	Calcite	Quartz	
Jobe-Hueco	JH	Calcite	Quartz	
Rainbow-Baker Pit	RB	Calcite	Quartz	
A-Rock Brazos River	BR	Calcite	Quartz	
Vulcan-Mexico	VM	Calcite	Quartz	

Table 3.2. Molecular weights for selected compounds

Compound	Molecular Weight (g)
Calcite	100.091
Dolomite	184.407
Quartz	60.0855
Albite	524.48
Kalinite	546.674
CaO	56.08
MgO	40.305
SiO_2	60.086

Next, to estimate the original calcite in the sample, it is first necessary to subtract the amount of CaO produced by the decomposition of dolomite (CaO_{dol}). Dolomite decomposition yields CaO in a 1:1 M.W. ratio, or 56.08g CaO / 184.407 g dolomite = 0.3041.

$$CaO_{dol} = \% \text{ dolomite} \bullet 0.3041 \quad \text{(Eq 3.7)}$$

Then, CaO from calcite decomposition (CaO_{cal}) equals total CaO (CaO_{tot}) less the amount released by dolomite:

$$CaO_{cal} = CaO_{tot} - CaO_{dol} \quad \text{(Eq 3.8)}$$

Now that CaO_{cal} is known, the original percent calcite can be calculated. In a 1:1 ratio, 1 mole (100.091g) of calcite produces 1 mole (56.08) of CaO, giving a m.w. ratio of 100.091/56.08 = 1.785.

$$\% \text{ calcite} = CaO_{cal} \bullet 1.785 \quad \text{(Eq 3.9)}$$

3.4.5 Computational Method—Silicates

A similar process can be employed to determine original silicate content. First, assuming most or all Na_2O was produced by albite decomposition (see Table 3.1) gives the following formula:

$$\% \text{ albite} = Na_2O \bullet 8.46 \quad \text{(Eq 3.10)}$$

Assuming most or all K_2O was produced by oxidation of the potassium feldspars orthoclase and microcline (these two minerals will be referred to collectively as PF, potassium feldspars):

$$\% \text{ PF} = K_2O \bullet 5.8 \quad \text{(Eq 3.11)}$$

Calculating SiO_2 from albite ($SiO_{2(alb)}$):

$$\% SiO_{2(alb)} = \% \text{ albite} \bullet .6874 \quad \text{(Eq 3.12)}$$

Calculating SiO_2 from PF ($SiO_{2(PF)}$):

$$\% SiO_{2(PF)} = \% PF \bullet .6595 \quad \text{(Eq 3.13)}$$

Then the remaining SiO_2 must have been quartz prior to oxidation:

$$\% \text{ quartz} = SiO_{2(tot)} - SiO_{2(alb)} - SiO_{2(PF)} \quad \text{(Eq 3.14)}$$

3.4.6 Results

Oxide percentages for the eight aggregates are given in Table 3.3. A computer program written in the SAS language was developed to calculate mineral content according to Eqs. 3.6-3.14. The results of running this program on the oxide residue data are given as Table 3.4. As a methodology check, the remaining unexplained mineral content is given as a column in the table.

Table 3.3 Phase II chemical analysis results

Source	Agg.	Type	SiO_2	CaO	MgO	CO_2	MnO	Fe_2O_3	Al_2O_3	Na_2O	K_2O	TiO_2	Other
McKelligan	Dolomite	(DL)	6.53	34.9	13.0	42.9	0.02	0.21	0.38	0.09	0.26	0.02	1.69
Western-T	S/L	(WT)	68.5	11.4	0.35	8.98	0.05	2.64	3.97	0.85	1.10	0.17	1.99
Bridpt+TinTop	L+S/L	(BTT*)	17.5	42.5	0.71	35.7	0.04	0.57	0.56	0.15	0.30	0.04	1.91
Feld (TCS)	LS	(LS)	2.56	45.7	5.97	43.3	0.01	0.06	0.21	0.14	0.21	0.02	1.82
Fordyce	SRG	(SRG)	93.8	2.23	0.11	1.77	0.01	0.76	0.63	0.18	0.32	0.01	0.09
Vega	SRG	(VG)	66.9	11.6	0.39	9.07	0.07	2.33	4.22	0.95	1.16	0.19	3.12
Ferris	L/S	(FR)	14.2	42.1	0.43	34.4	0.10	3.70	0.87	0.17	0.26	0.06	3.71
Scotland	Granite	(GR)	71.3	1.50	0.63	0.59	0.03	1.52	14.3	4.40	3.83	0.29	1.61
TXI-Boonesville		(BO)	5.26	49.8	.034	40.0	0.03	0.40	0.41	0.06	0.14	0.02	3.54
McKelligan #2		(DL2)	7.31	35.2	12.4	42.8	0.02	0.21	0.42	0.11	0.29	0.03	1.21
Ferris #2		(FR2)	12.5	42.8	0.44	35.4	0.10	3.56	0.76	0.17	0.28	0.06	3.93
TCP-Celburn #51		(CL)	18.8	41.3	0.49	34.7	0.05	0.72	0.62	0.19	0.31	0.04	2.78
Ingram Whitehead		(IW)	23.9	38.7	0.44	31.2	0.05	0.77	0.69	0.21	0.32	0.05	3.67
TXI-Tintop #2		(TT2)	33.6	34.1	0.35	27.9	0.06	0.91	0.74	0.16	0.32	0.05	1.81
Pioneer Landess Pit		(PI)	14.7	42.8	0.42	34.7	0.09	3.31	0.65	0.15	0.25	0.05	2.88
Jobe - Hueco		(JH)	17.5	41.7	1.62	35.1	0.02	0.45	1.01	0.16	0.35	0.06	2.03
Rainbow-Barker		(RB)	32.8	34.6	0.41	27.9	0.06	0.98	0.69	0.21	0.36	0.05	1.94
A-Rock Brazos Pit		(BR)	55.6	20.2	0.43	16.4	0.03	0.89	2.31	0.64	0.93	0.11	2.46
Vulcan-Mexico		(VM)	0.27	53.1	0.55	43.8	0.01	0.03	0.23	0.18	0.28	0.04	1.51
Sandstone-Samp. 1		(SA1)	97.5	0.07	0.02	*	*	1.03	0.55	0.12	0.05	0.02	0.66
Sandstone-Samp. 2		(SA2)	96.0	0.10	0.04	*	*	2.01	0.55	0.12	0.10	0.02	1.10

*These aggregates combined in a 50/50 blend when tested in the laboratory for concrete properties.

3.4.7 Discussion

In general, the procedure performs very well in describing the mineral content of the original sample. No conflict was found with the original crystallography analysis (Table 3.1). Most of the oxide residue is accounted for, with a maximum of 8.96 percent unexplained for aggregate (FR). This is probably due to the large amount of ferric minerals found in this aggregate and not addressed in the analysis.

Additional checks could be made by calculating the amount of Al_2O_3 and CO_2 remaining after the expected amounts are subtracted. For instance, all or most CO_2 should come from calcite and dolomite, and all or most Al_2O_3 should result from sodium and potassium feldspar decomposition. A large remainder of either of these compounds would indicate that a significant amount of some undetected mineral was present.

Of course, the real test of the procedure will be the enhanced predictive ability of the new models, which will be based on mineral content instead of on oxide residue.

Table 3.4. Calculated mineral composition (%)

	Aggregate	Calcite	Dolomite	Quartz	Albite	Potassium Feldspars	Remainder
1	BTT	73.98	3.245	15.51	1.269	1.77	4.23
2	DL	29.87	59.42	5.01	0.76	1.54	4.3
3	FR	73.87	1.97	12.22	1.44	1.54	8.96
4	GR	1.11	2.88	31.05	37.23	22.63	5.1
5	LS	66.53	27.29	0.94	1.18	1.24	2.82
6	SRG	3.70	0.50	91.53	1.52	1.89	0.86
7	VG	19.68	1.78	56.93	8.04	6.86	6.71
8	WT	19.42	1.60	59.35	7.19	6.50	5.94

CHAPTER 4. COMPUTER MODELING OF AGGREGATE PROPERTIES RELATED TO PORTLAND CEMENT CONCRETE PAVING

4.1 STATUS OF THE CRCP ANALYSIS PROGRAMS

The family of CRCP programs simulate the early-age behavior of continuously reinforced concrete pavements. These programs can be used to predict crack spacing, crack width, steel stresses, frictional forces, and displacements based on volume changes caused by temperature differentials and drying shrinkage. A substantial amount of input data relating to pavement design, environmental factors, and loading must be provided to the programs.

Many changes and additions have been made to the CRCP program since Adnan Abou-Ayyash wrote the original CRCP-1 version in 1973. Currently, only versions 4, 5, 6, and 7 are used, with versions 5, 6, and 7 simply modifications of version 4. (In 1990, Moon Won [Ref 5] introduced an updated CRCP program capable of simulating material variance in the form of random normal variation to concrete tensile strength. This revision was included in CRCP-5 and CRCP-7.) Phase II testing under this project enabled the development of normalized curing set curves for eight coarse aggregates commonly used in Texas pavements (Ref 2); these models have been incorporated in CRCP-6 and CRCP-7. Figure 4.1 reveals the relationship between versions and revisions.

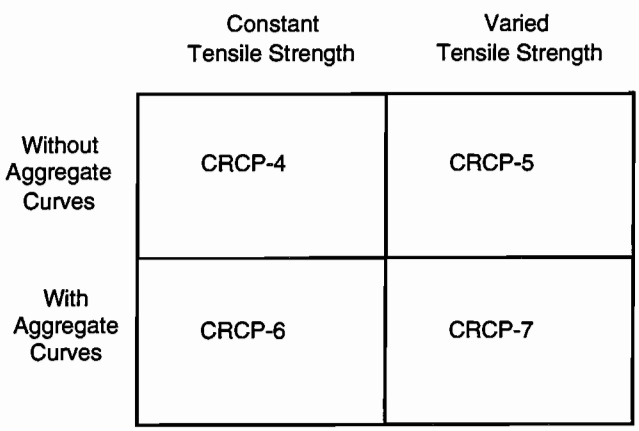

Figure 4.1. Nomenclature for CRCP program versions

Although CRCP-7 can be considered the "current" version of CRCP, it is still being tested and revised. Additionally, it has been streamlined and no longer performs some of the functions of its predecessors. It also takes much longer to run than versions 4 or 6. For these and other reasons, a decision was made to retain and support the previous versions of CRCP. Users can quickly run version 4 or 6 when only mean crack spacing is needed, or switch to 5 or 7 if a crack spacing distribution is desired.

4.1.1 IBM PC Versions of the CRCP Program

Recently, versions 4 through 7 were modified for IBM PC (or compatible) operation. In order to make them more user-friendly, modern pre- and post-processor subroutines were appended. User input data are passed from the front-end driver to the existing FORTRAN calculation module, with the results of the analysis then transferred to the post-processor for display. Figure 4.2 illustrates the concept.

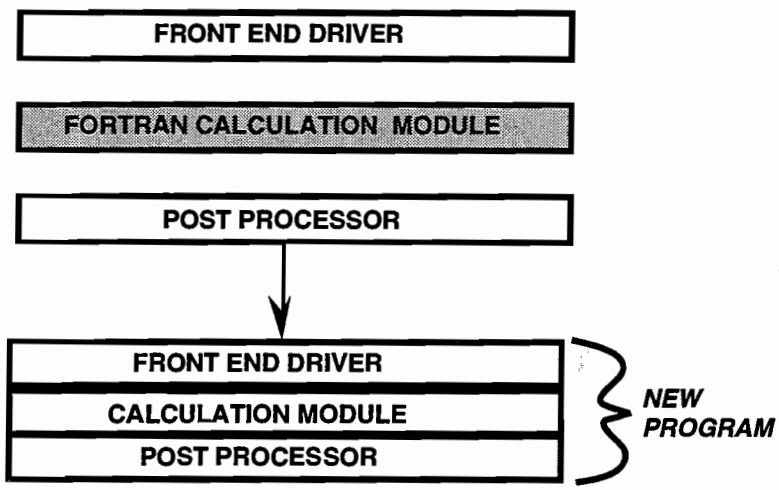

Figure 4.2. Conceptual diagram of new CRCP system

User input is accomplished via a series of "smart screens" that automatically expand and truncate data items based on parameters of the problem already entered. Reasonable default values are provided for each data item, but may be overridden by the user. Some of the input screens also operate in a "spreadsheet" fashion, calculating input data from fields already entered. An example input screen is shown in Figure 4.3.

Additionally, the new PC versions of the CRCP program use a "worksheet" concept for storage of user input data. This method greatly facilitates running multiple problems (e.g., sensitivity analysis), since data from each problem are retained and may be easily edited and resubmitted. Since the internal worksheet format is the same for all four versions of the CRCP program, data may be freely and easily exchanged between the different programs.

4.1.2 Output Summary Screen

Figure 4.4 shows the output summary screen. This screen has been standardized for all the CRCP versions, so some elements may be present or missing depending on which version was run. Output items are highlighted to indicate critical values, such as excessive steel stress, cracks too closely spaced, or excessive crack width. In the top right corner, a histogram is

presented showing predicted crack spacing distribution (cumulative or individual). The output summary may be screen-printed using a single keystroke.

CRCP-7 Screen 4

CONCRETE PROPERTIES

Pavement Thickness (in) 8.0
Thermal Coefficient (microstrains). 6.30

Aggregate Type: Granite BDG/TT Limestone
Dolomite Western-T SRG
Vega Ferris - Other -

Curing Time (days)	Tensile Strength (psi)	Compress. Strength (psi)	Elastic Modulus (psi)	Drying Shrinkage (in/inE-6)
1	182	1,265	2,619,341	11
3	306	2,707	3,331,953	31
7	381	3,877	3,660,227	67
28	444	4,999	3,704,000	195

Tensile Strength Coefficient of Variance. . . . . 20 %

F1 - CONTROL

1 psi=6894.757 Pa
1 inch=2.54 cm

Figure 4.3. Example input screen from CRCP pre-processor

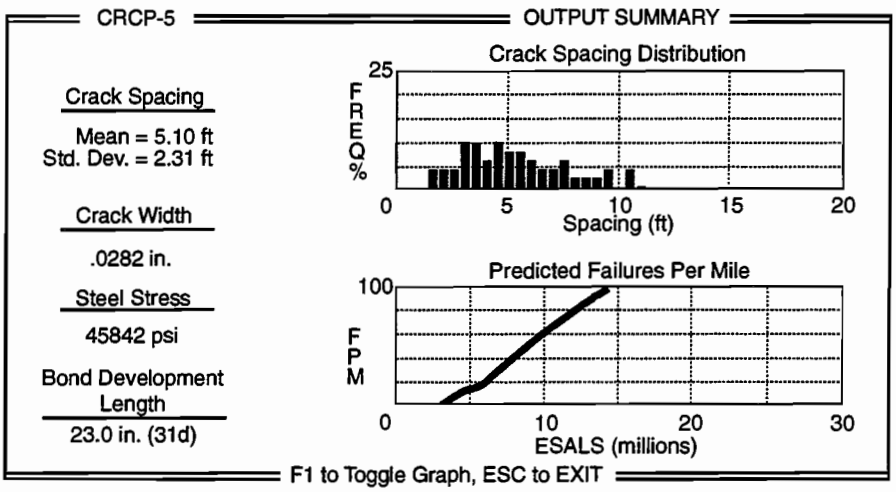

* 1 foot = .3048 m
** 1 inch = 2.54 cm
***1 psi = 6894.757 Pa

Figure 4.4. CRCP program output summary screen

4.1.3 Incorporation of Phase III Models into the CRCP Program

The descriptive models developed as a result of Phase III testing will be incorporated into the CRCP program. This will, at a minimum, give CRCP the ability to predict crack spacing, crack width, steel stress, and other properties for Portland cement concrete cast with blended limestone and siliceous aggregates. Additionally, since CHEM2 will replace the existing program CHEM1, and will have the added features of being able to predict thermal coefficient, tensile strength, compressive strength, modulus of elasticity, and drying shrinkage for blended and unblended aggregates, these improved and enhanced chemical models should also be added to the CRCP program. The net result is that the program will have enhanced predictive ability for limestones and siliceous river gravels, a result of the additional data on these aggregates that will be collected during the Phase III testing.

4.1.4 Methodology

To design pavements according to a desired level of performance using different aggregates, a predictive model is needed. The first step will be accomplished by CHEM2, which will predict concrete material properties based on the chemical composition of the aggregate. These properties will then be used as input to the CRCP programs to predict pavement performance based on such additional factors as steel design, thickness, environmental, and loading factors. By running CRCP at various levels of these factors, a reasonable design can be developed for the new aggregate or blend.

4.1.5 Discussion

Option 1: Values for 1, 3, 7, and 28 days predicted by CHEM2 for each concrete property can be entered directly into CRCP-5 by selecting "OTHER" as the aggregate type. Advantages: no modification is needed for the CRCP programs or front-end drivers. This saves the user a considerable amount of time and effort. Disadvantage: The user would have to type up to 17 numbers from CHEM2 output sheet into CRCP.

Option 2: If blend shapes approximate one of the known aggregates (probably limestone or SRG), the user need only select limestone or SRG, and type in the 28-day values from CHEM2. The CRCP program will backcalculate the 1-, 3-, and 7-day values. Advantages: Only four numbers need be transferred, and no modification is needed. Disadvantages: Presumably less precise than method 1.

***Option 3*:** Prepare CRCP-8 program. Additional aggregate types would be added, probably including something like "LS/SRG 50-50," "LS/SRG 75-25," etc. These would be normalized curves so that the user could either accept the entire default curve, or type in the 28-day value and have the program backcalculate the earlier values. Advantages: Presumably more precise than Option 2 (but not Option 1) and it is the easiest to use. Disadvantages: Requires a substantial amount of reprogramming, and the program worksheet would not be compatible with earlier versions of CRCP.

4.1.6 Recommendations

Prior to analyzing the results from the Phase III testing, it is impossible to tell whether Option 3 will be needed, or whether Option 2 will be sufficient. Option 1 will work in any case, at only a slight inconvenience to the user. It is estimated that most of the user's time will be spent modifying the other inputs to CRCP, such as bar size, percent steel, pavement thickness, etc., as the user attempts to find an acceptable design given the predicted aggregate properties. Based on this preliminary analysis, Option 1 is recommended, at least for the present.

In any event, it is recommended that the existing or proposed versions of CRCP be modified to provide a default 28-day thermal coefficient based on aggregate selection. This modification could be made with a minimum of programming effort and would provide some convenience and support to the user.

4.2 IMPROVED PERFORMANCE PREDICTION OF CRC PAVEMENTS

4.2.1 Introduction

Continuously reinforced concrete pavements (CRCP) were developed to reduce excessive maintenance problems associated with joints. Although CRCPs are less prone to joint-related distress, specific distresses are occurring. These distresses reduce the anticipated performance of CRCP under varying weather and traffic conditions. This section summarizes the current performance prediction method and proposes a more rational method of determining the actual performance of CRCP. Besides the ability of predicting actual performance, this new method can also be used to optimize different variables to achieve a desired performance level. In this study parameters that are unique to CRCP and influential in the fatigue life of CRCP will be discussed and used to develop criteria for fatigue life prediction model. These parameters will include crack spacing distribution, longitudinal reinforcement, soil conditions, weather conditions, traffic density and load distribution, sequence of load application, material, load, and weather variability. Load variation is an important factor that was not considered in most of the fatigue life formulations, since the damage of applied load to damage of standard load is the power of their magnitude ratio.

4.2.2 Objective

This section describes the CRCP performance and introduced a realistic performance prediction model.

4.2.3 Method of Analysis

Texas has many miles of CRCP in high traffic volume areas and in locations with variable weather conditions. Since traffic volume and weather conditions vary from one place to another, one can expect different performance levels for identically designed CRCPs. To overcome the effect of traffic volume variation and weather variation, the design should be adjusted according to the desired performance level. As part of the Project 1244, the authors developed a framework to systematically analyze what is available and what can be done to improve the prediction of CRCP

performance in Texas. The main framework is shown in Figure 4.5. Three main parts of the framework were accorded varying degrees of importance. Among these, the behavior and response process is the most commonly investigated and modeled process. Although individual processes by themselves are important for the prediction of CRCP performance, their interaction should receive the same level of investigation. This section briefly describes the interaction between the processes that affect the early-age behavior and fatigue life of CRCP built in Texas. Following the description of this interaction, the optimization process is explained. The optimization process includes several processes or subsystems. Because of the size of the framework, and because the literature abundantly addresses each process, only a part of the CRCP optimization system was selected. The response of CRCP is often modeled without considering either early-age CRCP behavior or the interaction of early-age behavior with performance of the pavement. Thus, the response model of CRCP was excluded in this study. Instead, early-age behavior, fatigue modeling, and the interaction of these two were investigated.

Early-age behavior of CRCP determines the initial crack spacing distribution. Since average crack spacing is a function of early-age behavior of CRCP, and since average crack spacing affects the remaining life of the pavement, the relationship between early-age behavior and remaining life becomes important. The CRCP life span can be divided into the three phases shown in Figure 4.6. Phase I includes the early-age effects on the average crack spacing. During this phase average crack spacing drops significantly and becomes almost constant before Phase II starts. In Phase II, CRCP is exposed to varying environmental conditions and traffic loads. Slab segments remain the same until the cumulative damage is more than what the slab segments can carry. When this happens, further cracking occurs. Phase III is the beginning of pavement failure that is aggravated by a continuous reduction in average crack spacing. Since average crack spacing almost remains constant during Phase II, it is safe to say that the average crack spacing at the end of Phase I influences the starting time for Phase III. Using this relationship, the interaction of early-age and failure period of the CRCP can be quantified to optimize CRCPs. In addition to the average crack spacing, this study used the crack spacing distribution in the calculations.

Structural performance of CRCP can be measured by calculating the structural damage to the pavement. Since punchout is the most severe structural failure, modeling of punchout will help to accurately estimate the time when the pavement will fail. Previous works on punchout modeling include simple assumptions that can affect the accuracy of model. These assumptions result in the incorrect application of Miner's fatigue formula and the incorrect selection of crack spacing distribution. All of these problems in the punchout model reduces the overall accuracy of the model. A brief description of these problems will clarify the reasons why a new model is needed. First of all, accumulated stress at any one slab segment, which is surrounded by two transverse cracks, may not be identical to the stress of another slab segment of the same length. In this case the bending stress is transverse to the pavement. This is because some of the slab segments retain their length while other slab segments may have further cracking and achieve the same slab length over time. The bending stress caused by wheel load is inversely proportional to the slab length. In other words, slab segments of short lengths are expected to fail.

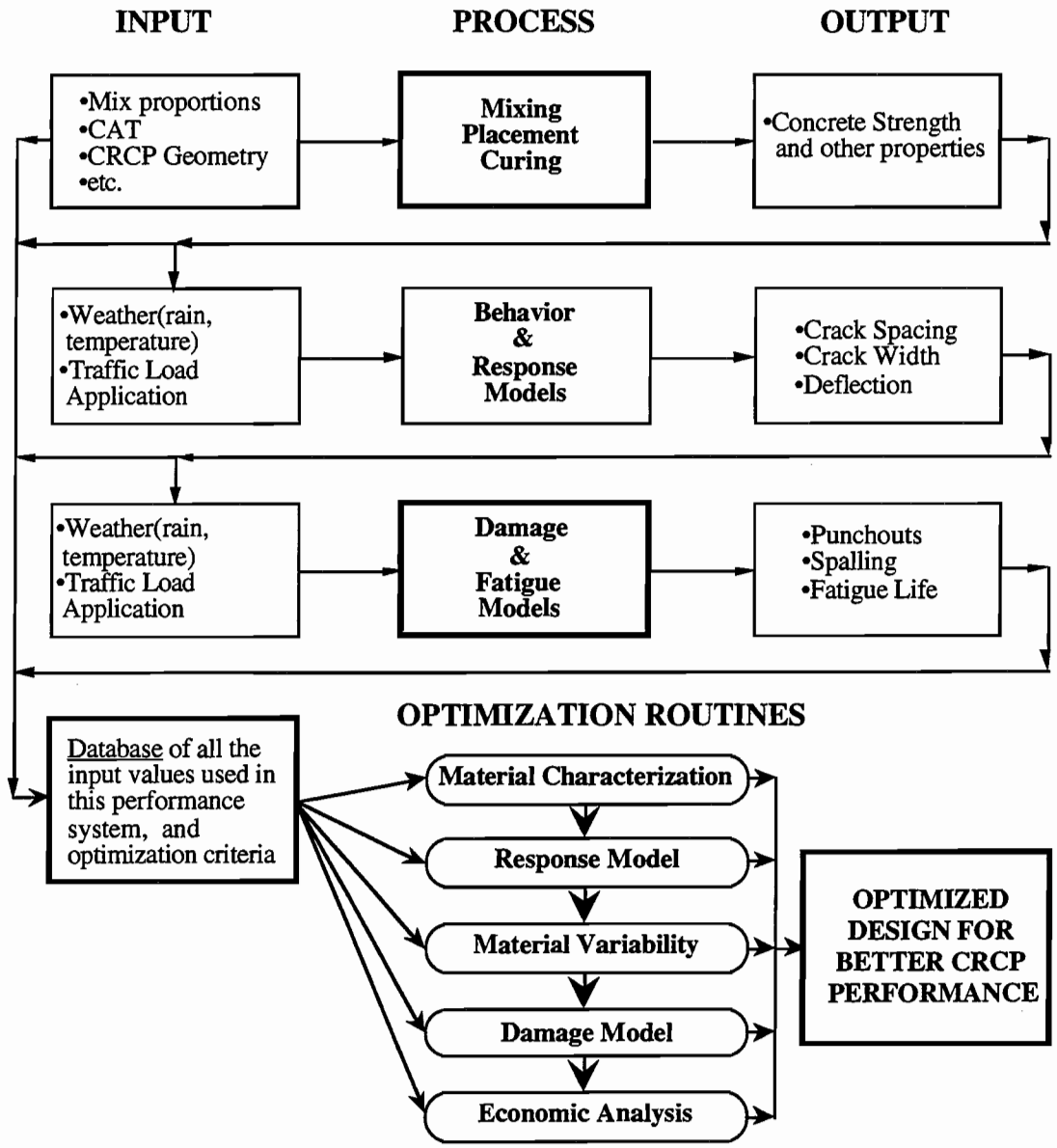

Figure 4.5. Framework of the CRCP performance optimization

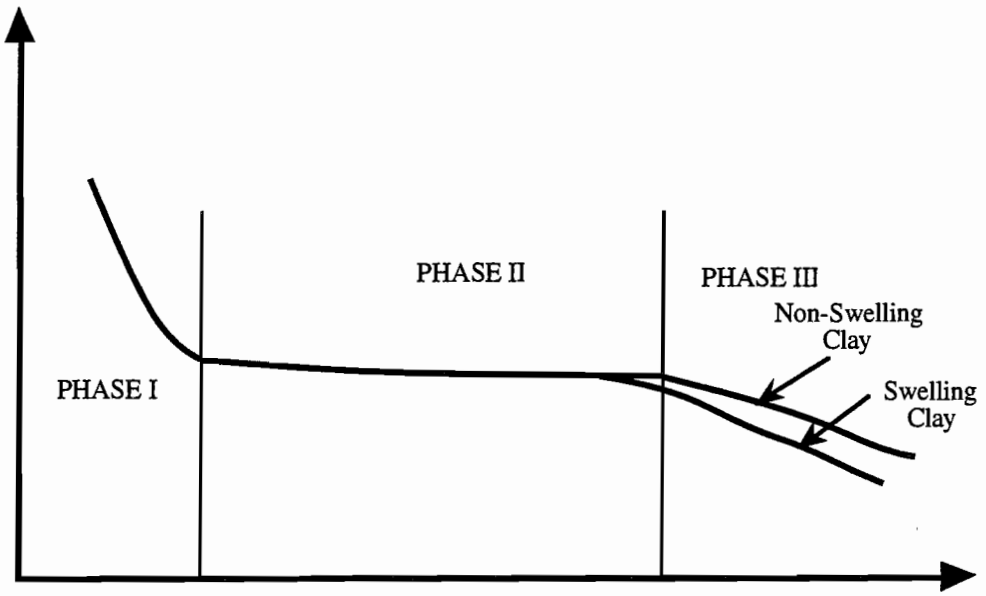

Figure 4.6. Conceptual drawing of time dependency of average crack spacing

4.2.4 Data Collection

The punchout prediction model was verified using data from Project 1244 test sections located in Houston. The condition surveys of these test sections cover early-age condition as well as current information about the condition of the pavement.

The Houston test sections included:

(1) SH 225

(2) SH 6 and Huffmiester

(3) SH 6 and Patterson

(4) Beltway 8 and Antonie

(5) IH-45 and Hardy Toll Road

More detailed information on each test section was provided by Suh (Ref 3).

4.2.5 Procedure

Final data from the Houston test sections were collected during spring 1992. Data accumulated since the construction of these pavement sections are used for analysis. Important data collected in these field surveys included crack spacing. The progress of average crack spacing with time can be used as an indicator of pavement performance level. The average crack spacing, which starts with a large value, decreases with time and with the contribution of environment and traffic. The trend in the average crack spacing indicates how the pavement performs. There is an optimum range for average crack spacing for a good performance. The lower and upper limits of

this range are 3.5 ft (1.0688 m) and 8 ft (2.4384 m), respectively. When average crack spacing ($\overline{X}$) is greater than 8 ft (2.4384 m) the cracks on both sides of the average slab segment become too wide to prevent water percolation. By the same token, if $\overline{X}$ becomes shorter than 3.5 ft (1.0688 m), then the probability of having longitudinal cracks between average slab length increases. This will result in punchouts, a distress manifestation.

The use of average crack spacing for performance is necessary but not sufficient for a complete characterization of the pavement behavior. The range for optimum crack spacing is for the whole spectrum of the crack spacing of the particular pavement section.

The length of the test sections varied from 230 ft (70.104 m) to 250 ft (76.2 m) (the test sections located at SH 225 were 250 ft (76.2 m) while the other test sections were 230 ft (70.104 m) long). At every test location there are eight sections (nine at SH 225) divided into two groups, with four sections each.

Reinforcement is continuous in CRCP construction. Consequently, the beginning or end of each section includes the reinforcement of the previous or the following section. Hence, for analysis purposes, both ends of any section should be excluded to some length to eliminate the effect of the reinforcement of the other section in the crack spacing calculations. This distance is assumed to be 15 ft (4.572 m) by Suh (Ref 3). Because this value was thought reasonable, it was adopted for this analysis.

4.2.6 Analysis

This section describes the crack spacing analysis. The procedure included the assumptions made and the steps used to start and complete the analysis.

4.2.6.1 Assumptions. The raw data collected from the test sections cannot be directly used for analysis, since the sections are connected to each other and since some revisions should be performed before using the raw data. The first assumption is the selection of the effective length of each section to be included in the crack spacing analysis. The 15-ft-long (4.572 m) sections that were excluded in the analysis are shown in Figure 4.7. Thus, only those cracks occurring in the effective segment of the CRCP section (Cracks 2, 3, 4, 5, and 6) are included in the crack spacing analysis (i.e., the cracks numbered 1, 7, and 8 are excluded from the analysis).

The following comparison shows the difference between what is currently used for performance prediction and what is proposed:

Current:
- Cumulative traffic loads
- Age

Proposed:
- Rate of traffic load application
- Rate of environmental change (rain, temperature, relative humidity, etc.)

Many agencies use cumulative traffic loads as an indication of the performance of CRCP. But accumulated traffic load does not yield sufficient information regarding how and when the traffic loads were accumulated. To overcome this limitation, rate of traffic load application is being proposed for the analysis of pavement performance. Age of CRCP is used along with cumulative traffic load for performance evaluation. Since environment is the other important factor in the performance of CRCP, the rate of environmental change, which includes temperature, relative humidity, and rain, is also proposed to replace age in the CRCP performance evaluation.

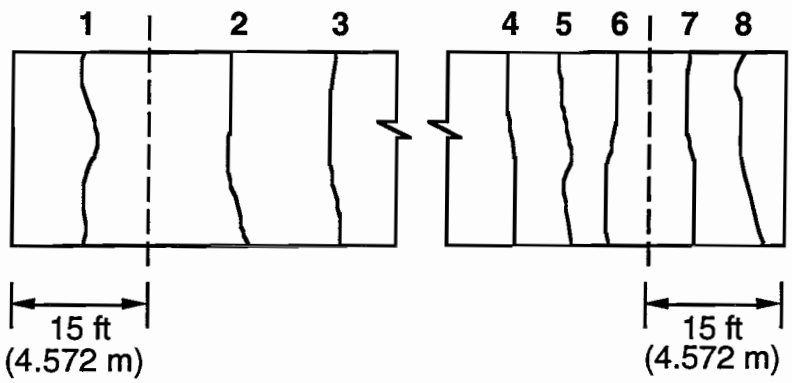

Figure 4.7. Typical test section crack survey analysis

4.2.6.2 Analysis. Current criteria and the formulas used for fatigue calculations of continuously reinforced concrete pavements cannot simulate all real-world conditions. More suitable criteria are needed to accurately estimate the life of CRCP under variable conditions of weather and traffic loads.

4.2.7 Results

The Houston test sections provided the primary data used in this study. Observations at these locations revealed the relationship between early-age behavior and crack spacing distribution at a later age. Although average crack spacing distribution is currently being used to evaluate CRCP performance, distribution reveals more information. Figures 4.8 through 4.10 show the average crack spacings for the various test sections.

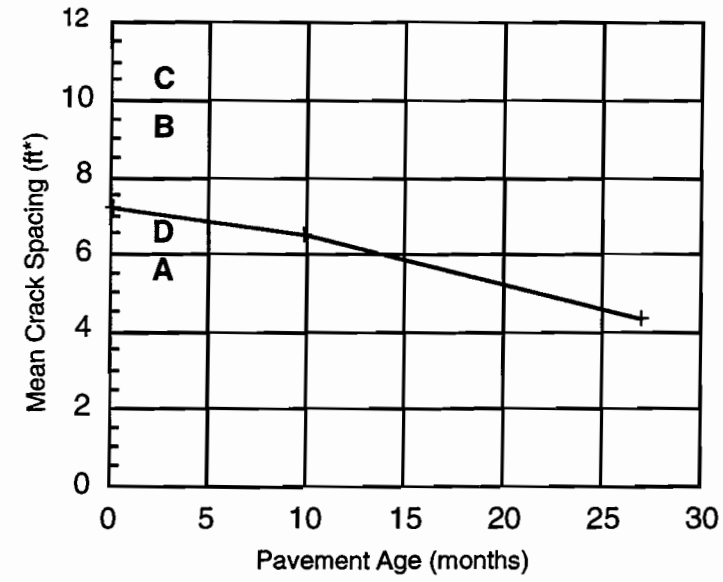

* 1 foot = .3048 m

Figure 4.8. Average crack spacing of different sections as a function of age, IH-45 section (SRG)

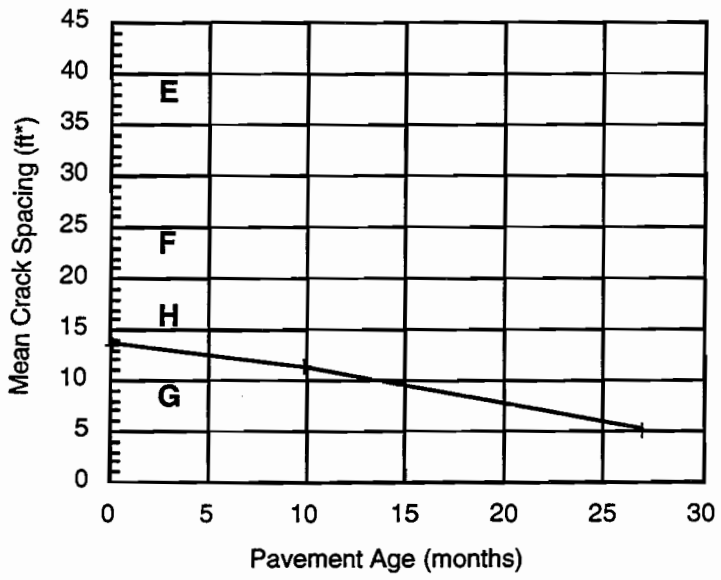

* 1 foot = .3048 m

Figure 4.9. Average crack spacing of different sections as a function of age for IH-45 section (LS)

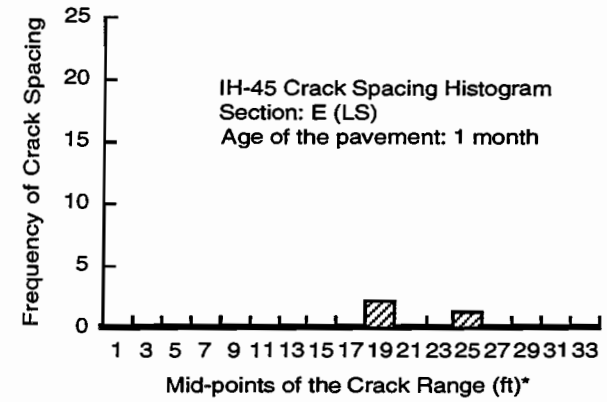

(a)

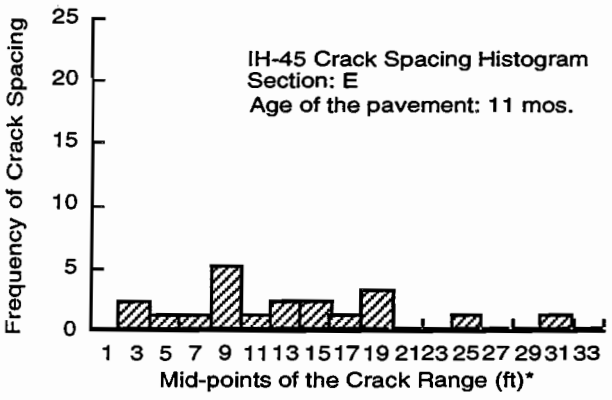

(b)

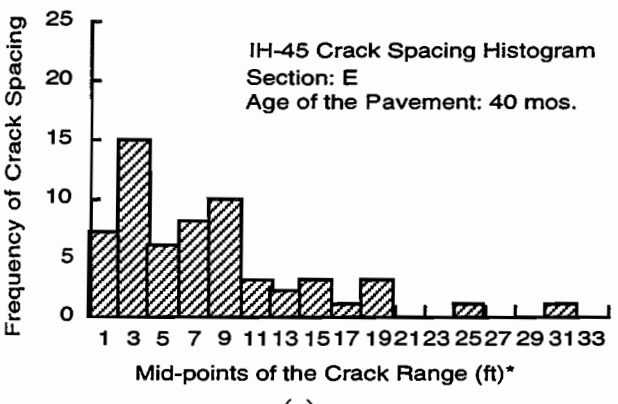

(c)

* 1 foot = .3048 m

Figure 4.10. Crack spacing distribution of section E as a function of age for location IH-45 (LS) at (a) 1 month, (b) 11 months, (c) 40 months

4.3 LABORATORY STUDIES ON THE EFFECTS OF AGGREGATE BLENDS ON PROPERTIES OF PORTLAND CEMENT CONCRETE

4.3.1 Background

Coarse aggregates comprise over 70 percent of the volume of any concrete mix. Each coarse aggregate source has its own chemical make-up, which influences the properties of the concrete in which it is used. Whereas an individual aggregate type may provide some of the desired properties, blends of aggregate types can be used to create a balance to produce properties desirable for a pavement design. This project will show that the mineralogy of the aggregate can be used to predict physical and mechanical properties of the mix, which in turn can be used to create blends that fit the needs of a pavement.

4.3.2 Laboratory Study

This study focused on two major types of aggregates, crushed limestone (LS) and siliceous river gravel (SRG). A lab investigation was conducted in which four sources were used.

Supplier	Company Name	Location
Group 1	Texas Crushed Stone	Georgetown LS
	Pioneer; SRG	Houston
Group 2	Young Bros, Inc.	Mexia LS
	LaGrange Conc. & Aggr.	LaGrange SRG

A mix design was created in which only the coarse aggregate and the volume of the fine aggregate were changed. Two groups of testing were created, as shown above. Within group 1, a batch was made of 100 percent LS, 67 percent LS, 33 percent SRG, 50 percent LS, 50 percent SRG, 33 percent LS, 67 percent SRG, and 100 percent SRG. Group 2 had four batches. A 50/50 batch was not made because the results of Group 1 proved to be relatively linear. From each batch twenty-four 6 in.-diameter x 12 in. (15.24 cm diameter x 30.48 cm) cylinders and three 4 in. x 4 in. x 15 in. (10.16 cm x 10.16 cm x 38.1 cm) bars were made .

4.3.3 Testing

Cylinder testing was performed at 1, 3, 7, and 28 days. Tests included Compressive Strength (Ref 6), Splitting Tensile Strength (Ref 7), and Elastic Modulus using an extensiometer. The bars were used to measure Drying Shrinkage (Ref 8) and Coefficient of Thermal Expansion (Ref 9).

4.3.4 Results

The results, described below, support the hypothesis that the properties varied linearly as the percentages changed. The finished project will include an analysis of the chemical and physical relationships, including the modeling of these relationships. The models will be used in the CHEM and CRCP programs discussed in this report.

4.4 FRACTAL ANALYSIS OF AGGREGATE SURFACE TEXTURE

4.4.1 Introduction

Concrete aggregate is a major and a critical component of the concrete mix. It has been well established that the characteristics of aggregate particles have a significant influence on the properties of the concrete. Aggregates are obtained either directly as natural gravel or as crushed particles from large rock masses. In either case, the aggregate particles do not have a definite geometric shape (such as a sphere or a cube). During their formation, natural particles are subjected to the influence of all the natural processes (e.g., wind, snow, and rain). This will cause the particles to have irregular shapes. For particles crushed from parent rock masses, the size and shape of the particles depend on the location of faults/flaws within the rock mass. Once again, the resulting particles are of irregular shape. In the same manner, the surface texture of the aggregate particles is also irregular in nature.

The surface texture of aggregate particles determine the degree of bond between the cement paste and aggregate. This interfacial bond is a result of physical, chemical, and mechanical components. The mechanical interaction between the cement paste and the aggregate is directly affected by the roughness of the aggregate particle surface, i.e., the rougher the particle surface, the more surface area there is to adhere to the cement paste (thus creating a stronger mechanical bond). The other component interactions also depend on the surface texture indirectly, a result of its influence on the formation of reaction products at the interface.

Yet however important the aggregate characteristics, there are very few methods by which civil engineers can quantify them. Specifications, including ASTM's, do not explicitly contain limitations on shape, surface texture, and surface area, even though it is widely known that the aggregate particle size (and hence the total aggregate surface area) influences the concrete strength. It would be fair to assume that the absence of such specifications may be due to the lack of a well-accepted practical method to measure such properties.

There is an available ASTM Test for Index of Aggregate Particle Shape and Surface Texture based on the weighted average void content of specific sizes of aggregates that have been subjected to two different compaction efforts.

The fractal analysis of aggregate surface texture is a new technique introduced by Mandelbrot in the late 1960s. This is regarded as a very promising quantification method. Using this method, a fractal dimension can be calculated for each aggregate type that is directly related to the geometric characteristics of the aggregate particles. The fractal dimension is calculated from a photographic or video image of the aggregate particle(s) using statistical and mechanized means.

Natural shapes that can be characterized using fractals abound in nature. Fractal shapes can be in the form of clouds, rivers, coastal lines, ocean waves, and specific topography. Fractals have already being successfully applied in the medical and geophysical sciences.

4.4.2 What is Fractal Analysis?

A truly mathematical fractal is an expression used in geometry to describe objects of which the geometry is complex but the shape looks the same whether it is greatly magnified or viewed from a distance. In other words, the shape of a true mathematical fractal is composed of smaller shapes which are of the same form as the larger object at all scale levels. This is sometimes referred to as self-similarity.

Images of complex natural shapes and surfaces (e.g., aggregate particles) are not true mathematical fractals because they do not have self-similarity at all scale levels. Physical shapes have an overall size that places an upper limit on the range of applicable scales, and a lower limit set by the size of the constitutive particles of the body. Like any other mathematical approximation, fractals can only approximate physical objects over a range of values of parameters. Therefore, a reasonable definition of a fractal surface is a surface that may be accurately approximated by a single fractal function over a range of scales.

Complex natural shapes are intermediate forms of topological ideals of Euclidean geometry. Such an object (a fractal object) is described by the fractal dimension of the object which is unique to that object. Euclidean geometry gives the dimensions of 0, 1, 2, and 3 for dots, straight lines, surfaces, and bodies, respectively. The fractal dimension of a natural shape describes the deviation of a certain line, a surface, or a volume from their closest topological ideals. For instance, a broken line could have a dimension between 0 and 1, while a jagged line could have a dimension between 1 and 2 (since it partly fills the plane of the paper). A fractal line such as a jagged coastline (which is an often used example) has a fractal dimension greater than 1, but less than 2. A fractal surface, such as that of an aggregate, has a fractal dimension greater than 2, but less than 3.

To illustrate the fractal dimension and its calculation, a simple example of a fractal line first introduced by Mandelbrot can be used. If there is an irregularly shaped (non-straight) line, such as a coastline, measurement of its length can be an act of futility. The simple method would be to use a "compass" method, where a gauge of a certain length is used as a yardstick to determine how may of its measures would cover the whole coastline needing to be measured.

For a straight line, this can simply be mathematically represented by the following equation:

$$L = N \bullet y + f \qquad \text{(Eq 4.1)}$$

where

y = length of the gauge,

N = number of measures from the gauge of length y,

f = length of the segment smaller than y which may remain at the end of the measurement, and,

L = total length measured from this gauge of length y.

The above equation can be rearranged as:

$$L = (N+f/y) \cdot y \qquad \text{(Eq 4.2)}$$

In general, for any line including a fractal line, this relationship was generally described by Mandelbrot (Ref 10) as:

$$L = (N+f/y) \cdot y^D \qquad \text{(Eq 4.3)}$$

where he referred to D as the fractal dimension. For a straight line, D would have the value 1. As mentioned earlier, the topological dimension of a straight line is also equal to unity. Therefore, for a straight line, the topological and fractal dimensions are equal.

To see the general picture, look at Mandelbrot's example for measuring the distance between two points A and B along the coastline of Great Britain. The details of these measurements are given in Table 4.1.

Table 4.1. Data for measurement of a fractal length

Length of Ruler in km.* (y)	N + f/y	Length of Coastline in km.* (L) ~ (N + f/y)y
200	4.55	910
100	10.75	1075
50	28.25	1,412.5

* 1 km = .62137 mile

In Table 4.1, the length in the third column is approximately calculated by taking the fractal dimension (D) as equal to 1.0 (rearrange equation 3).

$$Ly^D = N+f/y \qquad \text{(Eq 4.4)}$$

The result of taking the logarithm of the above equation is:

$$D \log (y) = \log (N+f/y) \qquad \text{(Eq 4.5)}$$

According to the above equation, by plotting log (N+f/y) against log (y), the fractal dimension (D) as the negative slope of the graph is obtained. With such an exercise, the fractal dimension for this part of the British coastline from point A to point B is calculated from data in Table 4.1 as 1.3. This would yield a value of 4,500 km (2,796.2 miles) as the length of the coastline.

4.4.3 Analysis of Surface Texture of Concrete Aggregates

The measurement of the surface texture of aggregate particles is based on a two-dimensional fractal method in which the intensity of the image is considered as a mapping of the three-dimensional surface roughness or geometry.

The first step in the fractal analysis of surface texture would be the detection of the edge of the aggregate. The aggregate sample is placed on a background that contrasts with the aggregate particles and video-taped. The video frame is then digitized onto the computer where the digitized image contains a large grid of picture elements called pixels. In one image, there are 512 columns and 480 rows of pixels. Each pixel can take a brightness value ranging from 0 to 255 from a scale called the "grey scale," where 0 represents pitch dark, and 255 represents the brightest light. Owing to the contrast between the aggregate and the background, a rapid change in grey level occurs near the boundary of each aggregate particle. There are also techniques available to enhance the boundary of the aggregates.

Comprehensive mathematical formulations by Pentland gave proof of the following:

1. The fractal dimension of the physical surface which is representative of the "roughness" of the three-dimensional surface seems to dictate the roughness of the intensity of the image. If it is known that the surface is homogeneous (edge and the interior), an estimation of the fractal dimension of the surface by measuring the fractal dimension of the image intensity data can be made.
2. The fractal dimension of a surface is invariant with respect to linear transformations of the data and to transformations of scale. Thus, the image projection of the surface contours or the imaging process of the surface shape is simply a linear transform of three-dimensional contour or three-dimensional surface shape. Thus, the use of the fractal dimension of the image shape to directly infer the fractal dimension of the three-dimensional surface is possible.

Research performed for the Texas Department of Transportation at the Texas Transportation Institute, both under this project and others, have indicated that fractal dimension can be obtained from automated means and that the fractal dimension differs for different aggregate types. For example, siliceous river gravel particles have a lower fractal dimension for surface texture than crushed limestone particles. This is an indication of a higher entropy in the limestone aggregate particles, which will result in enhanced bonding properties between the aggregate and the cement paste.

This method of fractal analysis gives a very satisfactory tool for characterizing the surface texture of aggregate—a very important characteristic to be considered in the study of the interfacial bond between aggregate and the cement paste and, hence, in the study of concrete as a whole.

CHAPTER 5. ANALYSIS OF CRC PAVEMENT UNDER MOISTURE, TEMPERATURE, AND CREEP EFFECTS

5.1 INTRODUCTION

Continuously reinforced concrete pavements (CRCP) are constructed with closely spaced parallel rows of steel reinforcement placed in an uninterrupted, longitudinal configuration. Consequently, the pavement contains reinforcement (in approximately 60-foot (18.288 m) lengths) placed continuously end-to-end for long distances, with no transverse expansion joints. From a structural point of view, this type of pavement consists of an infinite continuum in one direction (i.e., longitudinal direction). However, owing to the combination of environmental effects and wheel loads, a characteristic crack pattern develops that consists of a distribution of transverse cracks. Initial cracking in CRCPs is primarily due to environmentally induced temperature and moisture gradients that cause slab curling. Field observations of initial cracks suggest that these cracks form within the first 24 hours after placement of the concrete. Subsequent cracks form as a result of the continuity of reinforcement (i.e., internal restraint), which inhibits free movement of the concrete matrix after the formation of initial cracks. Stresses that are developed at this stage are referred to as restraint stresses.

Various factors affecting the formation of cracks in CRCP at an early age are considered in this study. CRCP typically is allowed to develop a random crack pattern that is primarily governed by various environmental conditions at the time of construction, mix design factors, curing practice, etc. These cracks are also governed by other material factors, such as tensile strength of concrete and the type of coarse aggregate. Transverse crack intervals vary from 2 to 12 feet (.6096 to 3.6576 m), but sometimes may occur within 6-inch (15.24 cm) intervals, which is undesirable. Most of the transverse cracks form shortly after construction of the slab and sometimes may not be evident on the surface for a period of time. The final crack pattern (as observed on the pavement surface) typically stabilizes approximately 3 years after construction; however, 80 to 90 percent of the crack pattern typically develops between 28 to 90 days after construction.

The objective of this work is to develop a numerical framework to study the various factors affecting the crack formation in early-aged CRCP based on two-dimensional analysis (in terms of slab thickness and longitudinal dimension). The word *framework* is used because the focus of this effort is to identify and include models to address the development of transverse cracking in CRCP, to formulate a working analysis process with these models, and to illustrate some typical results from the analysis. The ambient climatic conditions and structural configuration of CRCP are the primary causes for the development of tensile stresses in the pavement. Of the different numerical models developed for this analysis, one pertains to the computation of shrinkage strains caused by the decrease in moisture content of pavement, while another pertains to the stresses resulting from the combination of shrinkage and thermally-related strains. The thermal strains are the result of a decrease in the temperature of the concrete that may occur under seasonal climatic changes.

5.2 BEHAVIORAL CHARACTERISTICS OF CRCPS

Design analysis of CRCPs is based on the determination of stresses and strains in the steel and concrete caused by restraint of environmentally induced volumetric changes and of wheel loads. This restraint also develops a characteristic crack pattern that influences the strength of the pavement. Hence, the prediction of crack spacing is also an integral part of the design process. Vetter (Ref 11) developed relationships for crack spacing in reinforced concrete and bond stress and tensile stress in concrete, with respect to the restraint shrinkage and thermal strains. Some of the assumptions made in the development of these relationships are the following:

1. Stresses owing to restraint of volumetric strains are uniformly distributed over the pavement section, i.e., plane sections remain plane within the concrete pavement.
2. Midway between the cracks, the change in length of the reinforcing steel and the concrete are equal, which means that strain compatibility exists in the bonded regions of the reinforcement. In these regions, there is no relative movement between the concrete and steel; therefore, no bond stresses or changes in stress in the concrete or steel occur.
3. The total bond force developed between the reinforcement and the concrete is equal to either the total tensile force in the concrete or the total change in the force in the steel. The force in the steel reinforcement is transferred from the steel to the concrete by the bond stress acting along the bar.

Other models developed by Won (Ref 5), and Palmer (Ref 12) for the prediction of crack spacing made improvements over Vetter's model, particularly in characterizing bond slip relationships. However all these models fail to consider the variation of shrinkage strains through thickness of the pavement. The consideration of uniform shrinkage with respect to the depth of the pavement may be a reasonable approximation for matured concrete, but a highly inappropriate approximation for early-aged concrete. The consideration of moisture and temperature gradients in the concrete pavement will also allow for important effects of consideration of curling and warping stresses in the analysis. Hence, a procedure is developed to compute moisture content at different depths of concrete based on diffusion theory developed by Bazant (Ref 13).

In the approach taken for consideration of moisture gradients in the slab, the finite element procedure is used for spatial approximation and the finite difference procedure for time approximation. The finite element method, used in this manner, has an added advantage of adaptability to any geometry with ease when compared with the finite difference method. Many empirical models are available in the literature to predict temperatures at different depths of a concrete pavement as a function of the ambient temperature at the pavement site.

A typical segment of CRCP in the first few hours after construction is illustrated in Figure 5.1. It is observed that the cracks are parallel to each other and transverse in direction. Figure 5.2 represents the assumptions used by Vetter to account for the longitudinal reinforcement on a per-unit area of pavement cross-section. Therefore, short pavement segments can be modeled for further analysis by approximating the slab as a three-layered system based on plane strain

assumptions. The middle layer is a composite layer consisting of steel and concrete connected by bond slip elements.

The rate of variation of material properties is very high prior to the concrete achieving complete maturity (i.e., before 28 days). Since this work was mainly interested in the stress state and behavior of concrete in the first 7 days of pavement life, consideration of this variability is important to this study.

Gardner and Poon (Ref 14) discussed time and temperature effects on various concrete properties (including their affect on the bond relationship). Experimental investigation was performed to study these factors. Laboratory molds were prepared in which compression, tensile, and bond strength tests were performed. It was found that temperature influences tensile strength in much the same manner that it affects the compressive and bond strengths. Bond strength and tensile strength are observed to be proportional to the power 0.8 of the cylinder strength at the appropriate age.

5.3 ANALYSIS FRAMEWORK

Temperature drop and drying shrinkage causes volumetric change in the cracked pavement that may develop further cracking owing to the restraint provided by the steel reinforcement. If the pavement is free to move, then it does not experience any stress (tensile or compressive), but if it is fully or partially restrained, then stresses are developed in the concrete, as illustrated in Figures 5.3 and 5.4. If the tensile stress in a given layer exceeds the tensile strength of concrete, then the concrete cracks. Typically, the strength of early-aged concrete is low; and, since the diffusion of moisture may be very high during this period, shrinkage strains can be dominant factors in the development of initial cracking and even in subsequent cracking. The following mathematical models were developed for estimating the shrinkage strains for the prediction of stresses leading to subsequent cracking. Their effect is combined with that of thermal strains to predict a final stress state in CRCP.

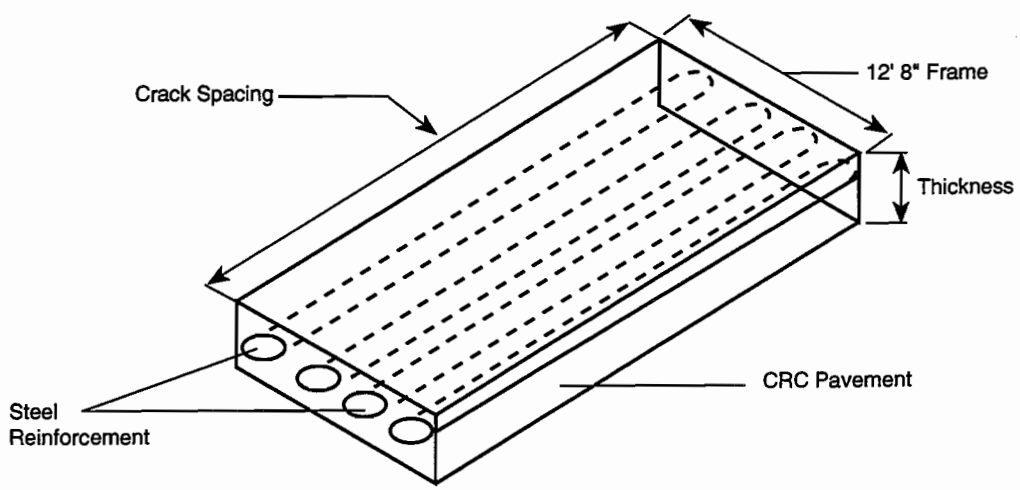

12' 6 " = 3.81 m

Figure 5.1. Typical model of CRCP between two adjacent cracks

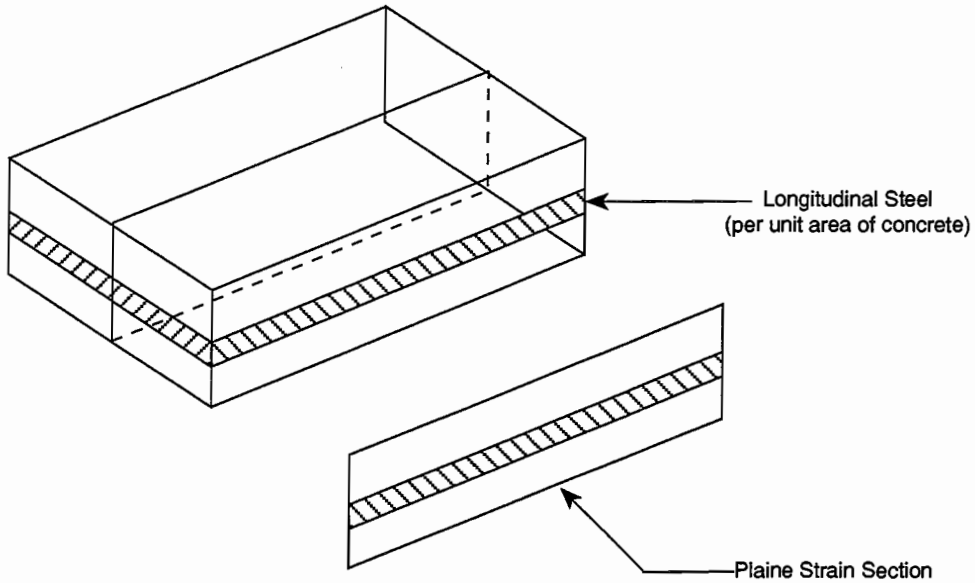

Figure 5.2. Three-layered view of pavement and cross-section considered for plan strain analysis

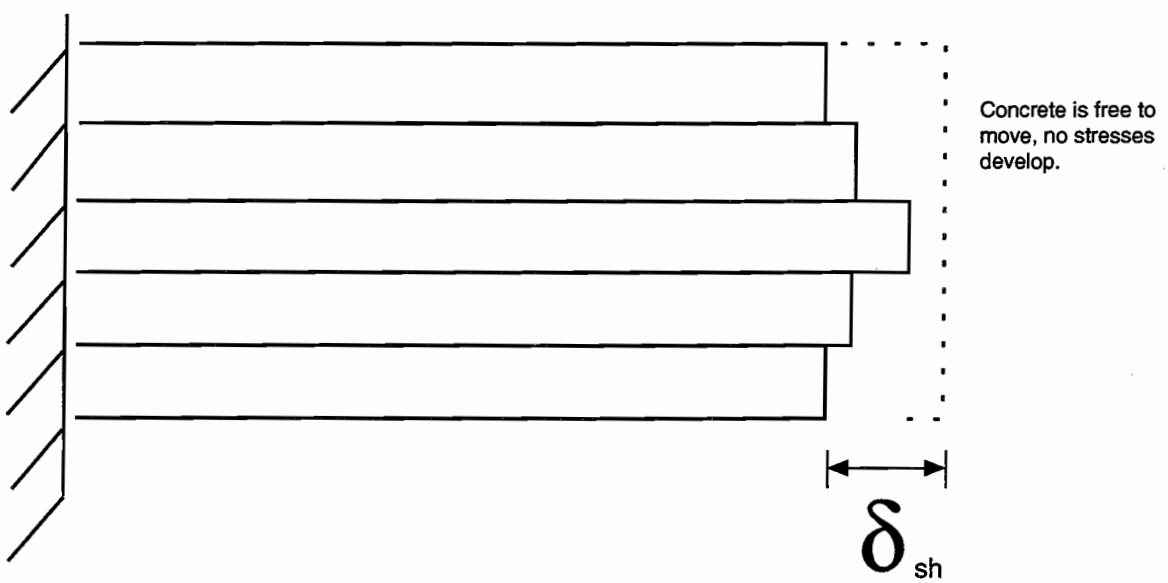

Figure 5.3. Unrestrained shrinkage

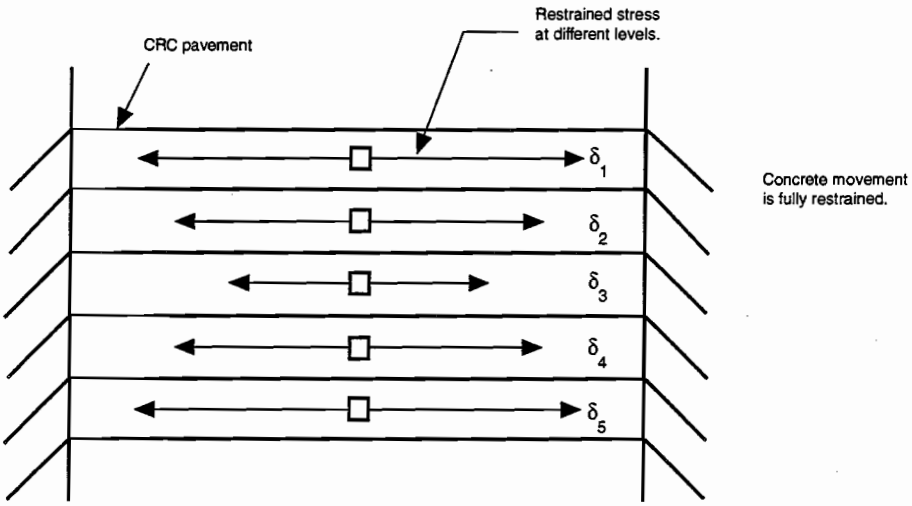

Figure 5.4. Restrained shrinkage

5.3.1 Drying Shrinkage Model

The prediction of drying shrinkage is based on the following model suggested by Bazant and Najjar (Ref 13):

$$\nabla\left(k_h \nabla(h)\right) + \frac{\partial h_h}{\partial t} + K\frac{\partial T}{\partial t} = \frac{\partial h}{\partial t} \qquad \text{(Eq 5.1)}$$

where

k_h = diffusivity of concrete,
h = percentage moisture content of the concrete at a given time,
h_h = percentage moisture content due to hydration,
T = is the temperature at different points in the concrete and at time intervals,
K = hygrometric coefficient, and
t = time.

The 'K' coefficient in Equation 5.1 is a conversion coefficient that converts temperature differentials into an equivalent change of relative humidity. An approximate equation for 'K' that is dependent on 'h' can be given as:

$$K = 0.0135\,h\,\frac{(1-h)}{(1.25-h)} \text{ per } ^\circ C \qquad \text{(Eq 5.2)}$$

1 °C = 9/5 + 32 °F

Equation 5.2 is an empirical approximation based on theoretical and experimental data. No flow boundary conditions are used on all surfaces for Equation 5.1 for plane problems. They can be described by the following equation:

$$k_h \frac{\partial h}{\partial x} n_x + k_h \frac{\partial h}{\partial y} n_y = 0.0 \qquad \text{(Eq 5.3)}$$

where n_x and n_y are direction cosines in x and y directions. The following are the imposed boundary conditions for environmental humidity at the surface of the pavement:

$$h = \hat{h} \text{ on } \Gamma_2 \quad t \geq 0 \qquad \text{(Eq 5.4)}$$

where

G_2 = boundary surface where environmental humidity acts, and
h = moisture content on surface (environmental humidity).

It is assumed at the initial condition of time 't' = 0 that h_0 = 100 percent (i.e., concrete is assumed to be completely saturated). The k_h term in Equation 5.1 is determined by the following equation:

$$(k_h)_t = k_d \left(\alpha_0 + \frac{1-\alpha_0}{1+\left(\frac{1-H_t}{1-H_c}\right)^n} \right) \qquad \text{(Eq 5.5)}$$

where

k_d = diffusivity of concrete at h = 1 and a given temperature (in.^{2}/day),
a_0 = min k_h / max k_h (a constant for a given concrete mix),
n = a constant which characterizes the distribution of h about k_h,
H_c = humidity value which corresponds to the average value of k_h, and
H_t = humidity value at the given time step 't'.

Diffusivity values of concrete are typically high for early-aged concrete; they rapidly decrease over the first 7 days as the concrete matures. Diffusivity values (k_d) used later in an example analysis are taken from laboratory experiments performed by Man Yop Han

(unpublished report, Texas A&M, 1989) using psychrometers embedded in hardening concrete; this provided data over several days, during which the variations in moisture caused by an imposed wetting and drying cycle were monitored. The variations in the measurements of this nature are, at a minimum, subject to the affects of the material parameters represented by the terms in Equation 5.5. Equation 5.5 provides an estimate of the expected value of K_h as it varies with time. Variability in K_h will be encompassed within the variations of a_0, n, and H_c, which may be defined in terms of any number of variance methods available in the literature (and which are not considered further in this study). However, the material parameter n varies between 6 and 16 (Ref 13) and is found from the "best fit" of computed diffusivity data to measured relative humidity data for a given mix.

The above nonlinear differential equation represents a classical boundary value problem. Bazant and Najjar (Ref 13) and also Grzybowski (Ref 15) solved this equation using a finite difference method. For generalized boundary conditions and geometries, the finite element method (FEM) is more convenient to use. In this study, the analysis uses the finite element method, treating the problem as a transient heat transfer problem. The solution is obtained using a semi-discrete approximation (i.e., spatial approximation is considered first, followed by an approximation in time). The differential equation is solved by an iterative procedure which converges to within a given tolerance. Temperature differentials and differentials of moisture loss caused by hydration (or self-desiccation) are specified as input. Moisture loss from the concrete pavement is converted into shrinkage strains at any vertical position in the slab using the following equation for plain concrete (Ref 16):

$$\varepsilon_{sh} = \varepsilon_{sh\infty}\left(1 - h^3\right) \qquad \text{(Eq 5.6)}$$

where h is previously defined, and the ultimate concrete shrinkage ($E_{sh\infty}$) is a material parameter of plain concrete. The following empirical expression is used to compute $E_{sh\infty}$:

$$\varepsilon_{sh\infty} = 1{,}330 - 970y \qquad \text{(Eq 5.7)}$$

where

$$y = \left(390\,z^{-4} + 1\right)^{-1} \qquad \text{(Eq 5.8)}$$

and

$$z = 0.381\sqrt{f_{cyl28}}\left[1.25\left(\frac{a}{c}\right)^{1/2} + 0.5\left(\frac{g}{s}\right)^2\right]\left(\frac{1+\frac{s}{c}}{\frac{w}{c}}\right)^{1/3} - 12 \qquad \text{(Eq 5.9)}$$

where

a/c = total aggregate/cement ratio,

g/c = coarse aggregate/cement ratio,

s/c = fine aggregate/cement ratio, and

w/c = water/cement ratio.

Equation 5.6 is assumed to be applicable to the analysis of shrinkage strain in CRCP, since previous studies have successfully applied the above expressions to concrete specimens in pure tension (Ref 17).

The analysis performed is unidirectional, and hence only one column of elements through the slab (Figure 5.5) is used for the specific cases considered in this analysis. The assumption of one-dimensional drying idealizes the drying conditions in actual concrete pavements. However, it is noted that if the subbase layer is stabilized with asphaltic cement or similar material, a certain amount of impermeability exists at the interface between the bottom of the concrete pavement and the top of the subbase. This assumption would not be applicable to all types of subbases. Shrinkage strains of this model are used as input for the stress model applied to CRCP.

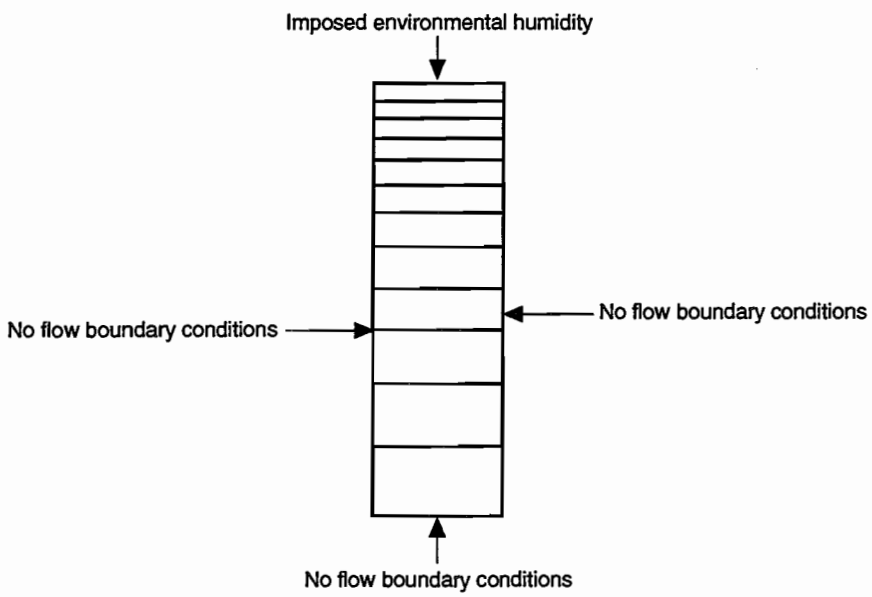

Figure 5.5. Finite element mesh for shrinkage analysis

5.3.2 The Stress Model

Finite element (FE) stress analysis was performed for imposed strains in early-aged concrete. The increase of strength and elasticity of concrete with age is accounted for in the analysis. Typically, the increase in strength of concrete at an early age (i.e., within the first few

days) is very high. The variation of modulus of elasticity and strength of concrete is given by following empirical equations (Ref 15):

$$f_c(t) = \frac{t}{A + Bt} f_c(28) \qquad \text{(Eq 5.10)}$$

$$E_c(t) = E_c(28) \left(\frac{t}{A + Bt} \right)^{1/2} \qquad \text{(Eq 5.11)}$$

where

t = time (days),

$f_c(t)$ = compressive or tensile strength of concrete at time 't' (psi),*

$f_c(28)$ = compressive or tensile strength of concrete after 28 days (psi),

$E_c(t)$ = modulus of elasticity at time t (psi),

$E_c(28)$ = modulus of elasticity after 28 days (psi), and

A & B = constants depending on concrete mix (A = 4.00 and B = 0.85 for moist cured concrete, cement type I).

* 1 psi = 6894.757 Pa

Characteristics of early-aged cracking behavior of CRCP may be illustrated in Figures 5.6 and 5.7, which summarize field data collected from a recently constructed CRCP section near Houston, Texas. It is interesting to note that the initial cracking development occurs quickly (say over a 3- to 5-day period) once cracking begins to develop. The effect of moisture and temperature gradients on early-age cracking may be reflected in the combination of frictional, curing, and warping stresses. The curling and warping stress are typically characterized in terms of the radius of relative stiffness (_). The range of _ - values for concrete pavements may vary between 36 to 42 inches (91.44 to 106.68 cm). Bradbury (Ref 18) pointed out that long slabs (sections of concrete pavements with joint or crack spacing [L] greater than or equal to 12_), as in the case of newly placed concrete pavements (whether jointed or CRC), develop maximum curling or warping stresses at a distance of 4.44_ from the joint or transverse crack. This effect, which is generally known and accepted from field experience, is manifest in actual pavements by cracks (whether random or controlled) occurring on the average at the interval pointed out above. Therefore, one would expect that stresses when combined with those due to frictional effects will contribute to cracking, at an early age, in CRCP at least at an interval of 4.44_.

The stresses that occur as a result of the restraint caused by the reinforcement may be accounted for at intervals smaller than this, since the stresses at intervals greater than L/_ of 4.44 are largely influenced by curling affects. Other factors also affect the rate of crack development,

including coarse aggregate type (as shown in Figures 5.6 and 5.7) and season or time of construction. It appears that an interval of L/_ equal to 4.44 or less may be appropriate to begin analysis of restraint cracking caused by reinforcement and frictional affects. In the example analysis discussed later, it is assumed that the pavement develops primary cracks at a spacing of 8 feet (2.4384 m), as influenced by slab curling and warping approximately equal to 50 percent of 4.4_.

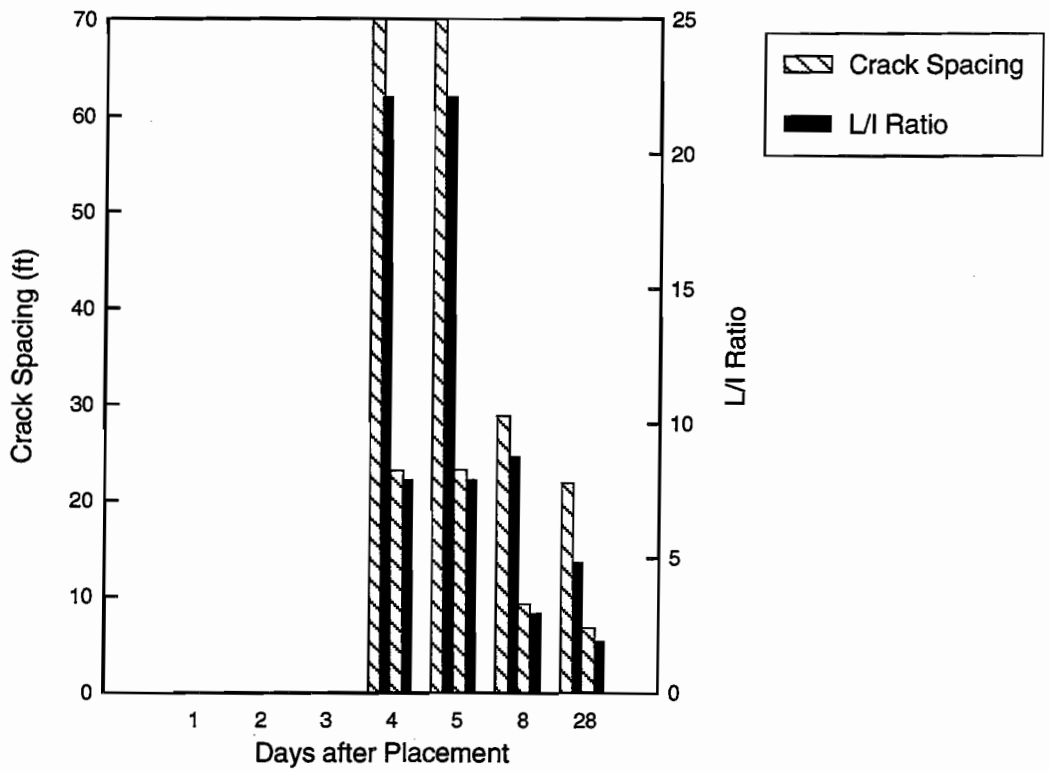

Figure 5.6. Early-aged crack evolution in limestone coarse aggregate

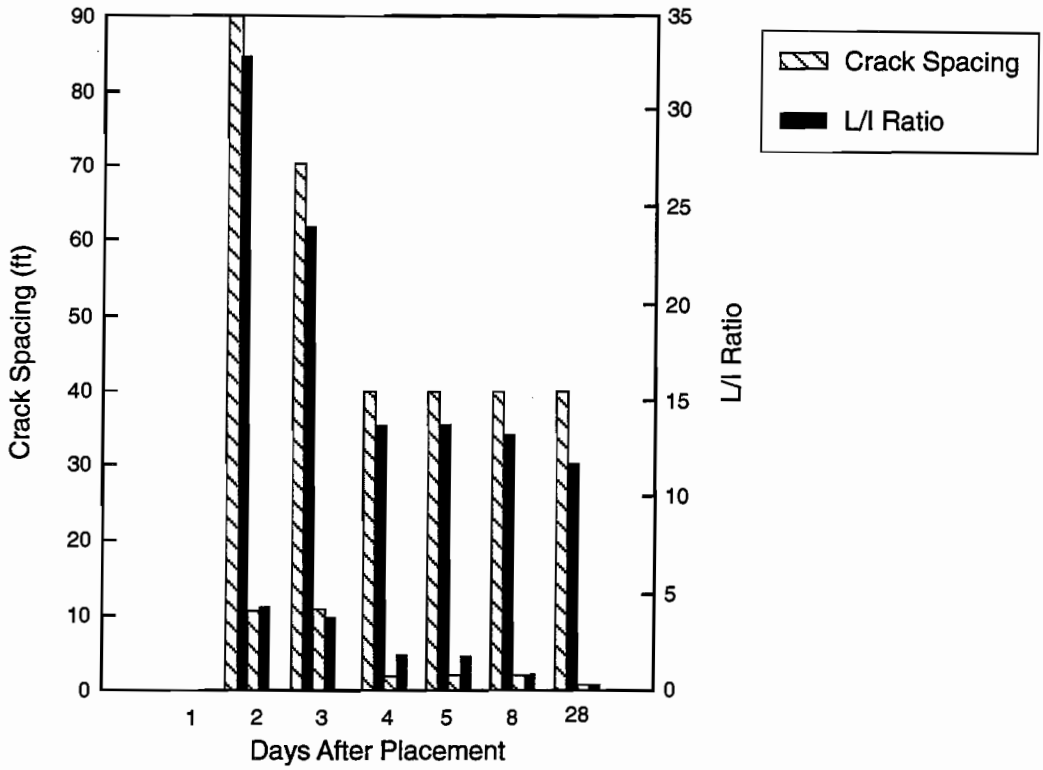

Figure 5.7. Early-aged crack evolution in silicious river gravel aggregate

Plane strain conditions are assumed for the stress analysis, and the properties of steel and concrete in the model are considered to be independent of each other. Bond slip elements are incorporated at the interface between concrete and steel. Analysis is performed to predict secondary crack formation. For modeling the concrete, consideration of the method suggested by Ngo and Scordelis (Ref 17) was taken, in which the concrete and steel are partitioned into two segments at the level of reinforcement. The thickness of these segments depends on the percentage of steel reinforcement in concrete. This approach is shown in Figure 5.8.

Eight-noded isoparametric elements with 3 x 3 Gaussian quadrature are used in the finite element analysis for both the concrete and the reinforcing steel. Strains are imposed by means of nodal forces. Stress transfer between steel and concrete owing to bond is modeled using a bond slip element. A slip element has two degrees of freedom per node, or four degrees of freedom per element at the interface of concrete and steel elements. It is assumed that x and y displacements of the spring element are independent of each other. The element is as shown in Figure 5.9.

Large values are given for the stiffness of the spring in the normal direction, so that the ratio of displacements in the normal direction to that of the reinforcing steel is approximately zero. The level of stiffness (depending on modulus of elasticity of the concrete and surface characteristics of the steel bar) is assigned as input to the stiffness in the direction aligned with the steel and is dependent on the bond-slip relationship at the steel-concrete interface. The bond-slip

function (as pointed out above) may vary depending on the bar pattern and the concrete properties. The spring stiffness is nonlinear and is approximated by the curve shown in Figure 5.10, which consists of two straight lines that are considered accurate enough to model the effect of bond-slip into the stress analysis. This is an approximation of the relationship suggested by Nilson (Ref 19) and recently validated by Jiang (Ref 20).

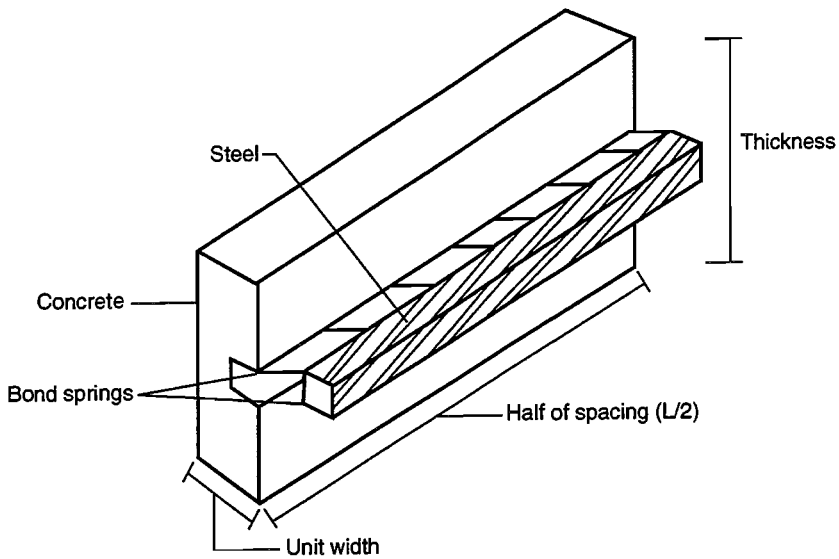

Figure 5.8. Three-dimensional view of finite element model for stress analysis

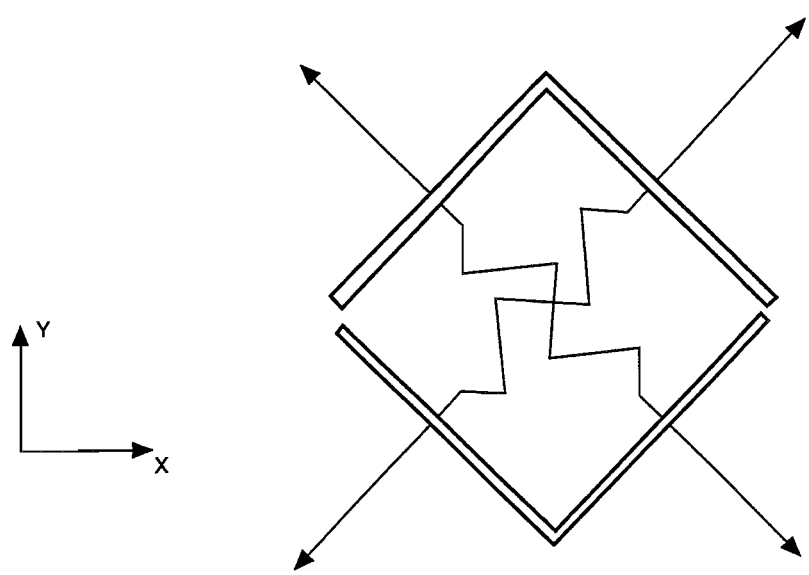

Figure 5.9. Spring element with four degrees of freedom

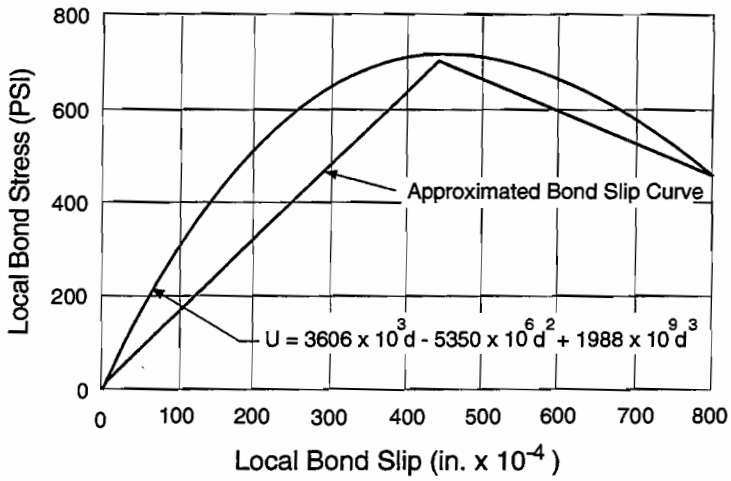

* 1 psi = 6894.757 Pa

Figure 5.10. Bond slip curves

5.3.3 Model Boundary Conditions

Boundary conditions are shown in Figure 5.11. Symmetry is considered and only one-half of the crack spacing is analyzed for stresses. The line of symmetry is modeled as pin connected. It is assumed that the pavement subbase is rigid and that the bond between the pavement and subbase is negligible. Consequently, because of the negligible effect of friction on the analysis, the pavement is supported on rollers at its base. This assumption appears to be appropriate because it has been noted (Ref 19) that, in the analysis of the structural response for CRCPs, the effect of subbase friction is negligible for secondary cracking. However, the approach to the characterization of bond-slip at the steel concrete interface may be applied to the friction between the concrete pavement and the subbase layer (Ref 21).

The stress-free boundary of concrete segment under consideration is taken as the crack face, which is assumed to have developed after the first few days (as explained previously) as a result of pavement curling stress. It is also assumed that formation of the crack releases all restraint along that boundary in the concrete. The steel is fixed on both sides, since it is continuous across the crack face and theoretically continues infinitely in a CRCP. Thus, steel restraint of the longitudinal direction causes stresses in the steel and concrete and affects the bond stress between concrete and steel.

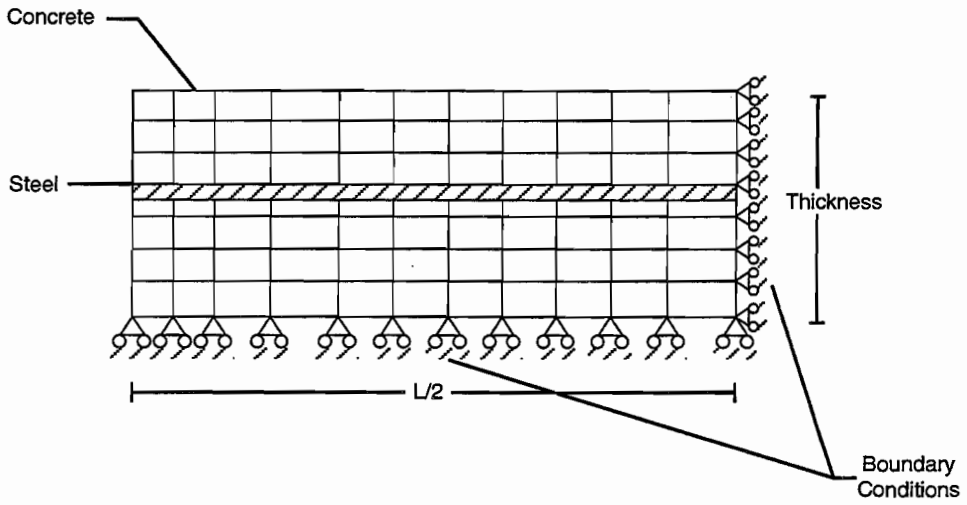

Figure 5.11. Boundary conditions and finite element mesh for stress analysis

5.3.4 Creep Model

Creep is defined as time-dependent deformation of a material subjected to sustained stress or loading. In the case where deformation is kept constant owing to some restraint, creep reduces stress in concrete, which is known as relaxation. Creep caused by thermal and shrinkage strains is included in this analysis. The method of superimposition of virgin creep curves is applied in this analysis and is similar to the approach by Grzybowski (Ref 15). At any time t, the creep function used to determine creep due to a load increment applied at time t_0 is given by:

$$\Phi(t, t_0) = \frac{1}{E(t_0)}\left[1 + \phi(t, t_0)\right] \qquad \text{(Eq 5.12)}$$

where

$E(t_0)$ = elastic modulus at age t_0 (psi),*

$\phi(t, t_0)$ = creep coefficient (ACI code),

t = actual age of concrete (days), and

t_0 = age of concrete at which load was applied (days).

* 1 psi = 6894.757 Pa

For every increment of stress Δs_i, the strain increment in the 'i'th time step owing to creep effect is given by the following equation:

$$\Delta\varepsilon_i = \frac{\Delta\sigma_i}{E(t_0)}\left[1+\phi(t,t_0)\right] \qquad \text{(Eq 5.13)}$$

The coefficient of creep in this analysis is suggested by the American Concrete Institute as a function of time and material properties. It is defined by the following equation:

$$\phi(t,t_0) = \frac{(t-t_0)^{0.8}}{10+(t-t_0)^{0.8}}\,\phi_\infty(t_0) \qquad \text{(Eq 5.14)}$$

where

t = time at which creep coefficient is computed,

t_0 = time at which load is applied, and

ϕ_∞ = ultimate creep coefficient, as given in ACI, depends on type of mix, specimen geometry, relative humidity, and age of concrete.

The ultimate creep coefficient is defined as the ratio of creep strain to initial strain. Its range, as specified in ACI, is normally between 1.30 and 4.15. The average value of the ultimate creep coefficient for moist, cured concrete is given by:

$$\phi_\infty = 2.35\,\gamma_c \qquad \text{(Eq 5.15)}$$

where Y_C is the correction factor, which depends on the relative humidity. This is given as:

$$\gamma_c = 1.27 - 0.067\,h \qquad \text{(Eq 5.16)}$$

where h is the moisture content in concrete.

5.4 EXAMPLE ANALYSIS

Four example problems are considered for examining various features of the model developed for the study of shrinkage and temperature stresses in CRCPs. The finite element mesh for the stress analysis model is optimally refined by considering mesh models with different aspect ratios.

The performance of the stress analysis model and its results are compared with Vetter's theoretical model (Ref 11). An example problem of uniform shrinkage is considered for the analysis to verify the model. The various parameters required for the analysis (both for the developed model and Vetter's model) are given below:

Crack spacing (L) = 8 ft (2.4384 m)

Concrete Poisson ratio = 0.18

Steel Poisson ratio	=	0.3
Concrete Elastic modulus (E_c)	=	4.29 X 10^6 psi*
Steel Elastic modulus (E^s)	=	29 X 10^6 psi
Percentage area of steel (p)	=	0.75%
Reinforcing bar diameter (d_b)	=	0.75" (1.905 cm)
Reinforcement cover	=	4.0" (10.16 cm)
Thickness of concrete slab	=	10.0" (25.4 cm)

* 1 psi = 6894.757 Pa

The following reduced equation of Vetter (Ref 11) is used for the computation of concrete stress in the pavement that occurs halfway between the transverse cracks due to drying shrinkage only:

$$f_c = \frac{-Q_0 + \sqrt{Q_0^2 + 4(Q_0)Z\ E_s}}{2} \qquad \text{(Eq 5.17)}$$

where

f_t = average tensile stress in concrete in the middle of the slab,

A = $4p/d_b$,

p = percentage reinforcement,

d_b = diameter of the reinforcing bar (in.),**

n = E_S/E_C,

E_S = modulus of elasticity of steel (psi),*

E_C = modulus of elasticity of concrete (psi),

u = average bond stress (psi),

z = shrinkage strain, and

L = crack spacing (ft).***

* 1 psi = 6894.757 Pa

** 1 inch = 2.54 cm

*** 1 foot = .3048 m

In the first example, the tensile stress in concrete is computed using Equation 5.17 and compared with the tensile stress computed using the finite element analysis. The results indicated for low shrinkage strains, the maximum tensile stress in the concrete, as computed by the FE model, is near the location of the steel reinforcement. However, note in Figure 5.12 that the location of the maximum bond and tensile stresses in the concrete becomes further away from the crack face as the shrinkage strains increase. This is may be primarily due to the varying level of

restraint of the steel reinforcement near the crack face, and to the nature of the bond-slip function. Also the FE model results indicate that the maximum tensile stress occurs further away from the crack face with increase in shrinkage strains where partial restraint (owing to breakdown of the bond) near the crack face releases tensile stress in the concrete. This leads to the maximum stress occurring at the fully bonded region.

To compare the results with Vetter's equation (Ref 11), the average concrete stress (average of all stresses along the section at which maximum bond stress occurs) is determined from the FE analysis and plotted in Figure 5.13.

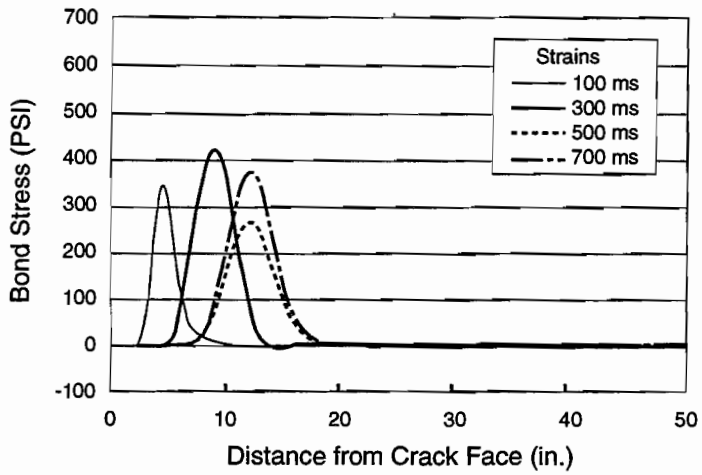

* 1 psi = 6894.757 Pa

** 1 inch = 2.54 cm

Figure 5.12. Comparison of average tensile stress obtained from Vetter's model

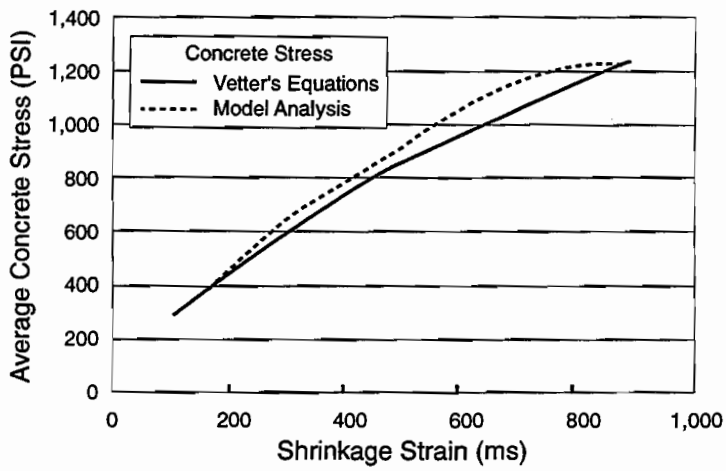

* 1 psi = 6894.757 Pa

Figure 5.13. Bond stress distribution along the reinforcement for uniform shrinkage strains

It can be seen that even though the maximum concrete stress obtained from the numerical model is high, the average stress is nearly equal to values obtained from Vetter's equations. As pointed out above, the bond stress distribution as computed from the FE model for various shrinkage strains are as shown in Figure 5.12. The Vetter approach assumes the bond to be uniformly distributed over the length of the bond development. In this sense, the FE model represents the bond distribution in a more realistic manner than does the Vetter equation. Stress contours for a shrinkage of 100 microstrain (ms) uniformly distributed along the depth are illustrated in Figure 5.14, while the slab boundary conditions are shown in Figure 5.11. This figure indicates, as pointed out previously, that the maximum stress occurs near the steel reinforcement in the vicinity of the fully bonded region. This point is further illustrated in Figure 5.15, which shows the maximum concrete stress distribution along the reinforcement for the analysis shown in Figure 5.14.

The second example considers a non-uniform, vertical shrinkage and temperature distribution; it is presented to further illustrate the model capabilities in terms of concrete cover over the steel reinforcement, bond stress-slip effects, and the percentage of steel reinforcement. It is pointed out that the Vetter approach does not consider the effect of rebar cover; nor are non-uniform shrinkage and temperature gradients considered. The shrinkage strain is allowed to vary through the depth of the concrete, and nonlinear moisture diffusivity is considered in the analysis.

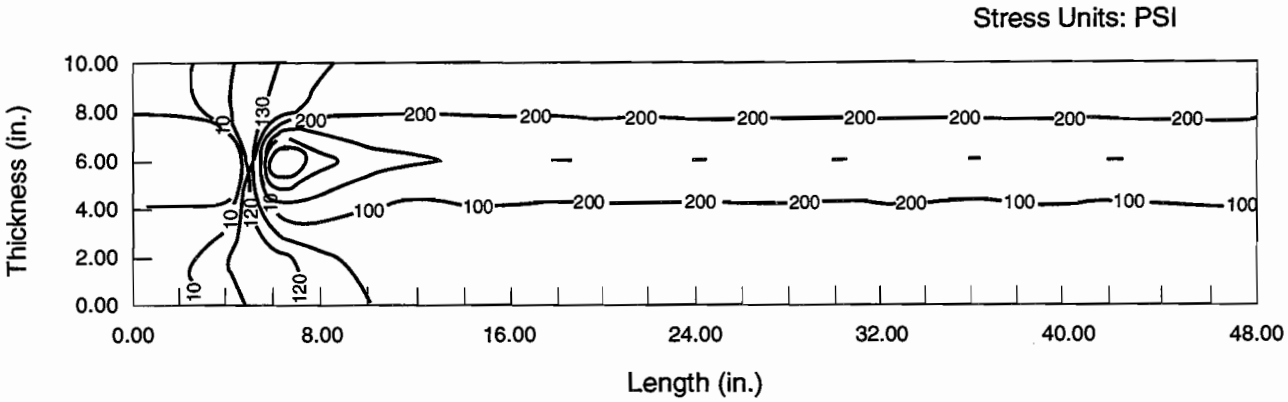

* 1 psi = 6894.757 Pa
** 1 inch = 2.54 cm

Figure 5.14. Contour plot for tensile stress in concrete for 100 ms uniform shrinkage strain

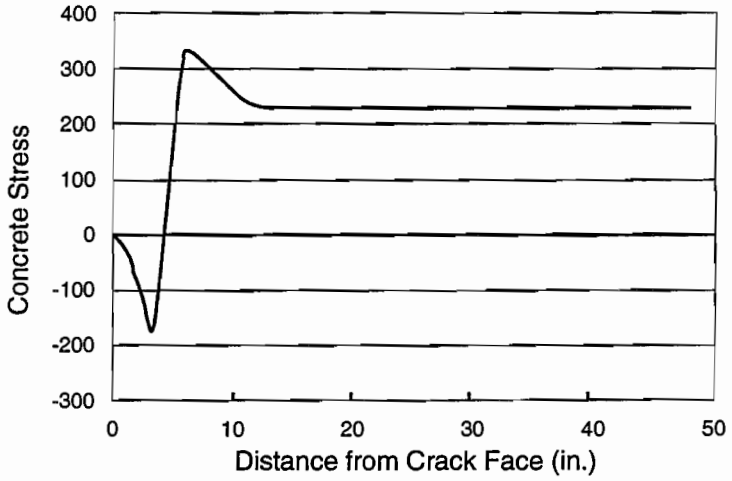

* 1 inch = 2.54 cm

Figure 5.15. Concrete stress distribution along the reinforcement for 100 ms uniform shrinkage strain

It is observed that the diffusivity constant in Equation 5.5 of the diffusion theory is nonlinear with respect to time. The variation of diffusivity is provided in unpublished data from a 1989 Texas A&M study. The following regression equation is developed from the data:

$$k_h = -0.00007750\, e^t + 2.36146257\, e^t + 0.24864235 \qquad \text{(Eq 5.18)}$$

where

k_h = diffusivity (in.^{2}/day), and

t = time (day).

A pavement with a thickness of 10 inches is assumed to illustrate the effects of the above factors in which ambient conditions are idealized. The variation of the ambient temperature and relative humidity for the pavement construction site conditions are approximated by a sine curve. The maximum temperature is assumed to be 90° F (32.2° C), and the minimum temperature at midnight is assumed to be 60° F (15.6° C). A 30° F (16.7° C) variation over a 24-hour period is assumed. Similarly, the maximum relative humidity is assumed to be 90 percent, and the minimum relative humidity is taken to be 60 percent, with a variation of 30 percent relative humidity over a 24-hour period. Analysis begins with the mean temperature and relative humidity. The sine curves of the relative humidity and temperature are shifted by a phase angle of 180 degrees; i.e., the maximum temperature and minimum relative humidity are observed at noon and maximum relative humidity and minimum temperature are observed at midnight. The variation of temperature along the depth of the concrete is taken into consideration with a gradient of +2 degrees and -1 degree per inch for the day and night (maximum and minimum)

temperatures, respectively. A thermal coefficient of 5 micro strains per degree Fahrenheit was assumed for the concrete and 6 micro strains per degree Fahrenheit for the steel reinforcement.

The results (Figure 5.16) show that the rate of diffusion of the moisture decreases with time. This is expected because the diffusivity constant decreases with time. It is also observed that, even though the net ambient conditions are constant, there is a significant amount of drying on the surface of the pavement, but little drying near the bottom of the slab, which may vary owing to the type of subbase. Shrinkage strains are computed from the pore moisture content using Equation 5.6. The maximum diffusion of moisture from the pavement observed at noon is a result of high temperature and low relative humidity. These shrinkage strains and temperature differentials are used as the input for three cases that are analyzed to study the effect of the reinforcement cover on the stress distribution in CRCPs. These cases are as follows:

1. The steel reinforcement at a depth of 2 in. (5.08 cm)
2. The steel reinforcement at a depth of 4 in. (10.16 cm)
3. The steel reinforcement at a depth of 6 in. (15.24 cm)

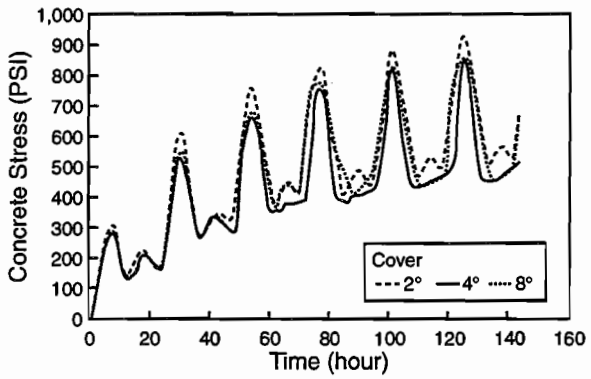

* 1 psi = 6894.757 Pa

Figure 5.16. Variation of pore moisture content with time and depth of pavement

Values for shrinkage strain and temperature differentials are taken from the strain model.

In the above analysis, it is observed that the location of the maximum concrete tensile stresses occur again at the level of the steel. This contradicts the commonly held belief that the maximum stresses occur near the pavement surface. Also, the maximum stress location is apparently at the point where the concrete is perfectly bonded to the reinforcement and the bond slip is nil. The effect that rebar cover is illustrated in the Figure 5.17.

It is observed from the analysis that a 2-inch (5.08-cm) cover of the slab steel produces greater tensile stress in concrete, when compared with 6 inches (15.24 cm) of cover. Field observations (Ref 3) have indicated that CRCPs with shallow rebar covers tend to develop, on the average, closer crack patterns than those with greater depths of cover. With respect to the perception that greater stresses result in a higher degree of cracking, past field studies tend to verify

this result. It is pointed out that this effect was not observed under a uniform shrinkage distribution, since the strain field was linearly distributed. As the steel is positioned nearer the high temperature and moisture gradient area, an increase in the concrete stresses result as a result of the bonding between steel and concrete increasing the level of restraint.

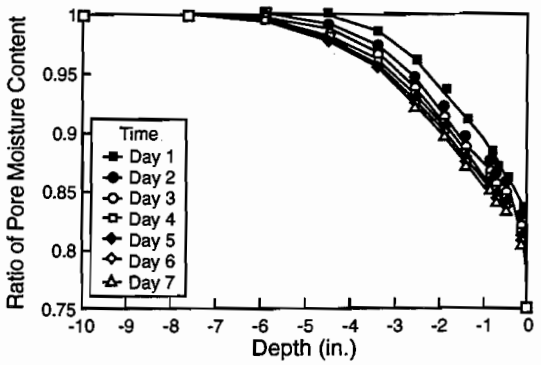

* 1 inch = 2.54 cm

Figure 5.17. Effect of cover on maximum tensile stress in cracked pavement

The third example demonstrates the effect of varying the percentage of steel reinforcement on the maximum tensile stresses and the effect of the percentage of steel on stress distribution in the pavement. Two cases are analyzed: (1) 2 inches (5.08 cm) of cover with 0.75 percent steel reinforcement, and (2) 2 inches (5.08 cm) of cover with 0.50 percent steel reinforcement.

The variation of the steel reinforcement is represented by varying the thickness of the reinforcement and the diameter of the reinforcing bar. Figure 5.18 illustrates the maximum tensile stress in concrete for these two cases. The variation of maximum tensile stress caused by the variation of the percentage of steel is not significant, even though stresses in the case of 0.75 percent steel are lesser than stresses in concrete with 0.50 percent steel, which is not consistent with other analytical models.

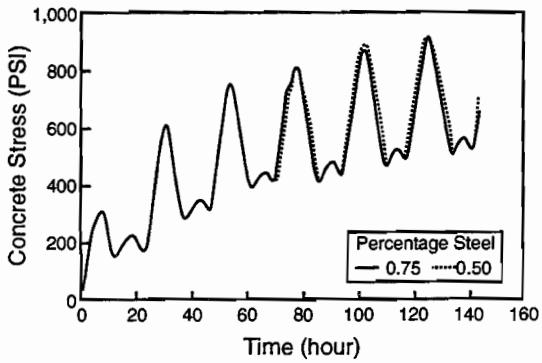

* 1 psi = 6894.757 Pa

Figure 5.18. Effect of % steel on maximum tensile stress in cracked pavement

The final example considers the effect of the bond stress-slip relationship. In the field, it is observed that the bond between steel and concrete varies significantly between epoxy-coated bars and ordinary deformed bars. An approximate variation of the stiffness of the bond slip elements is considered to show the effect of bond on stress distribution. Figure 5.19 illustrates the two bond slip relationships considered for this analysis.

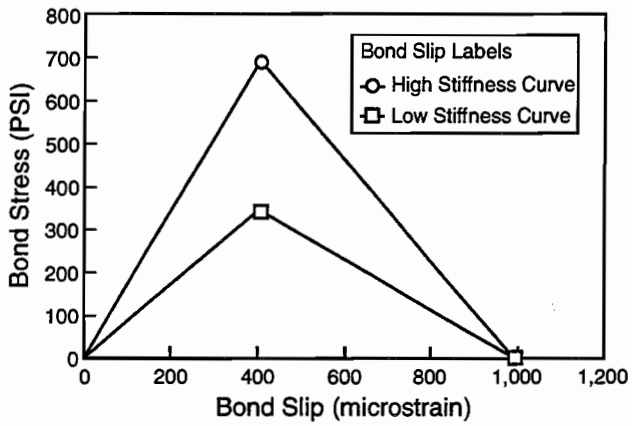

* 1 psi = 6894.757 Pa

Figure 5.19. Bond stress-slip relation

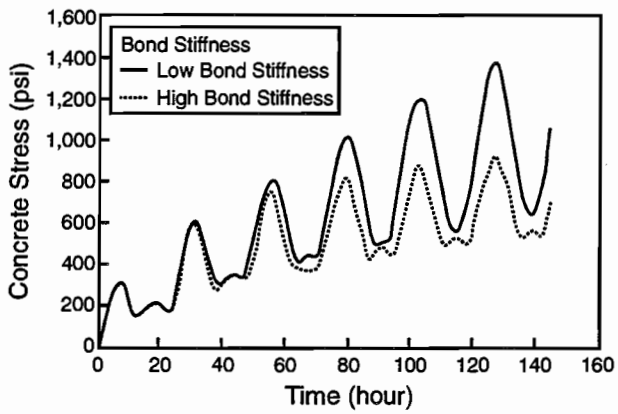

* 1 psi = 6894.757 Pa

Figure 5.20. Effect of bond stress-slip relationship on maximum tensile stress in cracked pavement

The slope of the bond stress-slip for low stiffness curve (Figure 5.20) is 50 percent of that for high stiffness curve. The analysis is performed for a cover of 2 inches, with the results illustrated in Figure 5.20. It is observed that in the first few hours there is no difference in the

stress between the two above-mentioned cases; however, after 60 hours, the stresses in lower bond strength increase significantly. This can be explained by the fact that the bond between steel and concrete fails (low stiffness curve) and, hence, gives higher tensile stress in concrete owing to the fact that all the stresses are carried by the concrete only. Also, tensile stresses in the concrete are high in both cases owing to the presence of steel in the high strain gradient area.

The above four example problems describe the potential capabilities of the analysis framework. Also, the effect of the ambient temperature and ambient humidity on the CRCPs is illustrated for various reinforcement covers and bond slip relationships.

5.5 SUMMARY

A procedure for a numerical analysis framework is developed to determine shrinkage strains and the corresponding tensile stresses in reinforced concrete slabs. Even though previous literature addresses these problems, most models do not consider either the non-uniform distribution of shrinkage strains or the bond slip variation in the concrete. In this paper, a framework is developed that considers not only these effects, but how they vary with respect to ambient climatic conditions in addition to creep relaxation.

Consideration of the effect of the various parameters, and the effect of their non-linearity with respect to time, is critical to a better understanding of the pavement behavior in first few days of its construction. The framework developed in this research incorporates various factors that are ignored in previous pavement models. This, relatively speaking, represents a step beyond previous research efforts to characterize stresses in CRCP.

The following are the conclusions resulting from the analysis of the example cases:

1. Vetter's equations or the later modified models may be applied for predicting the average tensile stress in the middle of crack spacing; however, it is observed that due to the bond between steel and concrete, maximum tensile stress in concrete is observed at the level of steel for pavements with 2 inches (5.08 cm) of cover, and in the middle of crack spacing for pavements with 6 inches (15.24 cm) of cover. Also, the maximum tensile stress predicted in this paper is greater than the average tensile stress predicted by Vetter's equations. Hence, for detailed stress analysis in the prediction of cracking, the assumption of uniform shrinkage and temperature gradients as considered in Vetter's approach may not be applicable.
2. The reinforcement cover may become a significant factor in crack development, especially under field conditions where the variation of temperature throughout a day is greater than what is assumed in this study (30° Fahrenheit (16.7° C) over a 24-hour period).
3. More detailed research should be performed toward determination of the bond-slip relationship between the steel reinforcement and the rebar because of its apparent significant effect on stress distribution in concrete. Further research needs to be performed to more accurately determine the bond stress-slip relationship. Determination of bond characteristics between steel and concrete for different types of steel bars, such as plain, deformed, or epoxy-coated bars is significant for the prediction of the actual state of stress in CRCP. Although there are some experimental

relationships that predict bond stress for a given slip, they are mostly pull-out types of experiments (steel bar embedded in concrete being pulled out and then studied for the strains developed in the bar and concrete). The validity of these models for the problems considered here should be studied further. Also, the model should be improved to consider different stiffness values for spring elements along the reinforcement since it is demonstrated that the bond stress-slip relationship varies along the reinforcement. The variation of bond stress-slip relationship with time should also be determined. The simplified assumption that this variation is proportional to the variation of the modulus of concrete was used in this paper. There is no available evidence in the literature to substantiate this assumption.

4. The analysis indicates a lack of sensitivity to the percentage of reinforcement on concrete stress. This may have been due to the FE representation used for the steel bar. It is recommended that further analysis of this effect be considered, perhaps using a different technique to represent the steel bar.
5. The model results should be verified with experimental results, which was beyond the scope of this particular study. Work is currently underway at Texas A&M University to obtain sufficient field data to valid analysis of the nature presented in this framework.
6. The model is limited to the prediction of maximum tensile stress. Hence, for a study of the actual crack mechanism and its propagation, a crack tip element should be included in the model. This will allow the model to provide a more realistic approximation of the field conditions.
7. The inclusion of all the ambient factors such as concrete creep model, temperature, and non-linearity of the diffusion model in the analysis leads to a better understanding of the behavior of the pavement and can aid in development of a reliable design procedure for CRCPs.

CHAPTER 6. TRIAL IMPLEMENTATION OF PRELIMINARY RESULTS

6.1 INTRODUCTION

Several significant findings have been developed in this study. These findings, which are summarized in Report 1244-4 (Ref 4), pertain primarily to the construction of continuously reinforced and jointed concrete pavements in Texas; guidelines for the preliminary implementation of these findings are also provided in the report. Various categories of these findings are addressed below.

6.2 ENVIRONMENTAL PAVING CONTROLS

The findings here indicate that other factors, such as climatic conditions *at the time of paving*, must be considered in addition to the steel design for CRCP or the spacing of the joints for jointed concrete pavement. These controls are recommended to minimize the occurrence of poor crack patterns or uncontrolled random cracks that can affect the performance of the pavement.

For the standard conditions and curing methods employed in hot weather, paving of concrete pavement should be restricted between the mid-day hours of 10:00 a.m. to 3:00 p.m., when the ambient temperature is expected to rise above 92° F (33.3° C). An alternative to this is the control of the temperature of the concrete to a maximum of 90° F (32.2° C) as delivered to the project site. Additional alternatives under consideration involve curing methods, since these methods do affect the pavement temperature, the development of strength, and the evolution of cracking. Further considerations are provided under section 6.7.

6.3 STEEL DESIGN

One of the primary functions of reinforcing steel in CRCP is to maintain crack widths to within sufficient limits to insure the level of performance over a given service period. This particular function is dependent not only on the bond characteristics of the steel, but also on the depth of cover provided by the concrete.

The percentage of steel reinforcement and the area of bond provided by the rebar in a reinforced section are significant factors in the formation of the crack pattern. However, other factors are also important, such as the thermal coefficient of expansion of the coarse aggregate and the temperature conditions at the time of construction. Owing to these affects, the design of the steel reinforcement needs to take into account the type of coarse aggregate to be used in the concrete mix. However, this design feature should not be implemented separately or without respect to temperature controls described above.

It is also recommended, whether or not early-aged saw cut techniques are employed to control the development of the crack pattern, that the transverse steel, which is used to support the longitudinal steel reinforcement, be placed on a 60-degree skew to minimize the incidence of transverse cracking at the location of the transverse bar.

6.4 SAW CUTTING

The use of early-aged saw cutting has been found in this study to function as well as or better than conventional saw cut techniques in the control and formation of cracking in both longitudinal and transverse concrete pavement joints. The development of cracking in CRCPs should not be considered the problem in the performance of this pavement type, since the formation of any crack will ultimately result in the reduction of stress at some other point in the pavement.

However, one should ideally use the forces of nature to advantage by encouraging cracks to form at specific locations and in a specific manner. One way to do this is through early-aged saw cutting, in which drying shrinkage is used to minimize the depth of the cut required to initiate cracking. The formation of cracking through the lowering of the fracture toughness of the concrete at the location of the saw cut provides a cost benefit by extending pavement life (regardless of the coarse aggregate type).

Research findings have indicated that the use of the early-aged saw cutting during CRCP construction can successfully control the crack pattern. Trial test sections implementing positive control of the crack pattern have demonstrated high randomness crack indexes, low incidence of spall delamination, uniform crack distributions, elimination of short crack spacing, and elimination of 'Y' cracks. Given these benefits, it is recommended that positive crack control techniques be implemented for the construction of CRCPs using river gravel or any other kind of aggregates.

It is important to note that the use of the early-aged saw cutting technique for positive crack control of the crack pattern must include consideration of other factors (e.g., the steel design) when determining an optimum transverse spacing of the saw cuts. Other factors are discussed subsequently with respect to positioning of the tie bars across longitudinal joints.

6.5 TIE BAR MODIFICATIONS

Tie bars are modified when positive crack control measures are implemented during the construction process; such modification simply consists of positioning the tie bar at a distance of 6 inches (15.24 cm) or more from a transverse saw cut location to prevent crack development from passing through the position of the steel reinforcement. This measure will help to protect the tie bar from coinciding with the location of a transverse crack, a situation that may deteriorate the integrity of the bond between the steel and the concrete pavement.

6.6 AGGREGATE BLENDS

Aggregate blends will allow the strengths of one aggregate type to diminish the weaknesses of another aggregate type, which should serve to rectify the performance deficiencies manifest in the pavements containing the aggregate types exhibiting the poorer engineering properties. Several properties relating to strength, thermal expansion, modulus of elasticity, etc., can be modified according to the percentage of each aggregate included in the blend. Trends noted in the development of the crack pattern are similar to those occurring in the engineering properties.

The recommendation for aggregate blends call for the use of limestone or crushed aggregates in the 1-1/2 to 3/4 inch (1.905 to 3.81 cm) sizes, and river gravels in the 3/4 inch (1.905 cm) to #8 gradation sizes. It is also recommended that the gradation specification for concrete mixes be modified to allow a third aggregate (in addition to the coarse and fine aggregates) to be included in the size range of 3/8 inches (.9525 cm) to #8 sizes. Aggregate blends of this nature will increase the unit weight, reduce the required amount of cement and the water/cement ratio, and improve the workability of the mix while maintaining the strength requirements.

6.7 CURING METHODS

The type of curing method employed during the construction of concrete pavements can have a significant effect on the development and control of cracking. Although a final recommendation cannot be made at this time, it may be advisable to apply a single coat of Type II curing compound for paving in temperatures of 90° F (32.2° C) or below, while two coats are recommended for paving in temperatures above 90° F (32.2° C). The use of polyethylene film curing is extremely effective in reducing pavement surface moisture loss. While the effect of this is to delay the development of cracking in CRCP construction, there is a concomitant increase in the curing set temperature of the concrete owing to the greenhouse effect of the film. This effect would tend to accelerate the rate of strength gain and decrease the permeability of the concrete.

In terms of positive crack control for both jointed and CRCPs, a combination of curing compounds is recommended so that two coats of curing protection are provided. The first coat should consist of an application of Type I compound, which applies a quick-setting, temporary curing layer. Upon completion of the saw cutting operations, one or two coats (depending on the climatic conditions) of Type II compound should be applied to insure proper set.

As a final note, it is recommend that instrumentation capable of monitoring the degree of moisture loss in the field be used to determine when to apply curing compounds; such instrumentation could provide a measure of quality control during construction.

CHAPTER 7. FUTURE WORK ACTIVITIES

7.1 FIELD IMPLEMENTATION OF RESEARCH FINDINGS

District 12 is implementing several findings reported in Chapter 5 in a major construction project on U.S. 290 between Hempstead and the Harris County Line. A variety of test sections, placed on a large scale, will serve to validate the methods and procedures when appropriately combined. The following items are to be considered in the test sections:

1. use of two coarse aggregate types;
2. use of skewed transverse steel;
3. use of three different curing methods;
4. use of early-aged saw cutting techniques;
5. placement of concrete under different climatic conditions and temperature controls; and
6. use of variation in crack control, aggregate blends, fly ash quantities, steel percentages, cure methods, and other miscellaneous items.

The construction of these test sections will permit the collection of additional temperature and moisture data, which can be compared with the results obtained from computer-generated numerical methods. This will be an interesting segment of the project, insofar as it will test how well simulation models can be used to predict strength and stress gain in the field based on measured material properties and predicted weather conditions at the time of construction.

The aggregate characteristics, which differ for each coarse aggregate type, make up a portion of the material properties that serve as inputs to the simulation models. These aggregate characteristics, which influence the performance of a given pavement type, can be predicted based on certain properties, including origin, chemical constituents, shape and texture characteristics, thermal expansion, and conductivity characteristics, among others. Thus, an aggregate classification framework should be organized and developed to quantify different aggregates with respect to their demonstrated performance.

7.2 OPTIMIZATIONS OF DESIGN FACTORS

The essence of construction quality control and quality assurance (QC/QA) is achieving the best combination of the available materials to produce the required level of pavement performance. In order to better understand these material combinations, an optimization process should be undertaken that will consider climatic conditions at the time of construction, material characteristics, and pavement behavior and performance.

Essential to this type of analysis will be the use of material and structural stimulation models that reflect the behavior of the pavement—particularly during the early stages of CRCP life when most of the cracking damage occurs.

Thus, several combinations of aggregate type, mix proportions, curing and construction methods, steel configurations, and climatic conditions should be considered as a minimum in developing a framework-optimized design procedure.

REFERENCES

1. Hankins, K., Y. C. Suh, and B. F. McCullough, "Field Evaluations for Coarse Aggregate Types: Criteria for Test Sections," Research Report 1244-1, Center for Transportation Research, The University of Texas at Austin, 1991.
2. Dossey, T., and B. F. McCullough, "Characterization of Concrete Properties With Age," Research Report 1244-2, Center for Transportation Research, The University of Texas at Austin, 1992.
3. Suh, Y. C., K. Hankins, and B. F. McCullough, "Early-age Behavior of Continuously Reinforced Concrete Pavement and Calibration of the Failure Prediction Model in the CRCP-7 Program," Research Report 1244-3, Center for Transportation Research, The University of Texas at Austin, 1992.
4. Jimenez, M. A. C., B. F. McCullough, and K. Hankins, "Monitoring of Silicious River Gravel and Limestone Continuously Reinforced Concrete Pavement Test Sections in Houston 2 Years After Placement and Development of a Crack Width Model for the CRCP-7 Program," Research Report 1244-4, Center for Transportation Research, The University of Texas at Austin, 1992.
5. Won, Mooncheol, K. Hankins, and B. F. McCullough, "Mechanistic Analysis of Continuously Reinforced Concrete Pavements Considering Material Characteristics, Variability, and Fatigue," CTR Research Report 1169-2, April 1990.
6. ASTM C39-86, Standard Test Method for Compressive Strength of Cylindrical Concrete Specimens.
7. ASTM C496-90, Standard Test Method for Splitting Tensile Strength of Cylindrical Concrete Specimens.
8. ASTM C 157-91, Standard Test Method for Length Change of Hardened Hydraulic-Cement and Concrete.
9. ASTM C 531-85 (Reapproved 1990), Standard Test Method for Linear Shrinkage and Coefficient of Thermal Expansion of Chemical-Resistant Mortars, Grouts and Monolithic Surfaces.
10. Mandelbrot, B. B., *The Fractal Geometry of Nature*, San Francisco: Freeman Press, 1982.
11. Vetter, C. P., "Stresses in Reinforced Concrete Due to Volume Changes," ASCE Proceedings, Paper # 1848, February 1932.
12. Palmer, R. P., Olsen, M., and Lytton, R. L., "TTICRCP — A Mechanistic Model for the Prediction of Stresses, Strains, and Displacements in Continuously Reinforced Concrete Pavements," Research Report 371-2F, Texas Transportation Institute, Texas A&M University, August 1987.
13. Bazant, Z. P., and Najjar, L. J., "Nonlinear Water Diffusion in Non-Saturated Concrete," *Materials and Structures,* Vol. 5, # 25, 1972, Paris.
14. Gardner, N. J., and Poon, S. M., "Time and Temperature Effects on Tensile, Bond, and Compressive Strengths," No. 73-31, *ACI Journal,* July 1976.

15. Grzybowski, M., and Shah, S. P., "Model to Predict Cracking in Fibre Reinforced Concrete Due to Restrained Shrinkage," *Magazine of Concrete Research,* Vol. 41, No. 148, September 1989, p. 125-135.

16. Bazant, Z. P., and S. T. Wu, "Creep and Shrinkage Law for Concrete at Variable Humidity," *Journal of the Engineering Mechanics Division*, Vol. 100, December 1974.

17. Ngo, D., Scordelis, A. C., "Finite Element Analysis of Reinforced Concrete Beams," Title No. 64-14, *ACI Journal,* March 1967.

18. Bradbury, R. D., "Reinforced Concrete Pavement," Wire Reinforcement Institute, Washington, D.C., 1938.

19. Nilson, A. H., "Bond Stress-Slip Relations in Reinforced Concrete," Report No. 345, Department of Structural Engineering, School of Civil and Environmental Engineering, December 1971.

20. Jiang, D.H., Shah, S. P., and Andoinian, A. T., "Study of the Transfer of Tensile Forces by Bond," *ACI Journal,* Proceedings, Vol. 81, No. 3, May-June 1984, p.251-259.

21. Nilson, A. H., "Internal Measurement of Bond Slip," Title No. 64.41, ACI Summary Paper, *ACI Journal,* July 1972